Binder Jet Additive Manufacturing of Copper

Optimizing the print and post-process parameters to achieve high density copper parts

MSc. Thesis

Mariëtte Houtkoop

TU Delft

CONCR3DE
YOUR 3D POWDERHOUSE

Binder Jet Additive Manufacturing of Copper

MSc. Thesis
by
Mariëtte Houtkoop

to obtain the degree of Master of Science
at the Delft University of Technology,
to be defended publicly Monday 18 December 2023 at 13:00

Student number:	4477367	
Project duration:	February - December 2023	
Thesis committee:	Dr. V. Popovich,	TU Delft 3mE/MSE
	Dr. F. Salari,	Concr3de
	Dr. O. Nejadseyfi,	TU Delft 3mE/PME

TU Delft

CONCR3DE
YOUR 3D POWDERHOUSE

Acknowledgements

I would like to show my gratitude to everyone who supported me during this thesis. Firstly I want to thank my thesis supervisor Dr. Vera Popovich of the TU Delft. For helping me through my project with constructive criticism and guiding me in the right direction.
Secondly I want to thank Dr. Farid Salari and Matteo Baldassari for not only giving me the project at Concr3de, but guiding me towards a solid end result. Thanks to the material development team as well who aided me with all my questions and all the other colleagues at Concr3de for giving me a nice working environment.
Thirdly I want to thank people from the TU Delft. Especially Hans Brouwer, who really gave all the right guidance for finding the working post processing conditions. The kindness, discussions and aid really benefited my thesis. I also want to show my appreciation to the mechanical behaviour team, the optical team and the XRD and Micro-CT operators.
At last I want to thank my family and boyfriend for supporting me throughout everything and believing in me. I am grateful for all your help.

Mariëtte Houtkoop
Delft, December 2023

Abstract

This research aimed to optimize the process parameters of small copper parts printed with binder jetting. The optimisation was distinguished by dividing the parameters in print and post-process parameters. Binder jetting is an additive manufacturing technique that combines layers of the material in powder form with a binder. After the printing process the printed samples need curing, debinding and sintering. The binder acts as a temporary glue to hold the shape and is later removed during the debinding. The sintering fuses the powder particles together, below the melting temperature. With binder jetting it is the aim to achieve the high density parts, as there is no compression of powder during the printing process. This often leads to low density parts with binder jetting.
The two problems that needed to be solved, were: how can the bleeding issues be stopped and at what temperature, time and environment can the printed copper be sintered.
Multiple print sessions were done to: first test the known print parameters, second optimize the print parameters and third, print with optimized print parameters. ThermoGravimetric Analysis (TGA) was conducted to determine the correct debinding and sintering temperature of the copper samples. The bleeding issues could be solved by adjusting the saturation level. The saturation level was reduced from 104 % to 72 %. The lower percentage gave 0.5 mm dimensional accurate samples and no bleeding issues.
Compression testing was done to compare the mechanical behaviour to that of conventionally manufactured copper. However the discs used for compression testing needed to be bigger in size than the cubes used for optimizing the sintering process. This lead to not fully sintered discs used for the compression testing. Meaning the achieved compressive strength and elasticity modulus were 1 % of conventionally manufactured copper. Three working sinter sessions were compared to see which gave the highest achieved density. Sintering 10 hours in argon at 1093 ℃ or in vacuum at 1080 ℃ both achieved the same high densities. Shell printed cubes performed better with an average density of 73 ± 8 % in argon and 74 ± 7 in vacuum. The samples placed on the top level inside the sintering oven achieved higher densities than in lower levels. Two shell printed cubes in argon achieved a density of 83 ± 0.5 % with a volumetric shrinkage of 40 ± 1 % and two shell printed cubes in vacuum achieved a density of 82 % with a volumetric shrinkage of 40 %. Solid cubes reached lower densities, with 67 ± 10 % in argon and 71 ± 7 % in vacuum. As with the shell printed cubes, the solid cubes have a high deviation due to the placement of the samples on different levels. The solid cubes had less volumetric shrinkage and rather high deviation due to the same reason, with 25 ± 16 % in argon and 35 ± 11 % in vacuum.
The density is measured with a caliper and with Archimedes which gave quite differ-

ent results. Densities measured with Archimedes were up to 22 % higher due to the porosity of the samples. All the measurements done by other copper binder jetted parts are done with Archimedes. Thus it seems the 74 % and 82 % is low when compared to 91 % density achieved in literature, but it is not known how accurate these measurements are.

Contents

List of Figures **vi**

List of Tables **viii**

1 Introduction **1**
1.1 Additive manufacturing of copper 1
1.2 Research question 1
1.3 Structure of Thesis 3

2 Literature Review **4**
2.1 The process 6
2.2 Printing copper 7
2.3 Binder jetting parameters 9
2.4 Post-Processing 11
2.5 Difficulties Binder Jetting 16

3 Methodology **25**
3.1 Printing and Curing 25
3.2 TGA 29
3.3 Debinding and Sintering 30
3.4 XRD 33
3.5 Dimensional accuracy 33
3.6 Testing of functional properties 35
3.7 Microstructural characterisation 39

4 Results **40**
4.1 Effect of Printing and Curing 40
4.2 TGA 44
4.3 Debinding and Sintering 47
4.4 XRD 52
4.5 Dimensional accuracy 55
4.6 Testing of functional properties 58
4.7 Microstructural characterisation 61

5 Discussion **67**
5.1 Printing and Post-processing of samples 67
5.2 Testing of samples 80
5.3 Characterization analysis 84
5.4 Comparison to wrought copper 89

6 Conclusions and Future Scope **93**
6.1 Recommendations for future research 95

A Printlog **97**
A.1 First session 97
A.2 Second session 98
A.3 Third session 103

B TGA graphs **106**
B.1 Debinding temperature 106

C Debinding and Sintering log **109**

List of Figures

1 An overview different AM classifications [4] 4
2 A schematic overview of binder jetting [8] 7
3 Post-processing steps of BJT copper parts [21] 11
4 Partial melting process of sintering powder [22] 12
5 Printing process of BJT [24] 13
6 Sintering profile of copper [26] 14
7 Surface of sintered and mechanically ground sample [28] 15
8 Dimensional differences between the real part and the BJT part [29] . 16
9 Normal printing versus shell printing [31] 18
10 Sintering and HIP of copper [9] 19
11 Oxide growth of copper [32] 20
12 Heating schedules and its rates 24
13 Flow chart of the thesis for binder jetting of copper 25
14 TGA machinery made by Setaram [38] 29
15 Dimensions of the alumina crucible inside the TGA 30
16 Used sintering equipment 31
17 Temperature graph with pyrometer and thermocouple [40] 32
18 Artec Space Spider Scanner 34
19 Caliper placement on cube 36
20 Set of broken dog-bone sintered in argon 36
21 Plastometrex Benchtop [43] 38
22 Printed samples P2 43
23 TGA and TGA derivative of sample T1 46
24 S9 green and sintered at 1095 ℃ samples, with natural cooling 48
25 S10 green and distorted sintered at 1093 ℃ samples, with natural cooling 49
26 S12 hollow cube and cube samples sintered at 1093 ℃ 50
27 S15 sample set at 1093 ℃ in argon for 10 hours 51
28 S16 sample set at 1075 ℃ in vacuum for 10 hours 51
29 S17 sample set at 1080 ℃ in vacuum for 10 hours 51
30 Sintered heat exchanger and gyroid next to green heat exchanger and gyroid 52
31 Printed samples P2 53
32 XRD samples 54
33 XRD sample of long curing 55
34 3D models of a green and sintered cube 56
35 3D models of a cone and its fused image 56
36 Dog-bone before and after tensile testing, sintered at 1080 ℃ in vacuum 61
37 SEM images of sample sintered in argon at 1093 ℃ 62

38 SEM images of sample sintered in vacuum at 1080 ℃ 62
39 EDS map of argon sample 63
40 XRD map made by EDS of argon sample 64
41 EDS map of vacuum sample 65
42 XRD map made by EDS of vacuum sample 66
43 Leaking powder during printing 69
44 Less leaking with upgraded reduction bed 69
45 Difference in binder saturation on cubes [45] 71
46 Particle shape of copper with a copper oxide shell [47] 74
47 Packing density versus sizes particles [48] 75
48 Fluid drainage binder in different powder particle shapes [34] 75
49 S4 samples 77
50 Droplets on plateau 78
51 Effect of adjustment cooling rate 79
52 Distorted heat exchanger 79
53 Plateau sample placement 81
54 Sintered broken off gyroid 85
55 Dummy sample for compression testing 86
56 Compressed sample with tear 87
57 SEM images of sample sintered in vacuum at 1080 ℃ and argon at 1093 ℃ 88
58 EDS map of carbon in different samples 88
59 EDS map of oxygen in different samples 89
60 View during print number 1 of print session 1 98
61 Leaking powder during printing 101
62 Prints during print session 3 105
63 TGA and TGA derivative of sample T2 107
64 TGA and derivative T4 108
65 S4 samples 110
66 Difference between sintered samples S7 (left T_s=1075℃) and S8 (right T_s=1090℃) 112
67 Samples S9 T_s=1095℃ 113
68 Samples S10 T_s=1093℃ 114
69 Samples S11 T_s=1094℃ 116
70 S15 sample set at 1093 ℃ in argon for 10 hours 117
71 S16 sample set at 1075 ℃ in vacuum for 10 hours 118
72 S17 sample set at 1080 ℃ in vacuum for 10 hours 118
73 Sintered heat exchanger and gyroid next to green heat exchanger and gyroid 119

List of Tables

1 Overview of AM processes and their materials [1] 5
2 Comparison of AM techniques to print copper [3] 8
3 Comparison of binder jetted copper properties to conventional manufactured copper properties 9
4 Comparison of shrinkage with different binders [26] 15
5 Improvement of density after sintering and HIP [25] 19
6 Improvement of the decreasing porosity after sintering and HIP [25] . 19
7 Comparison of shrinkage after sintering and HIP [25] 21
8 Heating schedules of different researchers (Atm = Atmosphere, RAtm = Reduced Atmosphere, H = Hydrogen, Ar = Argon, V = Vacuum) . 23
9 Parameters and chosen values for printing 26
10 Waveform M-Binder 27
11 Calculated saturation levels 28
12 Guaranteed chemical composition of copper powder by supplier . . . 28
13 Particle size distribution of copper powder 28
14 Specifications Artec Space Spider 3D Scanner [42] 34
15 Dimensions cuboids for electrical conductivity testing 37
16 Dimensions discs for compression testing 38
17 Prints from printing session 1 41
18 Prints from printing session 2 42
19 Prints from printing session 3 44
20 TGA input data 44
21 Debinding and sintering runs 47
22 Standard powder diffraction JCPDS, copper file No. 04-0836 [44] . . 55
23 Shrinkage measured with 3D Scanner 57
24 Directional shrinkage measured for solid and hollow cubes in different sinter atmospheres 57
25 Solid cube density measured with a caliper and a scale 58
26 Hollow cube density measured with a Archimedes 59
27 Dimensional accuracy measurements of green samples 59
28 Electrical conductivity measurements of cuboids in different atmospheres 60
29 Compressive strength measurements of different atmospheres 60
30 Tensile strength of sample sintered in vacuum at 1080 ℃ 60
31 EDS percentage of argon sample 64
32 EDS percentage of vacuum sample 66
33 Reasoning survival and accuracy of printed samples 68
34 Waveform M-Binder 72
35 Dimensional accuracy measurements of green samples 73

36 Achieved densities and standard deviations measured with caliper . . 80
37 Average measured shrinkage and density 82
38 Comparison electrical conductivity 83
39 Compressive strength measurements of different atmospheres 85
40 Property comparison 90
41 Comparison of measured densities for hollow cubes 91
42 Achieved densities of different researchers 91
43 Prints from printing session 1 97
44 Prints from printing session 2 100
45 Prints from printing session 3 104
46 TGA input data 106
47 Input data sinter session 1 110
48 Input data sinter session 2 112
49 Input data sinter session 3 117

Nomenclature

AM Additive Manufacturing

BJT Binder Jetting

DED Directed Energy Deposition

FDM Fused Deposit Modeling

HIP Hot Isostatic Pressing

MEX Material Extrusion

MJT Material Jetting

PBF Powder Bed Fusion

$SEBM$ Selective Electron Beam Melting

SHL Sheet Lamination

SLM Selective Laser Melting

VPP Vat Photo-Polymerization

1 Introduction

A part can be manufactured in multiple ways. A conventional way to manufacture a part is with Subtractive Manufacturing (SM), like CNC machining. The part starts as a block and more and more gets subtracted with hard tooling, until the desired form is left. It is a highly accurate method of manufacturing, but it leaves left-over material. Other possible manufacturing methods are casting and additive manufacturing. SM has the advantage that it is highly accurate. It can create complex shapes, but it will take a long time, while CNC is a relatively fast process for less complex parts. Furthermore SM works well for hard, brittle materials. Casting is better for softer materials, but the moulds can be very expansive. Additive Manufacturing (AM) can create very complex parts, for example an infill pattern like a honeycomb structure. Creating these kind of infills is not possible with conventional manufacturing methods. The processes in general are less accurate than SM and the parts are usually anisotropic, which are downsides of AM [1].

1.1 Additive manufacturing of copper

AM for metals is in high development since 2009 [2], thanks to the creation of the ASTM F42 Committee on AM technologies. Processes that can print metals with AM are powder bed fusion, direct energy disposition and binder jetting.

Copper is an interesting material due to its high thermal and electrical conductivity. Combine that with the geometrically complex shapes they can be used for the design and production of components for a wide range of sectors, including electronics and aerospace and the possibility of printing pure copper. But due to the high thermal and electrical conductivity and the lack of knowledge, it is proven to be rather difficult to produce pure copper parts with AM [3].

1.2 Research question

It is already difficult to produce pure copper with conventional production methods and even more for complex shapes. Using AM can help produce complex shapes in pure copper with hopefully less difficulties.
The aim of this thesis is to optimize the process parameters for achieving a high dimensional accuracy, high density small copper part printed with binder jetting.
Hereby a dimensional accuracy of 0.5 mm is wanted between the 3D model and the printed green part, a minimum density of 80 %. The optimization of the process para-

meters can be divided into the printing parameters and the post-process parameters. The focus lays on the post-process parameters, but finding the correct printing parameters are necessary to print accurate shapes. This is needed for the density and mechanical testing measurements. The correct printing parameters are also necessary to achieve strong enough green parts for transportation to clients. The correct post-process parameters are necessary to have fully sintered pure copper with a high density and an accurate shape.
The main question can be divided into the following sub-questions:

1. What are the optimized print parameters?
    (a) What layer height achieves ± 0.5 mm dimensional accurate shapes?
    (b) What saturation level achieves ± 0.5 mm dimensional accurate shapes with no bleeding issues?
    (c) What temperature and time need to be used for curing to achieve strong enough green parts that survive the depowdering process?
    (d) How many times can the copper powder be reused for the printing process?
2. What are the optimized post-process parameters?
    (a) What is the debinding temperature that burns out the binder?
    (b) What are the sintering temperature and time that sinter the samples?
    (c) Which atmosphere or atmospheres, to debind and sinter the samples in, achieves the highest density?
3. What is the effect of the above mentioned optimized process parameters on the functional properties?
    (a) What is the highest achieved density?
    (b) What is the shrinkage in the X-, Y- and Z-direction?
    (c) What is the highest achieved compressive strength?
    (d) What is the highest achieved electrical conductivity?
    (e) How do the achieved functional properties compare to conventional manufactured parts?

The parameters that will be outside the scope are the compression of the print bed for printing parameters and the gas flow and debinding time for the post-process parameters.
For this thesis the compression of the print bed is too time consuming to consider, as there needs to be something designed and tested to give the same compression to

the powder bed every time. The gas flow is put on the lowest setting for the lowest temperature difference inside the sintering furnace when sintering in argon. The debinding time was tested in TGA, with older measurements and the given time gave successful results Furthermore the focus is on the copper parts being fully sintered, the debinding is a small factor in this.

The limitations for this project are the fragmented knowledge. There are some researchers that have successfully printed and sintered high density copper with binder jetting. This is however very specific to the type of printer used, powder provider and debinding/sintering furnace. Temperatures, times and atmospheres that work for some researchers will not work for other researchers.
Furthermore time is a limitation. This is a thesis for a master degree which takes around 9 months of work. It is expected to finish with all the results, but there are possibilities that not all results will be perfect as there is no unlimited time.

1.3 Structure of Thesis

The thesis is made up of five parts. A literature review, the methodology, the results, the discussion and conclusion.
The literature review, in chapter 2, explains the background information about what binder jetting is and how copper can be printed with binder jetting. It explains the parameters, the necessary post-processing steps and what the difficulties are around the process.
The methodology, in chapter 3, explains the methods that are used to achieve the answers to the research questions. It explains why these methods are chosen and how it can help the process.
The results are presented in the chapter 4. It shows the answers to the research questions per step taken in the thesis according to the methodology.
In the discussion, chapter 5, the results are discussed to see what the best solutions are and the reasoning behind the different results that can happen.
The conclusion of the thesis is given in chapter 6, together with future recommendations and research gaps.

2 Literature Review

Binder jetting is an additive manufacturing process. According to the ASTM 52900 standards by thee International Organization for Standardization (ISO, 2021), there are seven different kinds of processes for additive manufacturing methods. These processes are: Material Extrusion (MEX), Directed Energy Deposition (DED), Powder Bed Fusion (PBF), Binder Jetting (BJT), Material Jetting (MJT), Vat Photo-Polymerization (VPP) and Sheet Lamination (SHL). These categories all have their related technologies like Fused Deposition Modelling (FDM), which is the 3D printer we probably all know about. These seven different types are not the only way to classify different AM processes. AM can also be classified by the type of base material that is used or the medium used for processing. In figure 1 these different ways are visualised. The techniques that fall under the solid based, powder based and liquid based materials can all also be classified under the seven processes. For example LOM is a sheet lamination technique.

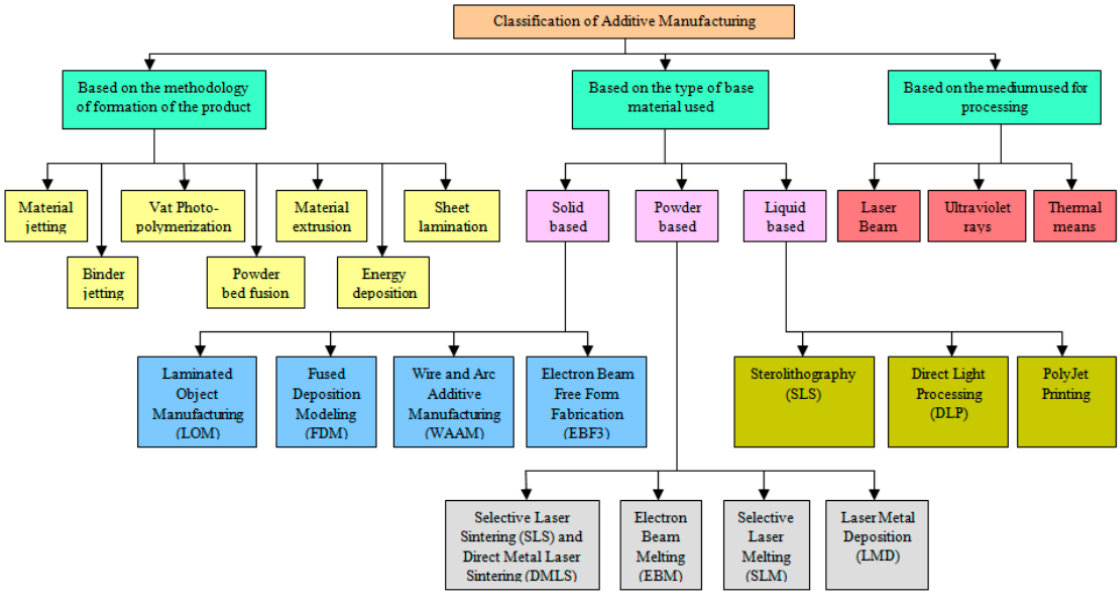

Figure 1: An overview different AM classifications [4]

Another way to divide the AM processes is by the type of feedstock/material. This can either be done by raw material input (feedstock): powder, liquid, wire or sheets or the type of material you want to print: metal, polymer, ceramics, etc. MJT and VPP are photo-polymer-based systems. BJT, DED and PBF are powder-based systems. MEX is a wire-based system, but DED can also print with wire. SHL uses

sheets of the desired material to create printed parts. In table 1 the seven different processes can be seen with the type of feedstock they use. It also shows the materials that can be printed with the processes and how the different processes consolidate the material. Some processes also use thermal cycles to further strengthen the material during the post-processing. The last column shows the different techniques/machines that fall under the process name. For example, techniques that fall under PBF are: Direct Metal Laser Sintering, Selective Laser Melting and Electron Beam Melting [1].

Furthermore it is also important to acknowledge that all processes have its benefits and drawbacks that can influence the type of process that needs to be chosen. The processes with the highest accuracy are VPP and PBF. The fastest process from CAD to finished printed part is MJT. Processes that can print multiple materials into one part are MJT, SHL, BJT, DED and MEX. But this is easier for some processes, like MJT and MEX than others. Processes that can print multiple colours are BJT, MJT, SHL and MEX. DED makes it possible to repair parts, but the process needs multiple post-processing steps [1].

Process	Feedstock	Material	Consolidation	Technique
PBF	Powder	Metals Polymers (Thermoplastics) Ceramics	Electron Beam Laser	DMLS SLM EBM
DED	Powder Wire	Metals Polymers (Thermoplastics) Ceramics Metal Matrix Composites	Electron Beam Laser Friction ARC	LENS WAAM
MJT	Liquid	Photo-polymer (Thermosets)	UV light	-
BJT	Powder	Polymers (Thermoplastics) Ceramics Metals	UV light*	-
VPP	Liquid	Photo-Polymers (Thermosets)	UV light	SLA
MEX	Wire	Polymers (Thermoplastics)	-	-
SHL	Sheet	Paper/Cardboard Polymers (Thermoplastics) Metals Ceramics	-	LOM

Table 1: Overview of AM processes and their materials [1]

*BJT can use UV light between each layer to consolidate the printed part, but this is not necessary as the part can be consolidated in an oven.

AM has a lot of capabilities: It can print multi-material parts, it can print assemblies, it can embed foreign components (for example stopping the print and inserting a foreign object into it) and it can print circuits, sensors and batteries [5]. There is a lot of freedom in the possibility of the design of the part. Almost anything can be printed in almost any kind of material and it is a relatively fast process, from 3D model to printed part.
But AM still has some big challenges. There is a lack of AM standards, making it difficult to use AM on a big scale. There is a need for qualification and certification of AM processes and parts [6]. Meaning that AM, for now, is a very good process for on-demand manufacturing of a very low production amount with a very specific design, like products for aerospace or biomedical industries [7].

2.1 The process

BJT was invented at MIT in the 20^{th} century. For each layer the process prints a binder into a powder bed to fabricate a part. It starts with a full powder feed tank and a build tank with some even layered powder. The powder feed tank ascends one layer level, while the build tank descends one layer level. The powder roller rolls the untouched powder from the powder feed tank onto the build tank. After which the printhead, above the build tank, deposits the binder into the powder on the specific design for the layer of the part. When the printhead prints the whole layer, which can be as thin as 10 µm, it moves away so the powder feed tank can ascend one level and the build tank can descends one. The powder roller rolls the new untouched powder onto the build thank and the process starts again, printing the new layer and so on, see figure 2. After all the layers are printed, the finished print, can be removed. Depending on the material, the print needs different post-processing steps [1].

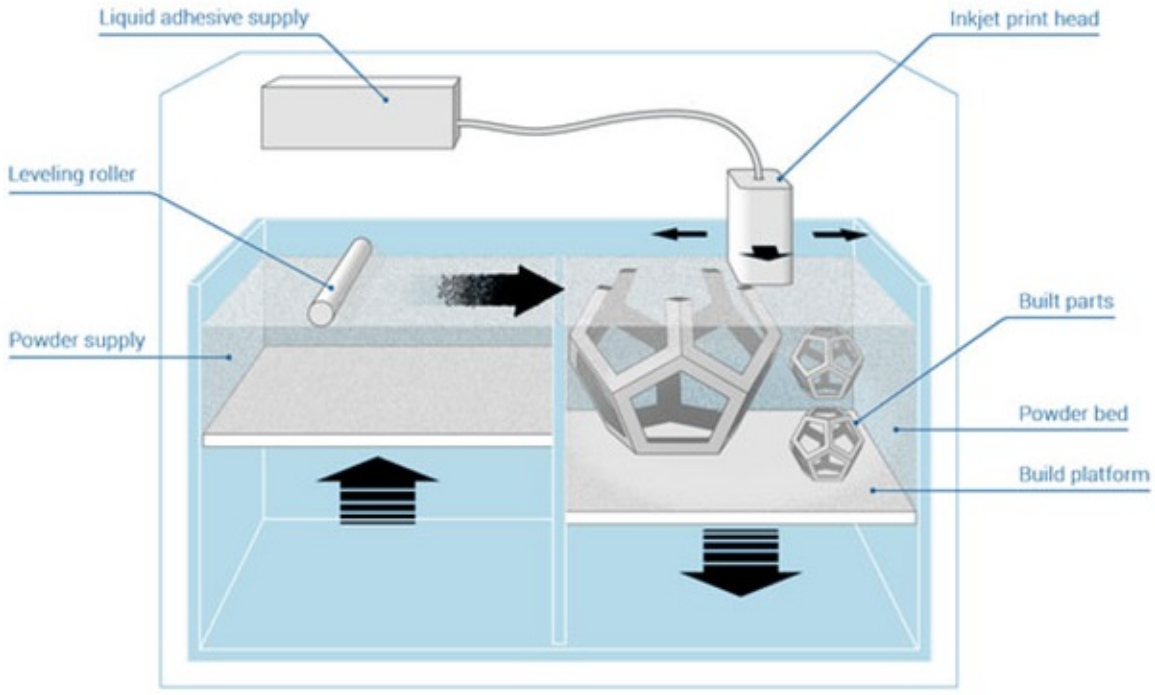

Figure 2: A schematic overview of binder jetting [8]

An advantage of BJT is the low energy process. Unlike other AM techniques that can print metals, BJT does not involve lasers and furthermore it is relatively fast and inexpensive [1]. The whole process is also scalable and does not need support structures due to the part being printed in a powder bed. The powder in the powder bed that was not printed can be reused for the next print [9].

A disadvantage of BJT is the low density of the printed part and the needed post-processing steps. Especially with the printing of metal parts. The printed parts do not only have a low density of around 50-60 %, they also need to be cured in an oven followed up by debinding and sintering in a furnace depending on the material. The printed parts possibly need other processes to improve the density up to 99 %, which is still proven to be difficult [9].

2.2 Printing copper

There are three pure copper additive manufacturing methods. Those are Selective Electron Beam Melting (SEBM), Selective Laser Melting (SLM), which are both a PBF process, and binder jetting [3].

The electron beam is the heat source of SEBM and goes over the part of the layer that needs to be printed. The electron beam locally melts the powder and thus forming a part. Once the electron beam has completed its path for the layer, the next layer of powder gets added on top of the already completed layer. The electron beams goes over its dedicated path for the new layer and the process repeats itself [3].
SLM is also a PBF process. Its process is the same as SEBM, but it uses a laser instead of an electron beam [3].
The density of BJT [10] and SLM [11] are measured with the Archimedes method, the density of SEBM is calculated with the ratio of the pores area versus the whole area [12].

Technique	BJT	SEBM	SLM
Costs equipment	Low	High	High
Energy process	Low	High	High
Process in vacuum	No	Yes	No
Post-processing needed	Yes	No	Yes
Affected by reflectivity copper	No	No	Yes
Limited to size	No	Yes	Yes
Supports needed	No	Yes	Yes
Average density	86.8 %	99.5 %	89.5 %

Table 2: Comparison of AM techniques to print copper [3]

Each technique has its advantages and disadvantages to print copper with, see table 2. A good reason to use BJT out of all AM techniques to print copper, is because BJT is a low energy process. It uses the binder to mend the parts together. The properties of copper are high thermal and electronic conductivity. Normally these properties are sought after, but they can create problems during the manufacturing process. For SLM it means that copper can reflect up to 98 % of the laser. This reflectivity can be reduced by lowering the wavelength of the laser. SEBM has low reflectivity and takes place in a high vacuum, which will minimize the oxidation. SEBM is just like SLM a high power process. But SLM and SEBM are still good AM techniques to print copper with, as they produce a higher density percentage than BJT. Furthermore it is dependent of the situation and budget, with BJT being relatively low and SLM and SEBM relatively high. All three techniques of printing are still in the development phase [3].

Table 3 shows the differences between the properties that can be achieved with binder jetting of sintered copper parts and conventional manufacturing of wrought copper

parts. The properties of the wrought copper in table 3 are the average values taken. The electrical resistivity of the wrought copper is conversed into electrical conductivity to match the other values of the binder jetted copper properties.
It can already be seen that the bimodal powder achieves the closest properties to the conventional manufactured copper. The bimodal powder is a mix of 5 and 30 μm, with a weight ratio of 27:73. The density of the binder jetted parts is measured with the Archimedes method [10].

	Binder jetted [10]			Wrought
Properties	25 μm	17 μm	Bimodal	[13]
Density	77.7 % ± 1.2	83.6 % ± 0.4	90.5 % ± 0.3	8.93 g/cc
UTS[1] (MPa)	82.0 ± 5.3	115.8 ± 9.2	144.9[a]	318
Elongation (%)	28.9 ± 1.6	48.5 ± 12.7	43.9[a]	26.6
Yield Modulus (MPa)	283.7 ± 24.2	238.8 ± 65.3	330.1[a]	-
TC[2] (W/mK)	245.7 ± 4.7	262.3 ± 8.2	293.5 ± 5.5	390
EC[3] (10^7 S/m)	3.0 ± 0.1	3.8 ± 0.4	4.7 ± 0.1	4.761

Table 3: Comparison of binder jetted copper properties to conventional manufactured copper properties

[1] UTS = Ultimate tensile strength
[2] TC = Thermal conductivity
[3] EC = Electrical conductivity
[a] Only one sample measured

2.3 Binder jetting parameters

There are different parameters that can influence the print during the printing process. These parameters can be divided by the raw material and the printing itself. The raw material parameters are: the powder (its shape and size) and the binder. The printing parameters are the saturation level, layer height [14], flow of the binder and how it is deposited, compactness feedstock and the printing speed. According to Shrestha and Manogharan [15] the saturation level and the feed-to-powder ratio are the critical parameters as they influence the densification the most.

Powder

The shape of the powder is important for the flowability of the powder. A good flowability guarantees a good print as the powder goes where it should be, it will not

stick to random places. The right amount of powder needs to be moved from the powder feed tank to the build tank. Spherical shapes have a better flowability than other shapes. Koseki, Suri, Earhardt and Kwon [16] found that a spherical shape shrinks less than irregular shapes.
The size of the powder is important for the properties that are wished to be achieved. Smaller particles can achieve better properties. But smaller particles also tend to agglomerate and/or aggregate, which reduces the flowability. The agglomerates occur due to van der Waals forces between the particles. The aggregates occur due to solid bridges between the particles [17]. Bigger particles are safer to operate with and the particles flow better [14]. But in table 3 it can be seen that bimodal powders can achieve better properties that are closer to conventional manufactured properties of said material.
Furthermore the powder size can influence the sintering process. A smaller particle is easier to sinter as bigger particles inhibit the densification as the driving force of the sintering is low [18].

Binder

The binder is dependent of the feedstock material, as not all binders can bind all the different feedstock materials. But not every feedstock material needs its own binder. For multiple different types of metals the same binder can be used. The same goes for organic materials. Different binders can also be used for the same feedstock material which can achieve a part with different properties [14]. Some binders will adhere nicely to the powder particles and fill in the holes between them, while other binders will only coat the powder particles, creating a weaker bonds between the particles [19]. Some binders will also leave a residue after the debinding step, while others are fully removed by pyrolysis.

Layer height

The layer height can control the resolution in the z-direction of the print. A smaller layer height will give a higher resolution, but the print will take longer. It will improve the surface finish by decreasing it [20]. A bigger layer height will print faster, but has a lower resolution. The layer height is also dependent of the powder size, as it usually needs to be three times the size of the particles [14].

Saturation level

The saturation level of the binder can impact the print significantly. Mostly the cured, printed part, also known as the green part, is impacted by this, as the binder is burned out after this stage. Too little binder will produce weak prints, making

them brittle. They can break during the depowdering process, as they are not strong enough to withstand a brush. A large amount of binder on the other hand can distort the green part. As there can be too much binder so it will bleed through to other layers or spread out. After curing and depowdering this will end in a distorted part [14]. This distortion can be enhanced by the sintering as was seen by earlier tests done by Concr3de in collaboration with the TU Delft.

Compactness feed-stock

To start a print, the powder is poured into the powder feed tank and it can be compressed. This makes room for more powder in the tank, affecting the properties of the printed parts. It increases the density, improves the surface quality and it creates a better dimensional control [20]. The size of the powder also has an impact on the compactness. As bigger particles are easier to compact than smaller particles [18].
During printing the powder can be compressed due to the feed-to-powder ratio. This is feed layer/layer thickness [15].

2.4 Post-Processing

After the part is printed it needs to undergo post-processing steps to give the green part the desired properties. Metallic prints need curing, debinding and sintering. This process can be seen in figure 3. It is important to see that sintering powder can leave small holes inside the sample, as the powder is not really compressed. These small holes are called pores.

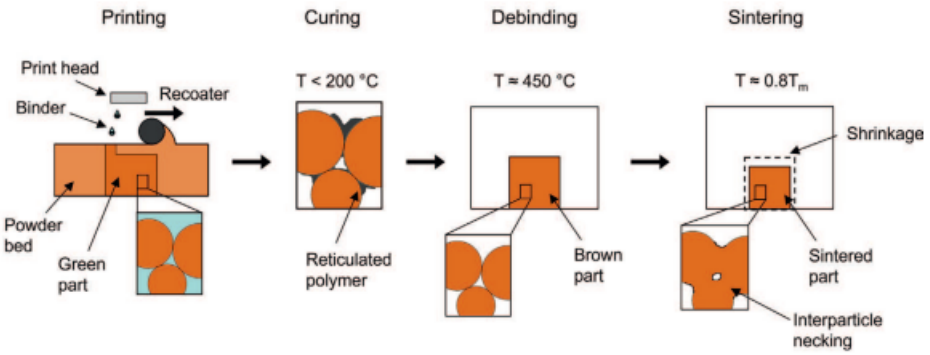

Figure 3: Post-processing steps of BJT copper parts [21]

During the sintering, the particles fuse together via neck growth, this is also called

necking, see figure 4. When the sample is fully sintered the sample has no more loose powder on the inside or outside [22].

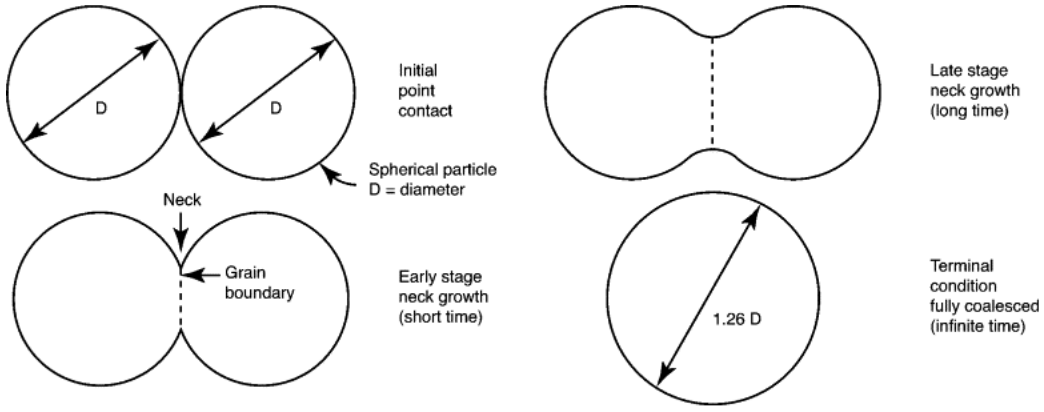

Figure 4: Partial melting process of sintering powder [22]

Curing

After the printer is done, the printed part sits on the building plate in the build tank, but it is still surrounded by loose powder. The building plate with the printed part and the loose powder need to be removed from the printer and put into the curing oven. This can be seen in figure 5. Almost all binders need some type of curing and the curing is dependent on the binder. The curing can initiate cross-linking for binders [23]. Usually curing temperatures do not go above 200 ℃, the temperature just needs to be high enough to strengthen the binder and not influence the powder. If the surrounding powder is removed before curing, it is possible the green part is too brittle and it will crumble beneath the touch of the brush. After correct use of the printing and curing parameters, the brush will not be able to destroy the printed part.

Depowdering

After curing, the part can be placed into a depowdering station. In the depowdering station the remaining powder can be removed, so all that is left behind, is the printed part. Removing the loose powder from the part can be done with soft or hard brushes depending on the used powder and binder. When the part is cured and depowdered it is called the green part. The process in figure 5 misses the debinding step, this is dependent of the printed material, but this can happen before or during the sintering process. The left-over powder in the depowdering station can be collected with a

clean vacuum. The retrieved powder can be sieved so only the powder untouched by the binder will be reused.

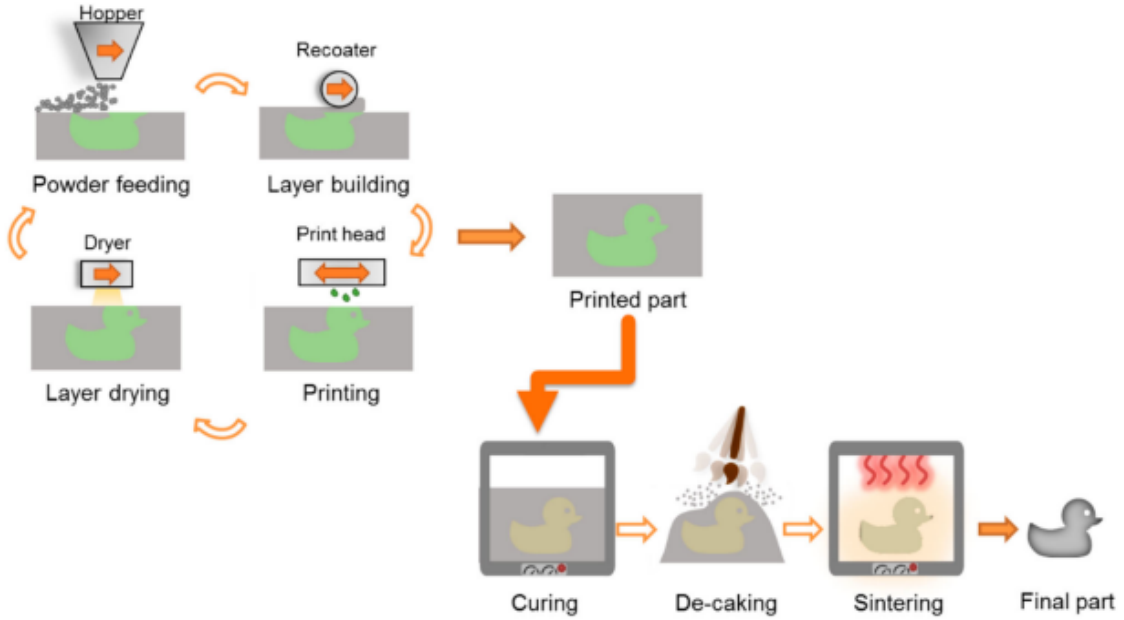

Figure 5: Printing process of BJT [24]

Debinding

For metal and ceramic parts debinding is an important step. Achieving a sample made of 100 % powder and not the binder is wanted. The debinding process removes the binder from the printed part, so the granules of the feedstock material all touch each other, see figure 3. The debinding is the first step into the densification process of the printed part. It can achieve higher material properties, consistency and accuracy. The debinding happens at temperatures around 400-600 ℃, but this also depends on the type of binder that is used. The binder is usually made of organic compounds and it will decompose at these higher temperatures. Holding the part at the debinding temperature can assure complete binder removal. But it is still possible that the binder will leave a small amount of residue in the printed part [23].

Sintering

Sintering strengthens and densifies the green parts. Sintering happens from 0.5 times the melting temperature to just under the melting temperature of the feedstock material. It melts the granules (partly) together so the printed part consists of one part

and not multiple small granules, see figure 3. The sintering transfers chemical bridges to mechanical bonding [23]. It increases multiple properties. For copper, sintering can bring the density up to 85 % [9] or even up to 99 % [25] with Hot Isostatic Pressing (HIP). In figure 6 an example of a sintering process of copper can be seen. In this process the copper is first held at 450 ℃ to burn out the binder. Followed by heating it to a higher temperature for the sintering. The graph has different temperatures and heating rates as it was tested to see which one gave the best outcome [26].

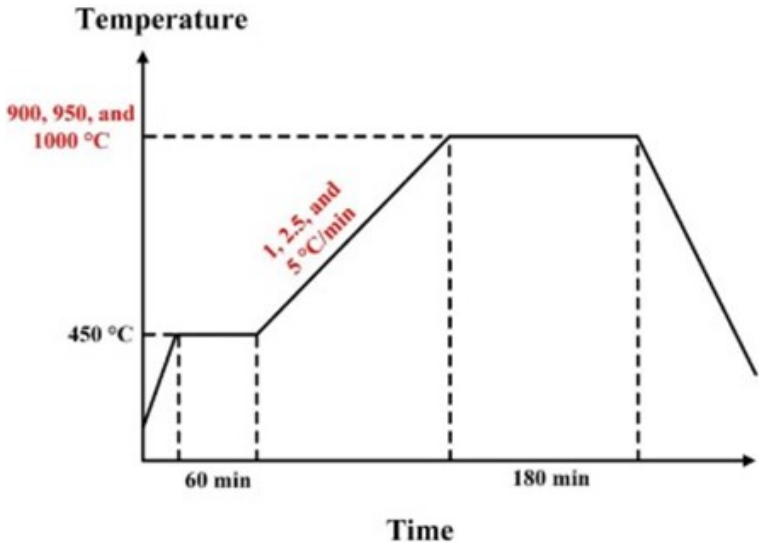

Figure 6: Sintering profile of copper [26]

Furthermore the sintering has many factors that can be adjusted. The material and granule size are important parameters for the sintering profile, as they determine the temperature, heating rate, sintering atmosphere and the holding time. When one of these factors is adjusted it can create a different outcome. The sintering atmosphere is important as it can influence the composition of the printed part. Oxygen or carbon can infiltrate the part for example and this is not wanted. Infiltrating carbon or oxygen can already happen during the debinding process as the temperatures are high enough to start possible chemical reactions. It is possible to combine the debinding and sintering into one step like it is done in 3. This is especially convenient when the part needs to be in an inert atmosphere during both debinding and sintering process.

Debinding but mostly sintering also has challenges. It causes shrinkage. The part has linear and volumetric shrinkage. Miyanaji, Rahman, Da and Williams [26] tested two different binders on copper and oversaw the differences. There was a difference in shrinkage, see table 4. The temperature, heating time and the heating rate can

also affect the shrinkage [27]. Another challenge is oxidation that can happen like said before, or a change in composition.

Type of binder	X (%)	Y (%)	Z (%)	Volumetric (%)
Solvent based binder	18.3	18.1	22.2	48.0
Aqueous based binder	17.3	17.1	22.5	46.8

Table 4: Comparison of shrinkage with different binders [26]

Surface treatments

Surface treatments are not wildly talked about in the printing process of binder jetting. The sintered parts can be grounded and polished to improve the surface roughness if that is necessary, depending on the function of the printed part. As can be seen in figure 7 that sintering can leave a surface roughness on the part that is easily removed with grounding [28].

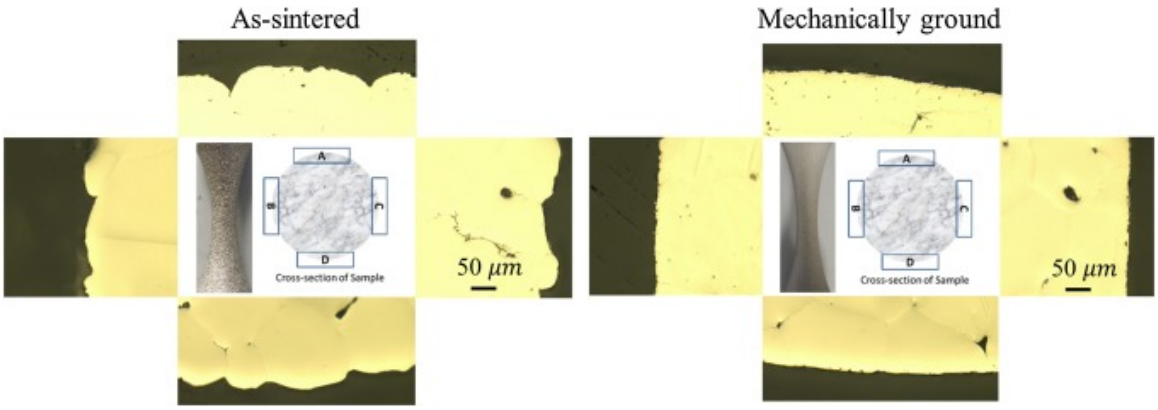

Figure 7: Surface of sintered and mechanically ground sample [28]

Lores et al. [24] showed that with the correct sintering profile the surface roughness could be as small as $R_a = 9$ μm, due to liquid phase sintering and large particle sizes were used (<150 μm). Lores, Azurmendi, Agote, Espinosa and García-Blanco [20] reached an initial surface roughness of $R_a = 5$ μm with sintering the part. The surface roughness was brought down further by 55 % with sand blasting and the surface roughness was overall reduced to 70 % with electropolishing, $R_a = 1.5$ μm. The surface does not have a homogeneous appearance yet. This is reached with HIP. HIP also decreases the final surface roughness to $R_a = 1$ μm, HIP is used before the blasting and polishing.

In figure 8 Mostafaei, Stevens, Ference, Schmidt and Chmielus [29] show the dimensional differences between the real denture frame work and the sintered binder jetted part. The binder jetted part shows slight differences in the range of ± 0.5 mm. In this case the binder jetted part was slightly thicker and polishing is used to reach the required dimensions. The part also had its surface roughness reduced by rubber polishing discs and an electric dental lab headpiece. Thus the surface treatments for a denture were necessary to achieve smooth and accurate finish. A reason for the polishing to increase the accuracy is the shrinkage that happens during the sintering. It is not perfectly predictable and differs in the Z and in the X-Y directions.

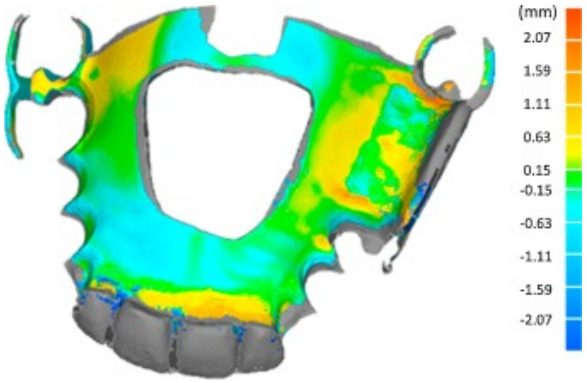

Figure 8: Dimensional differences between the real part and the BJT part [29]

2.5 Difficulties Binder Jetting

BJT for copper products has advantages and disadvantages. The advantages are almost no residual stresses, it is an inexpensive process, no need for supports [30] and non-used powder can be re-used. The disadvantages are low density and low mechanical properties. Furthermore there are also other difficulties: The binder can bleed too much into the powder bed of the build tank, ruining the print. But also attaining complete density and high purity of printed copper parts is difficult.

Bleeding binder

A bleeding binder during the printing of copper is a problem that occurs at the company, Concr3de, this literature review is done at. Concr3de requested a solution for this, as the binder bleeds into the other layers. After sintering this phenomenon is seen the best, as the samples come out distorted. Due to the viscosity of the binder that is used for copper, it is possible for the binder to bleed into other layers. This is also dependent of the size of the powder and the flowability. The binder that is used for copper, also called the m-binder, has a too low viscosity in combination with

the copper powder. The m-binder bleeds less with stainless steel printing. The low viscosity causes the binder to partly bleed into the layers below. This can adjust the geometry of the part as there is binder in places where it is not supposed to be.
A possible solution is to change the saturation level of the binder. But this is easier done with some machines than others. Furthermore it is possible that lowering the saturation level, to prevent bleeding, can make the print too brittle. As there is too little binder used to make a strong print.
Another possible solution is to add additives to the binder. The additive needs to change the viscosity, stopping the bleeding of the binder. But the additive will change the binder overall and can influence the part and its curing. Possibly making it brittle and ruining the print. Furthermore the binder still needs to be fully removed during the debinding process, which is not guaranteed with additives in the binder.
It is also possible to change the size of the powder to see which sizes or distribution makes the bleeding less. As the size can affect the flowability of the powder and maybe affect the bleeding issue.
Shell printing can also be a possibility to prevent bleeding. Shell printing is a form of printing used in BJT. Instead of depositing the binder each layer over the whole cross-section, only the outsides are deposited with binder. This leaves the core of the cube untouched by binder, see figure 9 for the differences. After printing the part will undergo the same post-processing steps: curing, debinding and sintering. The loose powder inside the cube will be sintered the same as the other powder that is touched by binder. Giving the same result as a normal print, only using less binder [31]. As less binder is used it is a possibility that the bleeding will be less. But it is also a possibility the print will distort more after sintering, as the outsides will bleed more than underneath the core. Another disadvantage is that it is not clear how the shape of the sample will be affected by shell printing.
Curing in between the layers with an IR lamp is another solution. This will dry out the binder almost directly after it is deposited on the layer. Creating a very small window for the binder to bleed into the lower layers.

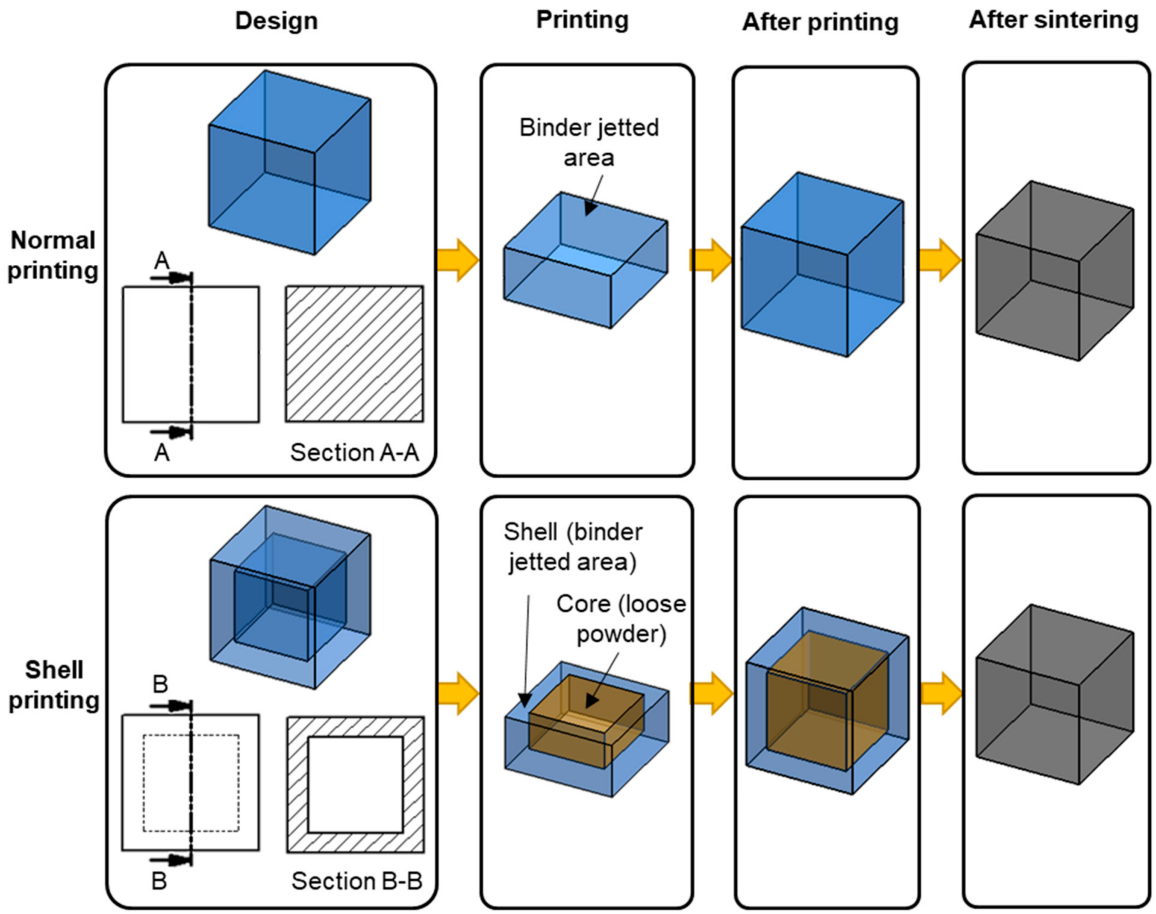

Figure 9: Normal printing versus shell printing [31]

Improving density and porosity

As was said in chapter 4 it is possible to bring the density up with sintering the copper parts. However this is still not very high. It is possible to bring this percentage up with Hot Isostatic Pressing (HIP). This technique uses high pressure to force the entrapped pores to overcome the surface energy driving force for the closure of pores. The pores dissolve and diffuse to the surface. Furthermore using HIP retains the shape of the part due to the isostatic pressure that acts perpendicular to the surface. HIP needs to happen after sintering, as the pores can only be effectively removed if the surface is devoid of pores. But BJT fabricated parts usually have surface connected porosity, even after sintering. Thus using HIP is still not widely documented for BJT [9]. Figure 10 shows the control variables for the BJT printing process, the sintering profile and the HIP variables that can be used.

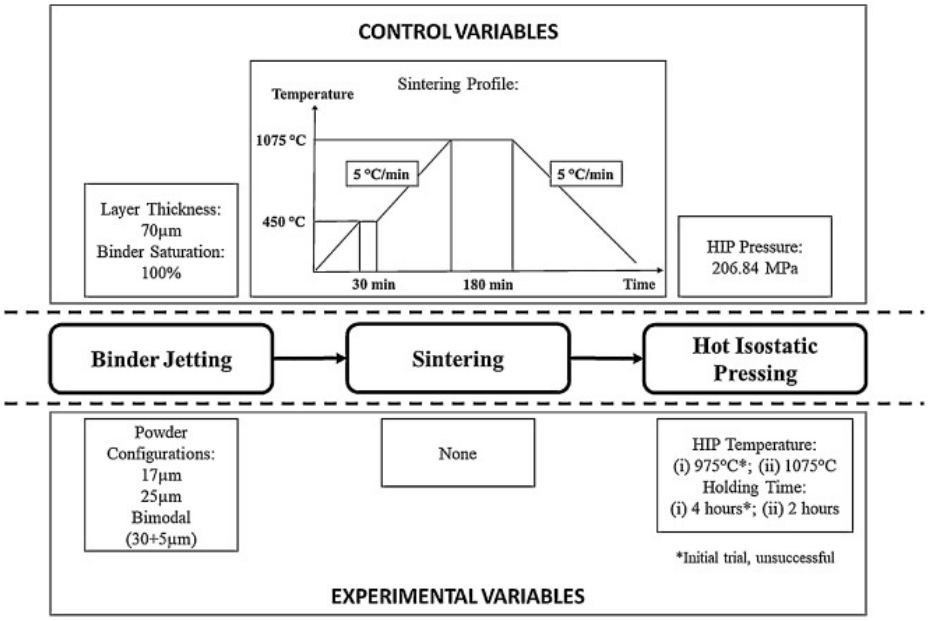

Figure 10: Sintering and HIP of copper [9]

It can be seen in table 5 how the density goes up after sintering and after HIP. Sintering already improves the density a lot. But HIP makes the density almost 100 % for all three samples, increasing it by 45 %.

Part Type	Green Density (%)	Sintered Density (%)	HIP Density (%)
A	55.13	93.46	99.24
B	54.97	93.89	99.78
C	54.88	94.34	99.38

Table 5: Improvement of density after sintering and HIP [25]

Increasing the density percentage for BJT parts goes hand in hand with decreasing the porosity. Table 6 shows the comparison of the average porosity of sintered parts and HIP parts. The sintered parts already have a relatively low porosity but HIP brings the porosity for all three samples down to around 0.1 %.

Part Type	Sintered Sample Porosity (%)	HIP Sample Porosity (%)
A	0.26	0.10
B	0.26	0.09
C	1.29	0.10

Table 6: Improvement of the decreasing porosity after sintering and HIP [25]

This shows that HIP is an excellent method to decrease the porosity and increase the density to almost 10 % of BJT manufactured parts. Although the properties were not tested after HIP. So it is yet unknown what the effects are on the part [25].

Oxidation

Copper goes through the process of thermal oxidation. At room temperature a superficial layer of oxide forms on the copper surface. This oxide layer prevents further oxidation of the copper because it limits the oxygen diffusion. The thermal energy, starting from 150 ℃, is enough to overcome the oxide layer. This means that oxidation of copper is already possible during the curing stage. Starting the oxidation of copper with cuprite Cu_2O, see reaction 1 [30].

$$2\,\mathrm{Cu} + \frac{1}{2}\,\mathrm{O_2} \longrightarrow \mathrm{Cu_2O} \tag{1}$$

$$2\,\mathrm{Cu_2O} + \mathrm{O_2} \longrightarrow 4\,\mathrm{CuO} \tag{2}$$

After 320 ℃, the Gibb's free energy is negative, making it possible to form tenorite CuO, next to the cuprite. If the metal is held long enough at a temperature above 320 ℃, all the cuprite will transform into tenorite, see reaction 2 [30]. The process of the oxide growth is displayed in figure 11.

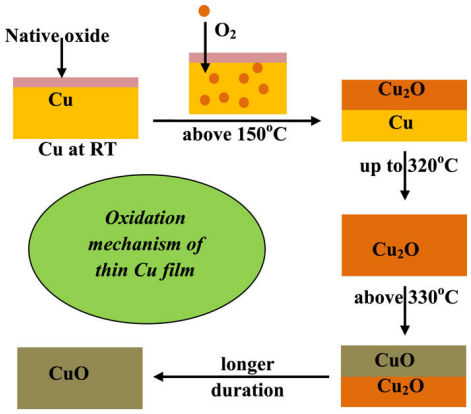

Figure 11: Oxide growth of copper [32]

A solution for the oxidation process is to do the debinding and sintering in an inert or vacuum environment. These environments can be hydrogen, argon, nitrogen or a combination of these gasses. They also each have advantages and disadvantages. Vacuum can help in elimination of pores during the sintering. As the vacuum helps

forcing the pores out of the sample. Nitrogen is cheaper than argon and hydrogen, but metals can be sensitive to nitrogen. If that is the case argon or hydrogen is chosen. But hydrogen is dangerous to work with as it can be explosive.
It is also possible to deoxidize the copper. It is seen during annealing reaction 3 can happen. Once CO is formed, reaction 4 can happen and with further heating the cuprite together with carbon can become copper and carbon dioxide, see reaction 5. Carbon is needed for these three reactions and thanks to the pyrolysis it is present. The binder will probably leave a small amount of carbon on the sample, making the reduction of copper oxides possible [33].

$$2\,CuO + C \longrightarrow Cu_2O + CO \tag{3}$$

$$2\,CuO + CO \longrightarrow Cu_2O + CO_2 \tag{4}$$

$$2\,Cu_2O + C \longrightarrow 4\,Cu + CO_2 \tag{5}$$

Shrinkage and distortion

The sintering causes shrinkage. The shrinkage happens in all the directions, x, y and z. The shrinkage in the x- and y-direction usually is similar. The shrinkage in the z-direction can be higher due to the gravity, but also the packing density between layers [34].
The biggest contributing factor to the shrinkage is the thermal gradient. Lowering the thermal gradient can make the shrinking more predictable [34].
In table 7 the difference can be seen between the shrinkage after sintering and the shrinkage after HIP [25].

	Shrinkage after Sintering (%)		Total Shrinkage after HIP (%)	
Part Type	X/Y	Z	X/Y	Z
A	14.35	16.91	15.52	18.77
B	14.14	18.57	15.56	19.30
C	14.25	16.91	16.16	19.70

Table 7: Comparison of shrinkage after sintering and HIP [25]

It can be seen that HIP causes more shrinkage, and just like after sintering the shrinkage along the z-direction is higher than the x- and y-direction. This causes the part to be anisotropic as the porosity between the layers is higher than within the layer.
One solution is to use theoretical modeling to predict the shrinkage of the part. Making it possible to design the part and achieving the correct measurements after

sintering [34].
Another possible solution is adding metal nanoparticles to the binder. But this has to be handled carefully as the nanoparticles can destroy the printer from the inside out. The printhead is very sensitive and expansive and when there are nanoparticles inside the binder it could clog the system. Bai and Williams [35] use a Metal-Organic-Decomposition (MOD) ink, which is particle free. But when the ink is heated it will precipitate metal nanoparticles. In this case there is no issue for the printhead as there are no particles in the ink that can possibly clog the system. In this case the MOD ink did generate a more dense core section, but the outer shell was more porous in comparison to a conventional polymer binder.

Sintering temperature and environment

Metals can react either sinter rather easy or very difficult. When they sinter easy, a temperature between half the melting temperature and the melting temperature works easily. When it is difficult to sinter the material, it is rather hard to find the correct temperature that fully sinters the samples. This is the case for the copper samples that were printed by Concr3de with their binder jet printer. The debinding temp is also not easy to find, you want all binder to be burned away without leaving residue. The wrong temperature can leave carbon on the sample, the same goes for the time. A good way to research the whole process, which is different for different binders and metal printed and size, are with TGA and DSC.
A Differential Scanning Calorimetry (DSC) can also be used next to the TGA. DSC measures the heat capacity over the time the temperature changes. The changes in the heat flow can be tracked and be measured as changes in the heat capacity. With DSC the thermal transitions are well seen.
With a ThermoGravimetric Analysis (TGA) the mass is recorded during the debinding and sintering process. When the heat treatment is done, it delivers a graph where the mass change is seen over the time the temperature changes. This make it clear to see when the binder is burned out and when the sample is fully sintered, as the mass decreases during these two steps. It is also possible to spot some type of oxidation, as the mass will increase due to the forming of tenorite and/or cuprite. But the oxidation of copper is dependent of the atmosphere. With TGA the weight changes are well seen.
The two techniques together give a well overview of which temperatures to choose for the heating profile. But the environment still needs to be chosen.

Researcher	Curing		Debinding		Sintering		Atm	Achieved density
	Temp [℃]	Time [h]	Temp [℃]	Time [h]	Temp [℃]	Time [h]		
Pisani [30]	180 180 180	2 4 6	470	4	900 900 1100	1 3 1/30	V V V	53 %
Kumar [25]	200	?	450	0.5	1075	3	RAtm	94 %
Bai [36]	190	2	450	0.5	1080 1080 1090	2 4 4	H/Ar H/Ar Air/V	85 %
Miyanaji [26]	?	?	450	1	900 950 1000	3 3 3	H H H	91 %
Choong [37]	200	2	350 800	1/12 3	1070	6	V/Ar	63 %

Table 8: Heating schedules of different researchers
(Atm = Atmosphere, RAtm = Reduced Atmosphere, H = Hydrogen, Ar = Argon, V = Vacuum)

Used sintering profiles

There are five articles on printing copper with BJT that made their sintering profiles known. Table 8 shows the different curing, debinding and sintering temperatures and times. The achieved sintered density can also be seen.
Some researchers tried different temperatures and hold times for the sintering. How some of these different profiles look can be seen in figure 12a to 12d. The cooling and heating rates are around 5 ℃ per minute and the holding times depend on the sintering temperature. Temperatures very close to the melting temperature of copper (1083 ℃) have a very short hold time while temperatures of 900 to 1000 ℃ have longer hold times from two hours up to six. The atmospheres are also different, some are in vacuum, some in hydrogen and some in argon with the combination of another gas.

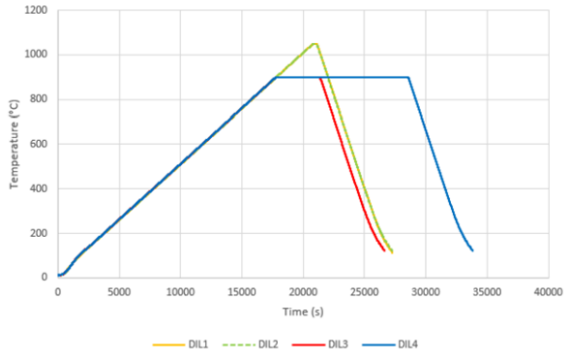

(a) Heating schedule Pisani [30]

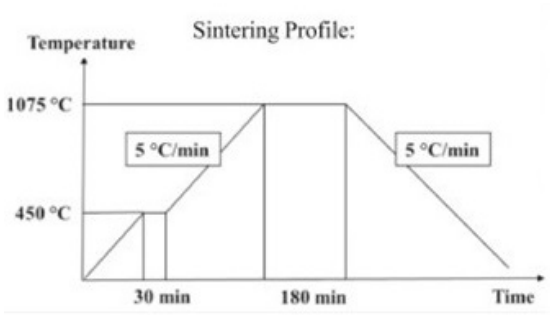

(b) Heating schedule Kumar [25]

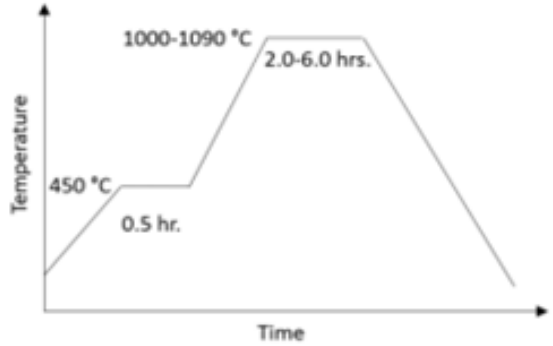

(c) Heating schedule Bai in Air/vacuum [36]

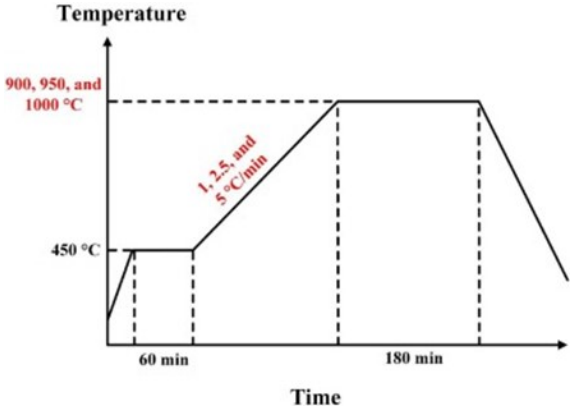

(d) Heating schedule Miyanaji [26]

Figure 12: Heating schedules and its rates

3 Methodology

The methodology of this thesis is explained in the following sections. Figure 13 shows the flow chart of all the actions that were done in chronological order. The different shapes have different meanings. The diamond shapes are products. The blocs are actions that are done and the ovals are data of knowledge that are used to give feedback on the actions.

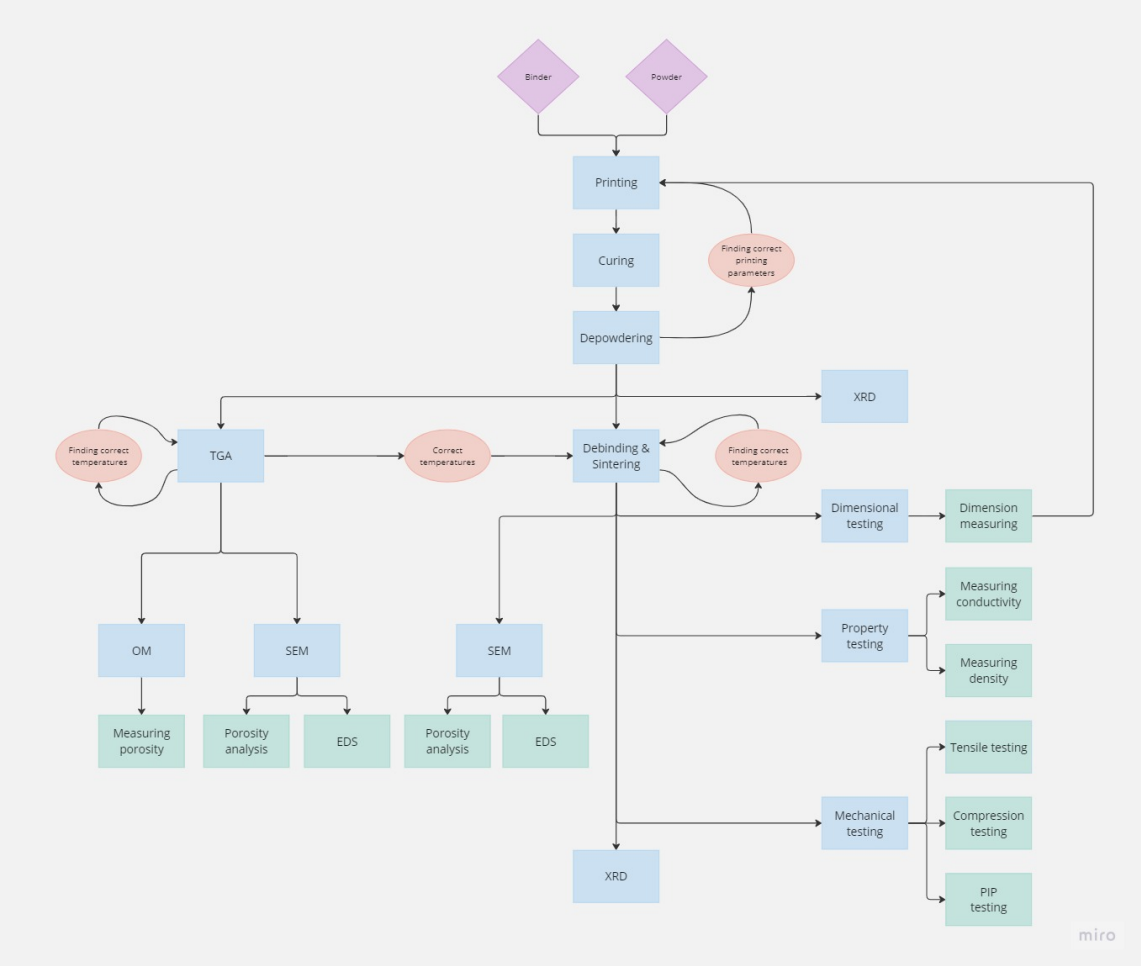

Figure 13: Flow chart of the thesis for binder jetting of copper

3.1 Printing and Curing

Printing the samples is the first important step. The printing parameters influence the accuracy and the strength of the samples. The essential chosen print parameters

are: the layer height and the saturation level.
The layer height determines the accuracy, the smaller the layer height, the more accurate the print will be, but it will take longer to be printed.
The saturation level is determined by the waveform of the chosen binder for the case of the Concr3de Armadillo and the X-speed of the printhead. This is different from other binder jet printers, like the ExOne, where the saturation level is measured in percentage.
The waveform is specially designed for every binder that is made and used by Concr3de. It is designed and measured in the dropwatcher, a machine that analyses the droplets that will be deposited by the printhead depending on the waveform. It can measure the amount of pL of binder and how it behaves under different X-speeds. The amount of pL can be converted into a percentage of saturation level. This conversion is done by formula 6 to 9. The R is the resolution of the printer and PR is the packing bed density. The formula was used for earlier research at the company.

$$\text{Saturation level} = \frac{\text{V}_{droplet}}{\text{V}_{air}} \tag{6}$$

$$\text{V}_{air} = (1\text{-PR}) \times \text{V}_{voxel} \tag{7}$$

$$\text{V}_{voxel} = \frac{\text{layer height}}{\text{R}^2} \tag{8}$$

$$\text{PR} = \frac{\text{powder bed density}}{\text{powder material solid density}} \tag{9}$$

The print parameters and the chosen values can be seen in table 9. It is important to acknowledge that not all the parameters are tried together. The different parameters are tried together until dimensional accurate shapes with no bleeding issues are the outcome. The different waveforms tried are 1 pulse (1P), 2 pulse (2P) and 3 pulse (3).

Print parameter	Chosen values
Layer height	50 micron and 100 micron
Waveform	1P, 2P and 3P
X-speed	20 %, 30 % and 60 %
Z-axis offset	0 and 1

Table 9: Parameters and chosen values for printing

$$\text{V}_{voxel} = \frac{\text{layer height}}{\frac{400}{0.254}^2} \tag{10}$$

$$\mathrm{PR} = \frac{156.48/30}{8.93} = \frac{5.22}{8.93} = 0.5841 \tag{11}$$

X-Speed	Two Pulse (2P) [pL]	Three Pulse (3P) [pL]
10%	78-85	85-105
20%	85-105	115-125
30%	115-125	130-140
40%	120-130	140
50%	125-145	-
60%	130-140	-

Table 10: Waveform M-Binder

The resolution of the printer is 400 DPI, the value needs to be converted to the metric system before it can be used in formula 10. The packing rate density is calculated by weighing 30 ml of copper powder, together with the density of wrought copper the packing rate density can be calculated in formula 11. It is important to note that the powder was little compressed during the packing bed density measurement. During the printing it is compressed more at the start and during the printing itself due to the roller and the possible z-axis offset. This difference in compression can give a difference in the true saturation level, as the calculated saturation level can go up to 2-3 % for saturation levels under the 100 %, above 100 % the percentage can go up to 7 %.
Table 10 shows the different values for the droplet size when the x-speed is adjusted for the two different waveforms. The saturation level of the 1P waveform was not calculated as it was not measured in the dropwatcher. The 1P waveform is only tested in the first print session. When compared, the saturation level of the 1P waveform with a 60 % X-speed is likely lower than 70 %.
Table 11 shows the calculated saturation level values for the different waveforms, X-speeds and layer heights. The droplet size is the average value taken for the corresponding X-speed. The 3P 60% value is extrapolated as the dropwatcher could not give the corresponding droplet size.

Waveform	X-speed [%]	Droplet volume [pL]	Layer height [μm]	Calculated saturation level [%]
2P	40	125	100	75
2P	60	135	100	80
3P	20	120	100	72
3P	30	135	100	80
3P	60	175	100	104
3P	60	175	50	209

Table 11: Calculated saturation levels

The fixed print parameters are: the binder, the size and shape of the powder particles, the spreading speed and the compression of the powder in the feed box.
The powder is copper powder, provided by the company Ampere Alloys. It is 99.95 % copper with spherical grain sizes of 5-25 μm. Making it a bimodal powder. The by the company guaranteed chemical composition can be seen in table 12 and the particle size distribution can be seen in table 13.

	Cu	O
wt%	> 99.9	< 0.03

Table 12: Guaranteed chemical composition of copper powder by supplier

	D10	D50	D90
Particle size [μm]	8.95	18.16	28.28

Table 13: Particle size distribution of copper powder

The binder used for the binder jetting of metals by Concr3de, is called the M-binder (metal-binder). The M-binder, and all the other binders used by Concr3de, are designed and tested by the company. The M-binder is compatible with the copper powder, but also with stainless steel.
The spreading speed is the speed of the powder that gets spread from the feed box to the print box by the spreader. This speed is set to 20 %.
The compression of the feed box can influence the porosity of the green and later sintered parts. The compactness can be adjusted by using a different force to compress the powder into the feed box. Due to the difficulty in applying different forces onto the feed box, the compactness is not taken as a print parameter. It is important to know that the force used, is done by hand. Thus the force can vary for every print.

It is tried to use the same force every time for a print, making it a parameter that is not used to see the influence of it on the prints.

The STL-files are printed layer by layer in the print box, with in between each powder layer, a layer of binder to temporary hold the sample together. When printing is done the samples are still embedded in loose powder in the print box. The content of the print box, the loose powder and the samples need to be transferred into the curing oven. The curing increases the strength of the binder. Making it possible to remove the samples from the powder bed, and depowder them without breaking. The curing temperature is dependent of the type of binder used. The temperature and time are fixed parameters.

3.2 TGA

ThermoGravimetric Analysis (TGA), is used to determine the correct temperatures, times and atmospheres for the debinding and sintering. The TGA can go through a debinding and sintering cycle while it measures the weight of the sample. The weight is displayed over time and temperature, making it possible to see when the sample gains or loses weight. In the case of copper binder jetting, the sample can gain weight due to oxidation, the forming of tenorite and/or cuprite, and it can loose weight by shrinking, where the porosity will decrease.

Figure 14: TGA machinery made by Setaram [38]

The type of TGA machinery used, is the Themys Duo made by Setaram. The TGA is shown in figure 14. The thermocouple inside of the TGA needs to be protected when hydrogen was used inside the chamber at temperatures above 1000 ℃. This is done by wrapping the thermocouple in protective material. Although this protects the thermocouple, it will also give an incorrect temperature that is measured inside the TGA. The temperature inside the TGA will be a few degrees above the temperature measured by the thermocouple. This needs to be taken into consideration when using other furnaces, as the input values, like the temperature, will be different. Possibly giving different results.

The samples prepared for TGA are small as they need to fit inside the alumina crucible. The crucible is shown in figure 15.

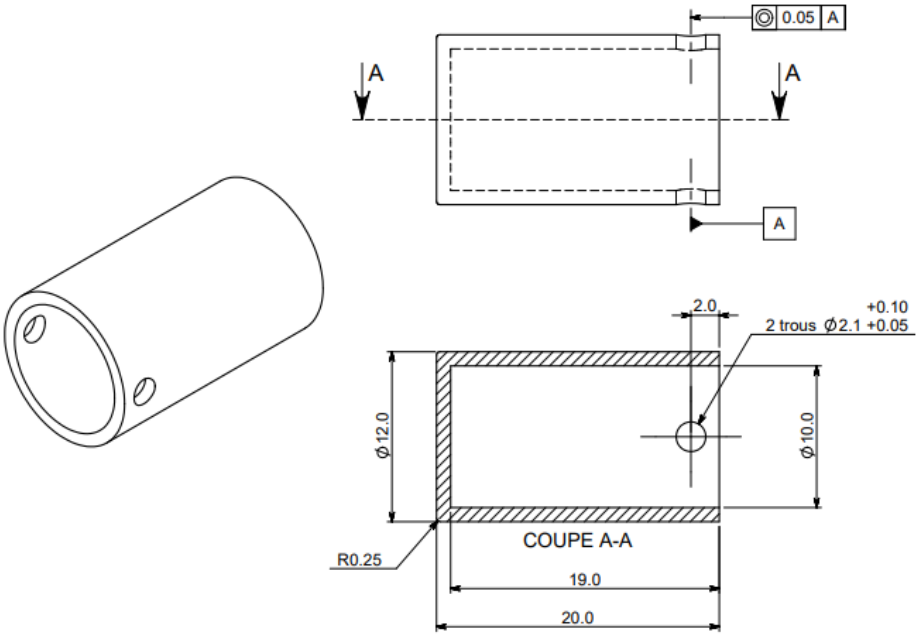

Figure 15: Dimensions of the alumina crucible inside the TGA

3.3 Debinding and Sintering

The debinding and sintering are necessary steps for producing metal samples with binder jetting. The debinding ensures a high purity by the burning the binder out via pyrolysis. The sintering melts the particles together. The debinding and sintering can happen in the same furnace as usually the same atmosphere is used for both processes and the sintering can happen right after the debinding.

The type of debinding and sintering furnace used, is the LHTG 200-300/22-1G made by Carbolite Gero 30-3000 ℃. The whole equipment of the furnace and the furnace itself can be seen in figure 16a and 16b. This type can go up to 2200 ℃, with a maximum heat rate of 10 K/min. The flow of nitrogen or argon can be adjusted from 50 up to 500 l/h and the usable space inside the furnace is 10 liter [39].

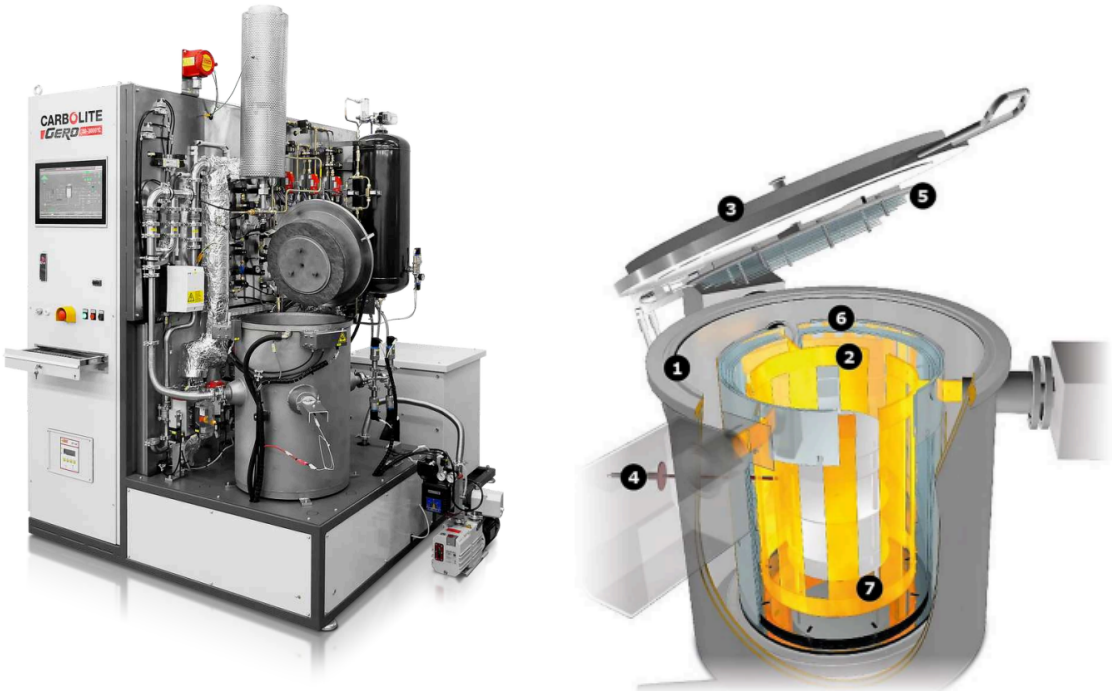

(a) The sintering furnace [39] (b) Inside of the furnace [39]

Figure 16: Used sintering equipment

The numbers on figure 16b equal to the following parts:

1. Water cooled vessel
2. Heating elements
3. Top cover (manually operated)
4. Thermocouple
5. Radiation shields at the top
6. Radiation shields at the mantle
7. Short circuit ring

The radiation shields are made of graphite. The samples are placed on a graphite tray that is placed inside the graphite bucket. One thing missing in figure 16b, is the pyrometer. The type of furnace used, measures the temperature with a combination of a pyrometer and a thermocouple. The pyrometer can only measure the temperature

from a certain temperature, below that it is measured with a thermocouple that can slide into the furnace. For temperatures up to 3000 ℃ the thermocouple is again outside of the furnace as only the pyrometer can measure up to these temperatures.

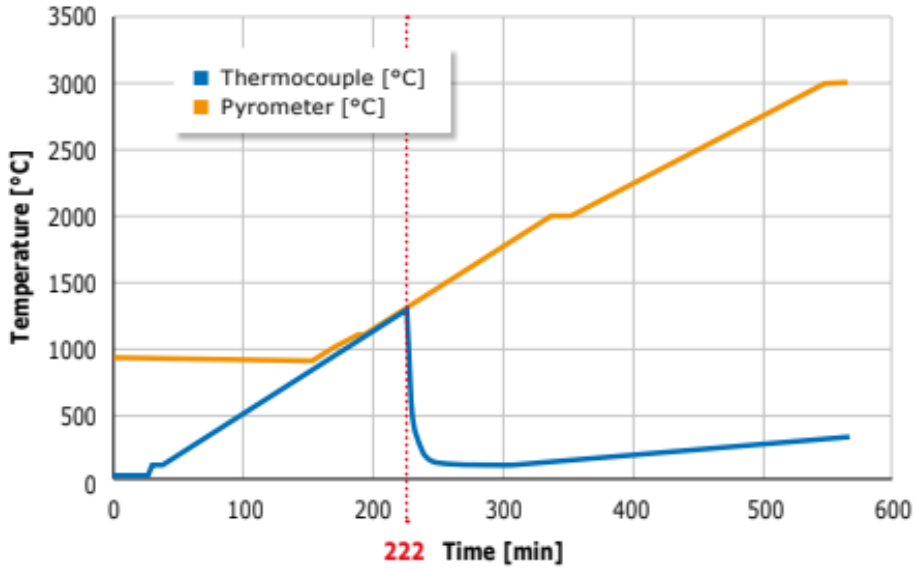

Figure 17: Temperature graph with pyrometer and thermocouple [40]

Figure 17 shows how the temperature is measured with the thermocouple and the pyrometer. The pyrometer can start measuring the temperature just below 1000 ℃. In this case the thermocouple is pulled out of the furnace after 222 minutes which equals a temperature of around 1300 ℃.

It is important to look at the placement of the thermocouple, as it is placed outside of the radiation shield. When a gas is used to sinter the samples, it will flow from outside the radiation shields to the inside of the radiation shields, via the top of the bucket. Meaning that, when there is a gas flow, the temperature next to the thermocouple (outside of the bucket), is different to the temperature right next to the samples (inside the bucket). The gas flow can influence the temperature due to the new gas not being preheated as it enters the bucket. Thus a higher gas flow will create a bigger temperature difference between the thermocouple and the samples.

The post-process parameters are the debinding temperature, sintering temperature, sintering time and sintering atmosphere. The debinding temperature is rather quickly determined with the TGA, the sintering temperature will be adjusted until the samples are fully sintered. When necessary the sintering time will be adjusted

as well. The change in sintering atmosphere will happen when the correct sintering temperature and time are found in argon. Then the correct sintering temperature and time will be tested in vacuum.

3.4 XRD

Although the atmosphere is specifically chosen to prevent oxidation, it is preferred to ensure it. X-Ray Diffraction, XRD, measures the diffraction peaks of the different crystalline phases [41]. In this case XRD can be used to see if there are any copper oxides in the green and sintered samples or if they are still pure copper.

The XRD machine used, is of the Bruker D8 Advance diffractometer Bragg-Brentano geometry and LynxEye-XET position sensitive detector. It uses Cu Kα radiation. With Soller slits 2.5 deg in diffracted beam and divergence slit V10mm, scatter screen, 45 kV 40 mA. There was no sample spinning and the detector was in High Resolution setting. The measurements are coupled TwoTheta/Theta scan, with a step size of 0.033 $^\circ$ 2θ and a counting time per step of 1s.
The software used to analyse the data is the Bruker software DiffracSuite.EVA vs 6.1.

3.5 Dimensional accuracy

Due to the porosity in binder jetting, the parts will undergo significant shrinkage during the debinding and sintering. To print the pieces and have them end up with the correct measurements can be difficult. With testing the dimensional accuracy the samples can be upscaled so they shrink the perfect amount. The dimensional accuracy can be measured in different ways. In this case a laser scanner and a caliper are used to compare the results. The samples are measured as green parts and as sintered parts. The laser scanner is an Artec Space Spider Scanner, see figure 18. It creates a 3D model which can be converted into a STL file or a Solidworks (sldprt) file for example.

Figure 18: Artec Space Spider Scanner

The part is placed on a stool which can be turned 360 degrees. This way the handheld laser scanner can be held still while the part is turned. The best results are when a sample is scanned in three rounds, one with the sample with the bottom on the ground, one with the top on the ground and another one with a different orientation. The laser scanner sends the three different scans to the computer where they can be fused together. The fusion is done by selecting the points on the different scans that should be the same point in the fused sample. When the area of the sample is either too reflective, too dark or all the sides are the same (like with a blank cube), a texture spray can be used on the sample. If the sample is too reflective or too dark, the spray will cover it with a white kind of paint. And when a cube for example, does not have distinctive sides, the spray can be sprayed on some of the planes to help recognize the points in the different 3D scans. The specifications of the laser scanner can be seen in table 14. The smallest cured samples are around the 10 mm in each direction. These samples will shrink a small amount, but should not shrink more than 50 %, thus being theoretically big enough to scan with the laser scanner.

3D accuracy	0.05 mm
3D resolution	0.1 mm
Starting size	From 5 mm
Data processing algorithms	Geometry and texture
Output formats: 3D mesh	OBJ, PLY, WRL, STL, AOP, ASC, PTX, E57, XYZRGB
Output formats: CAD	STEP, IGES, X_T
Output formats: Measurements	CSV, DXF, XML

Table 14: Specifications Artec Space Spider 3D Scanner [42]

The dimensional accuracy can also be measured with a caliper. The caliper has a res-

olution of 0.01 mm and can measure the smallest samples without giving errors. But the placement of the caliper is important as it can easily influence the results, even though these differences will be very small. The cubes can be easily measured with a caliper, unlike the dog-bones. Most measurements can be taken for the dog-bones, but the curvature can not be measured with a caliper.
It is possible to measure the total volume of the samples with the Archimedes principle. But only the volumetric shrinkage can be calculated and not the directional shrinkage.

3.6 Testing of functional properties

Density

The density can be measured in different ways. The following two methods are used to compare the results to each other, as they both have inaccuracies. The first method is measuring the density with the Archimedes principle. The second method is measuring the density with a caliper and a scale.
The volume can be measured with the Archimedes principle following the standard ISO 2738 Sintered metal materials, excluding hardmetals — Permeable sintered metal materials — Determination of density, oil content and open porosity. The density can be calculated by dividing the found volume by the weight. The volume cannot be measured with the original Archimedes principle as the samples are porous, which would give a false volume that comes out higher than it should be. The samples need to be impregnated with oil, but this still could give a wrong density. Hollow cubes are measured with Archimedes without the oil impregnation. Three hollow cubes of each sinter session are used and compared to their density calculation made by the caliper. The hollow cubes were chosen as they have a smoother surface compared to the solid cubes. The solid cubes have x, y and n engraved in the surface which leads to significantly more air bubbles which need to be removed.
The second method is to weigh the sample and measure the x, y and z dimensions with a caliper. To make up for the small dimensional differences in the cubes, three measurements are taken for each dimension. Figure 19 shows the three lines on each plane the caliper was placed.

Figure 19: Caliper placement on cube

Electrical conductivity

The electrical conductivity is measured with a FLUKE 177 true rms multimeter. Two sets of three broken dog-bone were used for the electrical conductivity test. The two sintering atmospheres that achieved the highest density were used on the two sets of broken dog-bone. One set of broken dog-bone used for the testing can be seen in figure 20. This set was sintered in argon at 1093 ℃. The other set was sintered in vacuum at 1080 ℃. All dog-bone were thin cuboids around the same length.

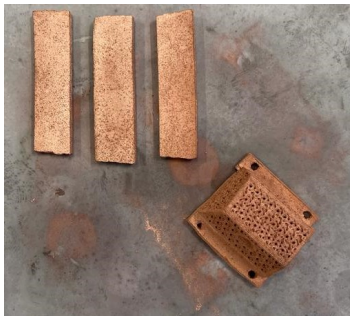

Figure 20: Set of broken dog-bone sintered in argon

To calculate the electrical conductivity the average length (l), width (w) and thickness (t) was measured of each cuboid. The measurements for each cuboid can be seen in table 15. For each dimension five locations were measured with a digital caliper and averaged. The resistance was measured with a two point probe placed on both ends of the cuboids.

Sample	Atmosphere	Temperature [°C]	Area [mm^2]	Length [mm]
1	Argon	1093	42.5	38.1
2	Argon	1093	40.3	37.5
3	Argon	1093	45.2	42.1
1	Vacuum	1080	35.8	38.7
2	Vacuum	1080	46.2	39.2
3	Vacuum	1080	49.0	39.8

Table 15: Dimensions cuboids for electrical conductivity testing

The resistance (R), length (l [m]), area (w [m] $\times$ t [m]) can be placed in formula 12 to calculate the resistivity (ρ) by dividing the resistance times area by the length [10]. The conductivity (σ) can be calculated with formula 13 by dividing 1 by the resistivity.

$$\rho = \frac{\mathrm{RA}}{\mathrm{l}} \tag{12}$$

$$\sigma = \frac{1}{\rho} \tag{13}$$

Mechanical testing

The mechanical testing helps defining the strength of the sintered parts, as the density is not up to 100 %. The mechanical tests that are being done are: compression, tensile and PIP testing. Compression and tensile strength is tested to see how binder jetted parts compare to conventionally manufactured parts. Profilometry-based Indentation Plastometry (PIP) obtains the stress-strain curve. In the case tensile testing cannot be done, PIP testing is a nice solution.
Compression testing is done according to the standard ASTM E9: Metal Compression testing. The test is done with three sintered discs for each of the three successful sinter sessions. The machine used for compression testing is the Zwick Z100. The measured samples and its dimensions are shown in table 16. The discs were tested with a speed of 0.028 mm/s and the measurement was stopped when the discs were compressed to half the original height.

Sample	Atmosphere	Temperature [℃]	Time [h]	Diameter [mm]	Height [mm]
1	Argon	1093	10	15.3	9.98
2	Argon	1093	10	15.2	10.45
3	Argon	1093	10	15.6	10.51
1	Vacuum	1075	10	15.5	10.22
2	Vacuum	1075	10	14.7	10.41
3	Vacuum	1075	10	14.4	9.72
1	Vacuum	1080	10	13.8	9.42
2	Vacuum	1080	10	14.6	9.70
3	Vacuum	1080	10	14.3	10.58

Table 16: Dimensions discs for compression testing

Tensile testing is done according to the standard ISO 6892-1: Tension testing of metals. Three sets of three dog-bone are used for the testing on the Zwick Z010. If less than three sets of three dog-bone are tested, the results will still be used to compare it to conventionally manufactured copper and other binder jetted copper results. The results or result will not be quantified, but it can still be compared to binder jet results as tensile testing is the only mechanical testing done. The test is done with a speed of 0.381 mm/min.

PIP testing is done on the Plastometrex Benchtop and can be seen in figure 21. The stress-strain data, the Brinell hardness and the surface roughness can be measured with the machine. The samples need to be grounded to a 1.5 µm finish and they must be flat. Two cubes sintered in the two atmospheres that achieved the highest density are tested.

Figure 21: Plastometrex Benchtop [43]

3.7 Microstructural characterisation

The microscopes are mainly used to look at the difference between the two hollow cubes that achieved the highest density in two different sintering atmospheres. The type of Scanning Electron Microscope (SEM) used, is the JSM-IT100. SEM is used to look at the porosity on the edge versus the inside of the samples. The SEM is also be used for an Energy-Dispersive X-ray spectroscopy (EDS) on the sample.

4 Results

The results are divided by the predetermined steps that are shown in the methodology. It is divided by the printing and curing, TGA, debinding and sintering, XRD, dimensional accuracy, testing of functional properties and microstructural characterisation. Only the important results are presented, a summary of all the results can be found in the different appendices.

4.1 Effect of Printing and Curing

The printing process is divided into different sessions. The first session was to get to know the printer and how the samples came out with the basic settings. The second session was to optimize the print parameters to achieve dimensional accurate prints and have enough samples to optimize the post-process parameters. The third session was to print dimensional accurate prints for the functional property testing. The extensive printlog can be found in appendix A, where the differences between each print of each printing session is explained and why the parameters were chosen.

First session to test print accuracy

The first session was the test print. Basic and difficult shapes were printed to see the outcome out of the printer and how they cure. The basic shapes, cubes (Cu) and hollow cubes (HC) where only 2 mm of the outsides gets deposited by binder, were further used for TGA. The difficult shapes, heat exchangers (He) and gyroids (Gy), were used to see how precise the prints could go. Table 17 shows how many different prints were done, which print parameters were used and if the prints survived the printing process, the removal of the print box and/or the depowdering. Prints further on are called ps#p#, where ps# stands for the printing session and p# stands for the print of that printing session.

Print	Shape	Waveform	X-speed [%]	Layer height [μm]	Amount printed [-]	Survived [-]
ps1p1	Cu	3P	60	100	11	11
ps1p1	He	3P	60	100	1	1
ps1p1	Gy	3P	60	100	1	1
ps1p2	Cu	1P	60	100	10	2
ps1p2	He	1P	60	100	1	0
ps1p2	Gy	1P	60	100	1	0
ps1p3	Cu	3P	60	100	4	4
ps1p3	HC	3P	60	100	4	3
ps1p4	Cu	3P	60	100	4	4
ps1p4	HC	3P	60	100	4	4

Table 17: Prints from printing session 1

Second session to optimize print parameters

The second session was to optimize the print parameters and print multiple sets of samples for the optimization of the post-process parameters. Mostly basic samples were printed, but a variety of shapes. These shapes are cubes (Cu) and hollow cubes (HC), discs (Di), cones (Co), dog-bones (Do), spirals (Sp) and gyroids (Gy). The cubes and hollow cubes are for comparing the saturation level, the cubes to check on shape distortion. The discs are for compression testing and the dog-bones for mechanical testing. The spiral and the gyroid are to test the accuracy of the printer. Table 18 shows the printed samples from the second printing session.

Print	Shape	Waveform	X-speed [%]	Layer height [μm]	Amount printed [-]	Survived [-]
ps2p1	HC	3P	60	50	9	9
ps2p2	HC	3P	60	100	9	6
ps2p3	HC	2P	60	100	9	2
ps2p3	Cu	2P	60	100	67	53
ps2p3	Co	2P	60	100	9	4
ps2p4	Do	3P	30	100	7	0
ps2p4	Di	3P	30	100	4	2
ps2p4	Cu	3P	30	100	8	2
ps2p4	HC	3P	30	100	9	7
ps2p4	Co	3P	30	100	9	5
ps2p4	Sp	3P	30	100	3	0
ps2p5	Do	3P	30	100	3	0
ps2p5	HC	3P	30	100	9	7
ps2p5	Co	3P	30	100	9	5
ps2p5	Cu	3P	30	100	9	0
ps2p6	Cu	2P	60	100	15	14
ps2p6	Di	2P	60	100	4	4
ps2p6	HC	2P	60	100	9	8
ps2p6	Co	2P	60	100	9	7
ps2p7	Cu	2P	30	100	15	13
ps2p7	Di	2P	30	100	4	4
ps2p7	HC	2P	30	100	9	9
ps2p7	Co	2P	30	100	9	8
ps2p8	Gy	3P	30	100	6	4

Table 18: Prints from printing session 2

Figure 22 shows the printed samples of the second print session inside the transport boxes. Box 1, figure 22a, shows the labeled compartments with the samples from print 1 to 4. Box 2, figure 22b, shows the printed samples inside of each compartment from print 5 to 8.

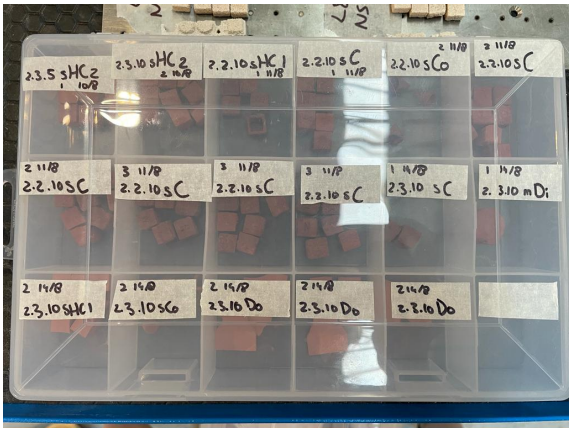

(a) Printed samples in box 1

(b) Printed samples in box 2

Figure 22: Printed samples P2

Third session to print dimensionally accurate shapes

The third session was to print dimensional accurate shapes with the optimized print parameters. The shapes printed are solid and hollow cubes for density and shrinkage measurements, discs for compression testing, dog bones for tensile testing and a complicated heat exchanger shape to test the dimensional accuracy. For each shape, at least five samples are printed for each post process cycle. There will be three sets of 4x5 shapes for the three different post process cycles. Table 19 shows the printed samples from the third printing session.

Print	Shape	Waveform	X-speed [%]	Layer height [μm]	Amount printed [-]	Survived [-]
ps3p1	Cu	3P	20	100	10	8
ps3p1	HC	3P	20	100	10	8
ps3p1	Do	3P	20	100	10	0
ps3p1	Di	3P	20	100	10	10
ps3p2	Cu	3P	20	100	10	8
ps3p2	HC	3P	20	100	10	7
ps3p2	Do	3P	20	100	10	0
ps3p2	Di	3P	20	100	10	8
ps3p3	Cu	3P	20	100	10	9
ps3p3	HC	3P	20	100	10	8
ps3p3	Do	3P	20	100	10	1
ps3p3	Di	3P	20	100	10	7
ps3p4	Do	3P	20	100	10	0
ps3p5	He	3P	20	100	4	2
ps3p5	Gy	3P	20	100	2	2

Table 19: Prints from printing session 3

4.2 TGA

Table 20, shows the input data of the TGA tests that were run. Appendix B will show the graphs of each TGA. They will be explained in the appendix, just like the reasons for the temperature changes.
Cubes from ps1p1 were used and cut into smaller pieces. Each piece got a name: T1 to T4.

	Debinding		Sintering		Atmosphere
Sample	Temp [℃]	Time [h]	Temp [℃]	Time [h]	
T1	600	3	1050	5	80% Ar 20% H
T2	450	3	1050	5	80% Ar 20% H
T3	400	3	1050	5	80% Ar 20% H
T4	400	3	1025	5	80% Ar 20% H

Table 20: TGA input data

TGA Debinding temperature

Figure 23a shows the graph from sample T1. The temperature is indicated by the red line, scale on the left in Celsius. The mass is indicated by the green line, scale on the right in milligrams. The whole cycle takes around 16 hours. Figure 23b shows the derivative in purple of the mass of figure 23a. It is taken at the big drop of mass in between the first and second hour. The peak of the derivative dissects the temperature slope around 1.4 hours and 367 ℃. Thus the biggest weight loss is done at this temperature, meaning the debinding happens at a lower temperature than originally thought. The mass keeps on decreasing until it reaches a temperature of around 450 ℃.
The second sample is tested at a lower debinding temperature to see if the the sample will correctly debind. The second sample had a lower debinding temperature of 450 ℃ to test if all the binder would burn out at a lower debinding temperature. The third sample was melted when it came out of the TGA. The reasoning behind this was a broken thermocouple, as the sintering temperature was the same as the earlier runs that did not melt. Thus the run was repeated, but with a lower sintering temperature to see if 400 ℃ was enough for the debinding. To ensure for all the binder to burn out of the samples, a debinding temperature of 450 ℃ was chosen. Appendix B shows the TGA graphs of the run T2 and T4 and they will be discussed in greater detail.

TGA Sintering temperature

It is interesting to see a slight increase in mass during the temperature increase after the debinding. This can indicate a small weight gain, after the weight gain, the mass slowly drops and keeps dropping at a faster rate during the cooling of the specimen after the sintered time is reached. Possibly meaning the samples need to be sintered for a longer period of time.

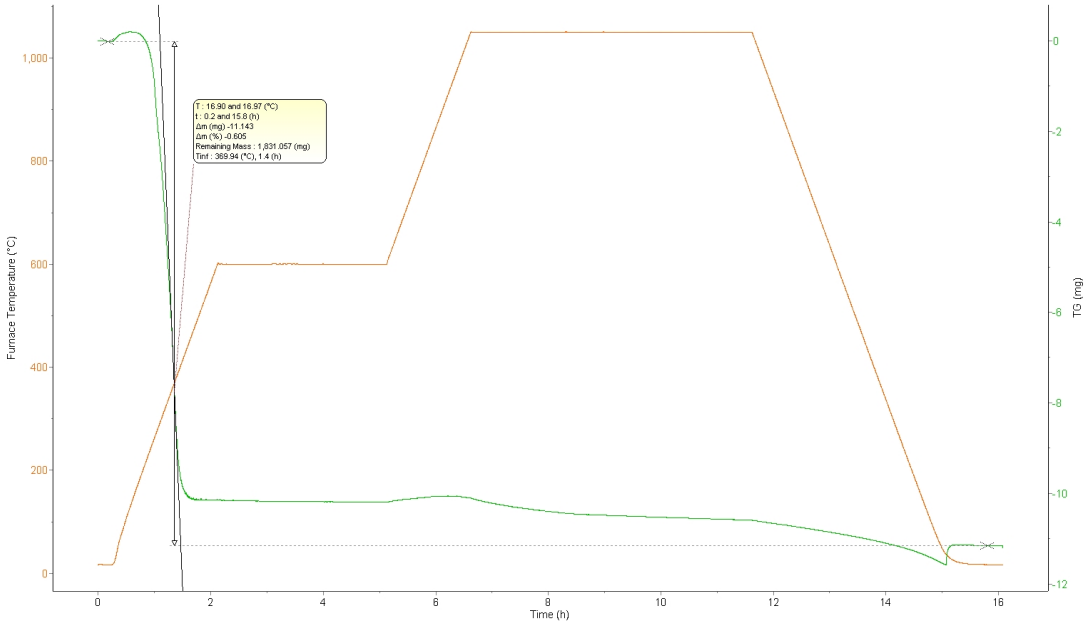

(a) TGA T1

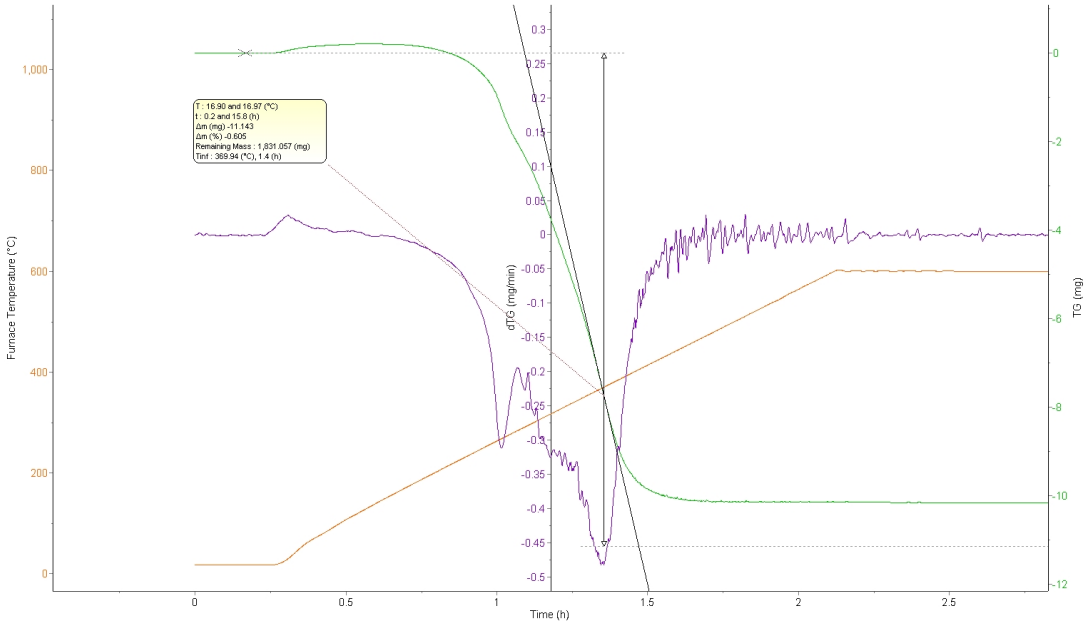

(b) TGA derivative T1

Figure 23: TGA and TGA derivative of sample T1

4.3 Debinding and Sintering

The debinding and sintering happened in multiple sessions after each printing session. The sinter and debinding sessions, from now on, called sinter sessions (S#) as the debinding and sintering happens as one process. All the sintering sessions can be seen in table 21. The debinding was always done in argon and the sintering was done in argon and vacuum. For the LHTG 200-300/22-1G furnace, it is not possible to start and end a session in vacuum. The debinding and final cooling stage were done in argon, the sintering was done in either argon or vacuum. Hence the vacuum sinter sessions still have a flow value of 150 l/h for the argon gas. In the beginning the sessions are cooled naturally, which is why there is a dash in the cooling rate cell. The separate results from all the sinter sessions, are shown in appendix C.

	Debinding		Sintering		Heating & cooling rate		Atmosphere	
Batch	Temp [°C]	Time [h]	Temp [°C]	Time [h]	Heating [°C/min]	Cooling [°C/min]	Type	Flow [l/h]
S1	450	3	1050	5	5	-	Argon	250
S2	450	3	1075	5	5	-	Argon	150
S3	450	3	1085	5	5	-	Argon	150
S4	450	3	1100	5	5	-	Argon	150
S5	450	3	1092	5	5	-	Argon	150
S6	450	3	1095	5	5	-	Argon	150
S7	450	3	1075	5	5	-	Argon	150
S8	450	3	1090	5	5	-	Argon	150
S9	450	3	1095	5	5	-	Argon	150
S10	450	3	1093	5	5	-	Argon	150
S11	450	3	1094	5	5	5	Argon	150
S12	450	3	1093	7.5	5	5	Argon	150
S13	450	3	1075	7.5	5	5	Vacuum	150
S14	450	3	1080	7.5	5	5	Vacuum	150
S15	450	3	1093	10	5	5	Argon	150
S16	450	3	1075	10	5	5	Vacuum	150
S17	450	3	1080	10	5	5	Vacuum	150
S18	450	3	1093	7.5	5	5	Argon	150
S19	450	3	1080	7.5	5	5	Vacuum	150

Table 21: Debinding and sintering runs

Up until session S9 there was no success in fully sintering the samples. As all the samples that came out of the furnace still had some loose powder on them. The first

fully sintered sample, on the outside, was sintered at T_s=1095 ℃ for 5 hours. Figure 24 shows the green bodies and the sintered samples. One sample is sintered perfectly, without any loose powder, but the other sample partially melted.

(a) Green cube and hollow cube samples

(b) Melted cube and sintered hollow cube, sintered at 1095 ℃

Figure 24: S9 green and sintered at 1095 ℃ samples, with natural cooling

Session S10 is done at a lower temperature at T_s=1093 ℃ for 5 hours. Three out of four samples came out fully sintered on the outside, but the cube on the left still had some loose powder on it. Furthermore the dog-bone was distorted during the

debinding and sintering as it curls up on the edges.

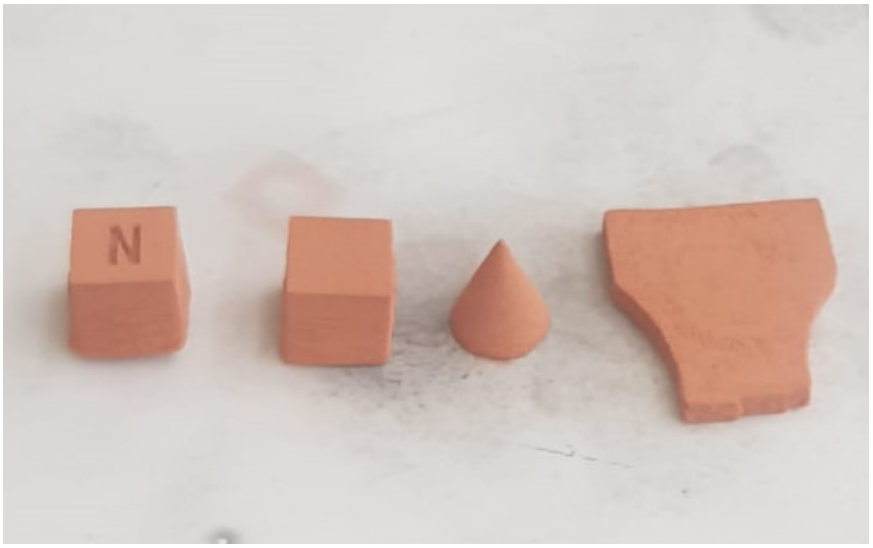

(a) Green cube, hollow cube, cone and dog-bone piece

(b) Sintered samples at 1093 ℃, with a distorted dog-bone piece

Figure 25: S10 green and distorted sintered at 1093 ℃ samples, with natural cooling

Session S12 is done at T_s=1093 ℃ for 7.5 hours in argon. Both cubes came out fully sintered on the outside and they were shiny. The sintered samples can be seen in figure 26. Session 13 is done at T_s=1075 ℃ for 7.5 hours in vacuum. Session 14 is done at T_s=1080 ℃ for 7.5 hours in. Both sets cubes came out fully sintered on the outside and had some shine to them.

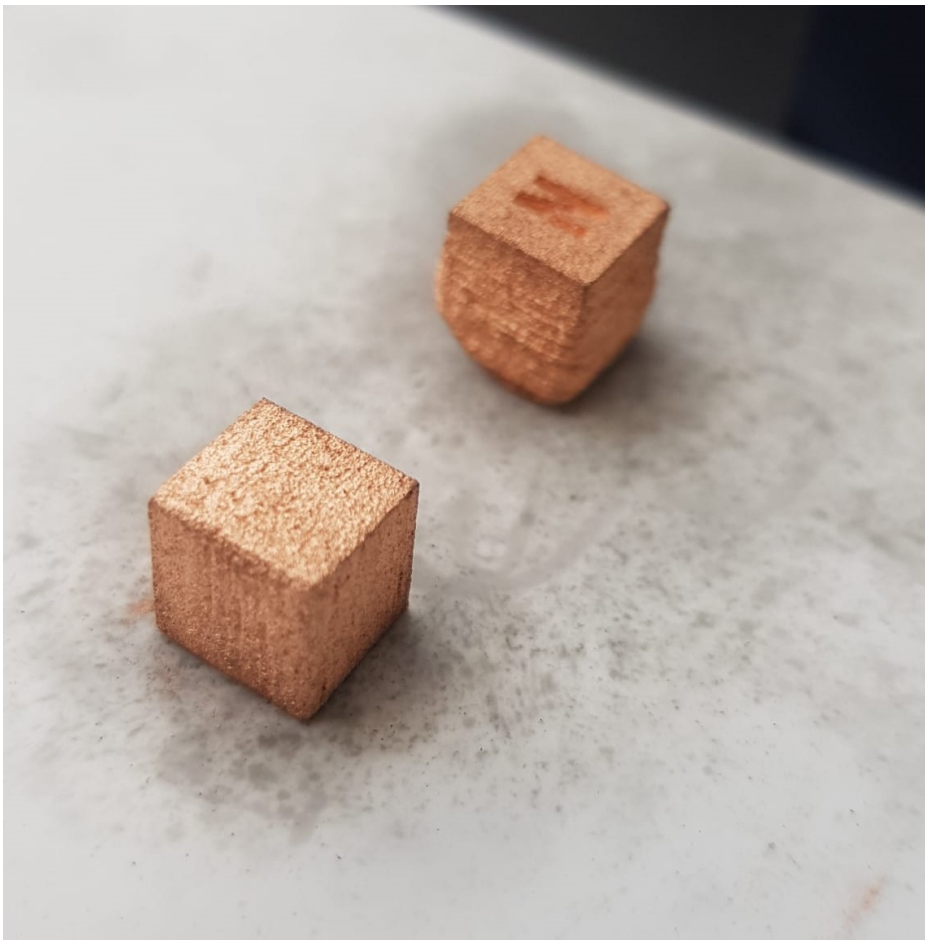

Figure 26: S12 hollow cube and cube samples sintered at 1093 ℃

Session 15, 16 and 17 were done with each five solid cubes, five hollow cubes and five discs. Due to the earlier sinter sessions, three final sinter atmospheres were chosen that fully sintered the samples. These sessions were argon at 1093 ℃ for 10 hours, vacuum at 1075 ℃ for 10 hours and vacuum at 1080 ℃ for 10 hours. The sinter time was increased to ensure each sample was fully sintered. The results of the three different sinter sessions can be seen in figure 27 for the argon session, figure 28 for the vacuum at 1075 ℃ session and figure 29 for the vacuum at 1080 ℃ session.

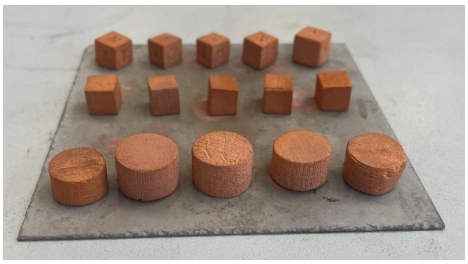

Figure 27: S15 sample set at 1093 ℃ in argon for 10 hours

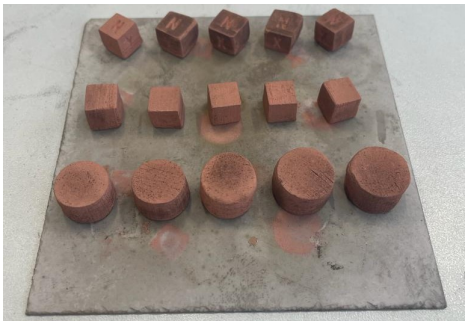

Figure 28: S16 sample set at 1075 ℃ in vacuum for 10 hours

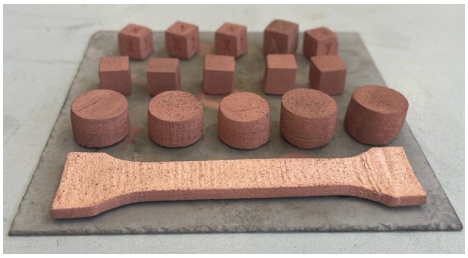

Figure 29: S17 sample set at 1080 ℃ in vacuum for 10 hours

Finally a heat exchanger and gyroid were sintered in argon at 1093 ℃ for 7.5 hours and in vacuum at 1080 ℃ for 7.5 hours. The heat exchanger was sintered for a shorter amount of time due to the thinness of the structure. The green and sintered heat exchanger and gyroid can be seen in figure 30.

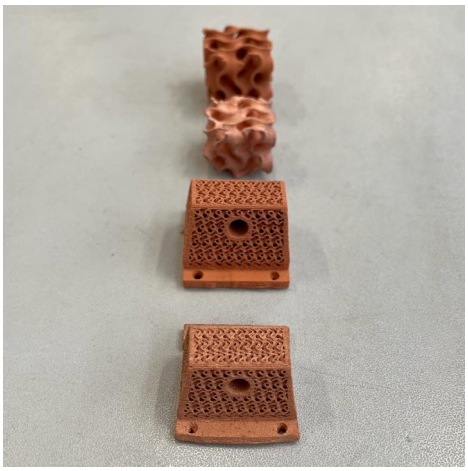

Figure 30: Sintered heat exchanger and gyroid next to green heat exchanger and gyroid

4.4 XRD

There are clear visual differences between multiple samples. Figure 31 shows the possible colour differences there were in between the printed and cured samples. At the beginning of the second print session there are some samples that were quite dark, see figure 31a. They were darker than other samples that were already used for sinter sessions. Another set of samples was quite dark when it was left to cure for around 15 hours instead of 3 hours, see figure 31b. The samples were left accidentally in the oven during the curing. Furthermore, samples with a higher binder saturation level appear darker than samples with a lower binder saturation. The samples in the top of figure 31c have less binder than the samples in the bottom.

(a) Dark samples 1

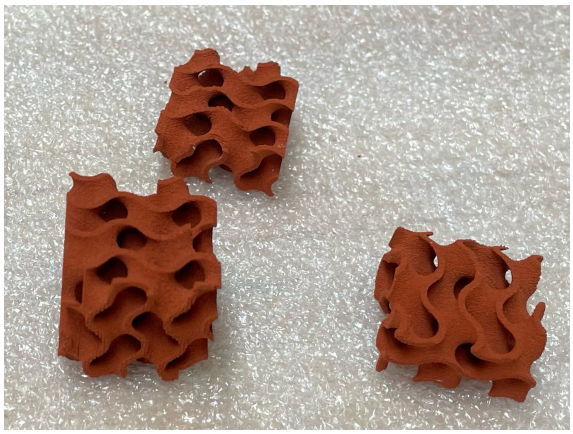

(b) Dark samples 2

(c) Colour difference between printed samples

Figure 31: Printed samples P2

XRD was done on three different samples:

- A hollow cube with 3P waveform, 30 % x-speed, from ps2p4
- A hollow cube with 2P waveform, 30 % x-speed, from ps2p7
- A gyroid with 3P waveform, 30 %, from ps2p8

For the hollow cubes, broken samples were chosen as the full-size was too high to fit into the holder. Both broken samples were around half the height of the original

hollow cubes. The gyroid has a difficult shape for XRD, thus small pieces of the shape were chipped off and grounded into loose powder.

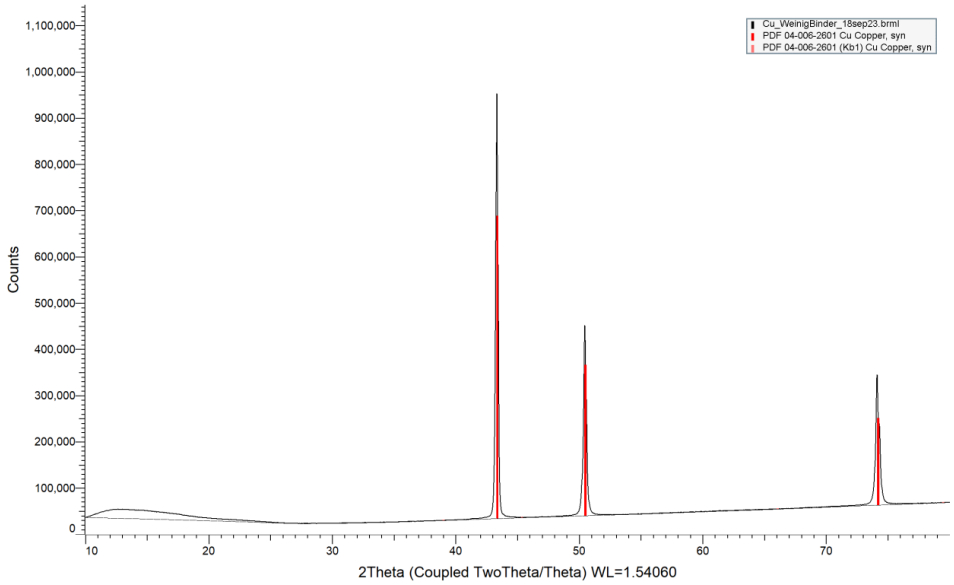

(a) XRD sample from ps2p4

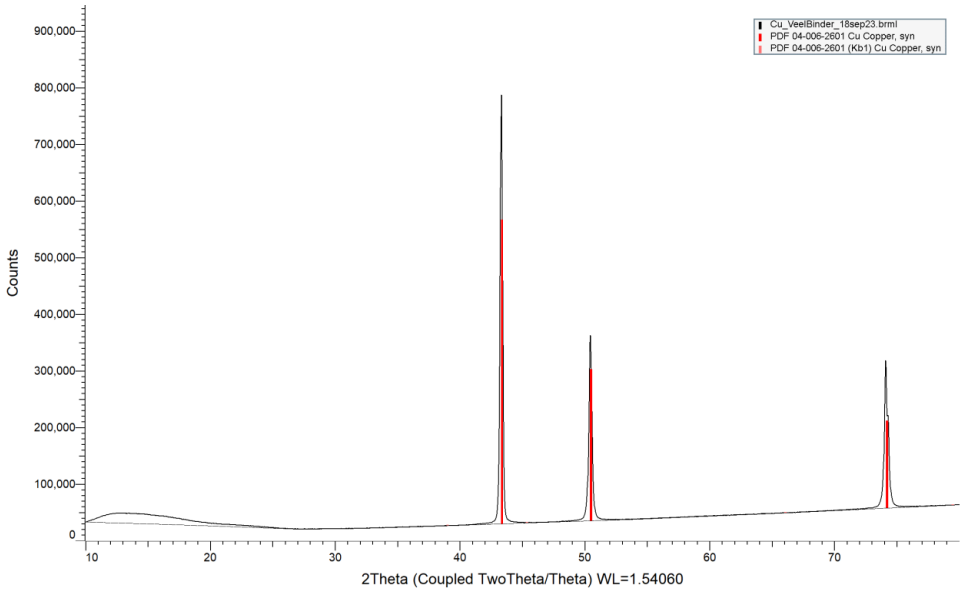

(b) XRD sample from ps2p7

Figure 32: XRD samples

Figure 32 shows the two XRD graphs of the samples with a different amount of binder in them. Figure 32a shows the hollow cube with less binder and figure 32b shows the hollow cube with more binder.

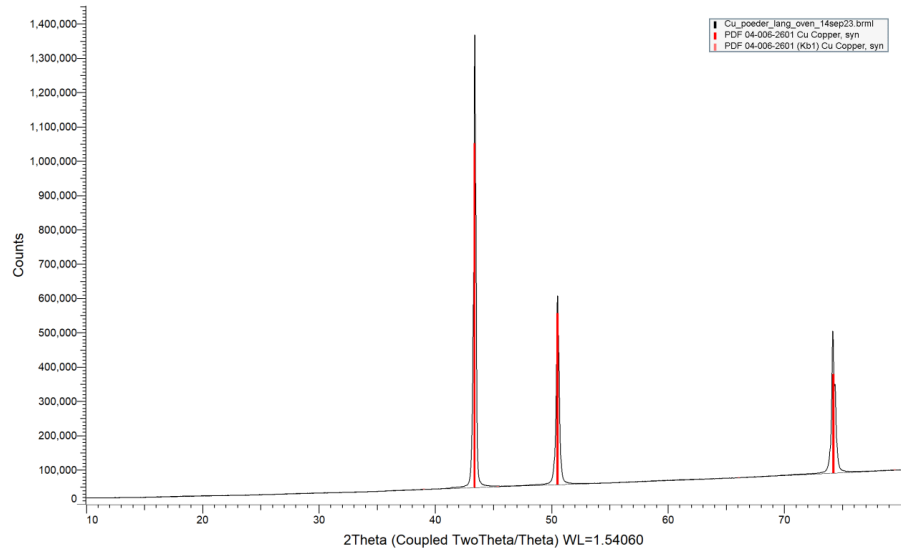

Figure 33: XRD sample of long curing

Figure 33 shows the XRD graph of the gyroid sample that cured in the oven for 15 hours instead of 3.
All three samples have three peaks. These peaks correspond to the (111), (200) and (220) copper planes for a face-centered cubic copper phase [44]. The standard 2θ values for copper powder can be seen in table 22.

2θ JCPDS Copper [degrees]	hkl
43.297	111
50.433	200
74.130	220

Table 22: Standard powder diffraction JCPDS, copper file No. 04-0836 [44]

4.5 Dimensional accuracy

Four samples were initially measured with the laser scanner: a green hollow cube, a sintered hollow cube, a green cone and a sintered cone. When fusing the different views of the green cube, the 3D objects were not very precise, as there were a lot of polygonals on the surface of each plane. These polygonals could be removed in the

software, but it was precise and time consuming work of only removing the protruding polygonals and polygonals directly on the surface. After removal of the polygonals and the fusion of the different views, there were still inaccuracies on the edges of the surface of the cube in the 3D models, see figure 34.

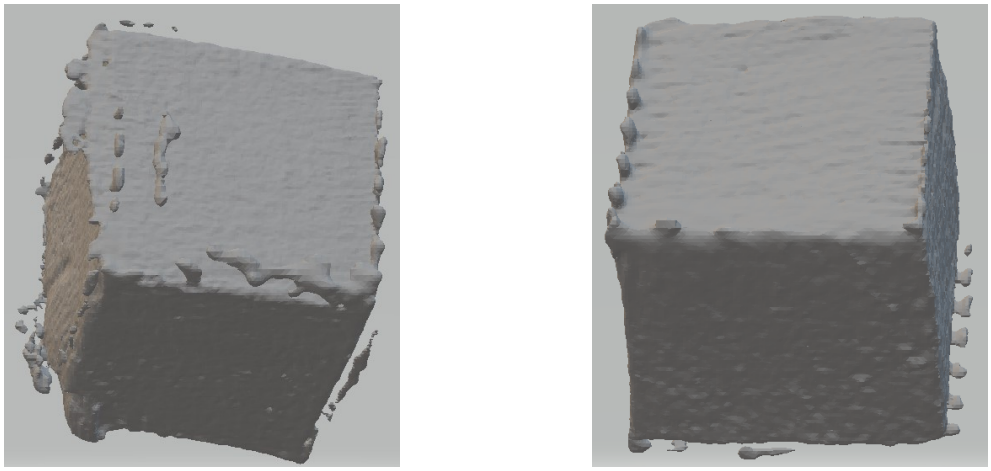

(a) 3D model of a green cube

(b) 3D model of a sintered cube

Figure 34: 3D models of a green and sintered cube

The cones were scanned with the 3D scanner as well, but these results were inconclusive. The cones were too small, as the 3D model had too much polygonals on its surface. Even after removal of much polygonals, the fusion of the different views resulted in an organic, non-cone shape. The scanned and fused 3D model of the cone can be seen in figure 35.

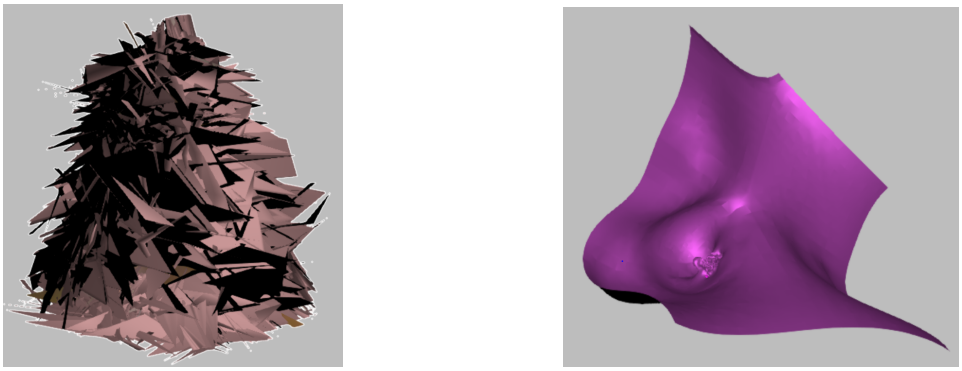

(a) 3D model of a cone

(b) Fused image of a cone

Figure 35: 3D models of a cone and its fused image

The 3D models of the cubes were opened in Paint 3D, where the dimensions were taken. Due to the inaccuracies of the 3D models, the calculated shrinkage is not precise. Thus the shrinkage is measured with a caliper too, to compare and average the results. The shrinkage measured with the 3D models can be seen in table 23.

	Green Part [mm]	Sintered Part [mm]	Shrinkage [%]
X	96	84	12.5
Y	95	83	12.2
Z	93	79	14.7

Table 23: Shrinkage measured with 3D Scanner

As the 3D scanner cannot accurately be used for the small samples printed and sintered, a caliper is used for the remaining samples. The caliper was used to measure the green and sintered cubes from different atmospheres to compare the shrinkage percentages. To accost for the shape inaccuracies of the cubes and hollow cubes, three measurements were taken and averaged for each direction. One measurement at the start, one in the middle and one at the end of the specified surface. Table 24 shows the averaged values in each direction and the calculated shrinkage of the two different cubes in each atmosphere and a green cube for comparison.

Shape	Atm	Temp [°C]	Time [h]	S X [%]	S Y [%]	S Z [%]	V S [%]
Hollow	Ar	1093	10	12 ± 4	11 ± 3	14 ± 3	32± 7
Hollow	V	1075	10	10 ± 4	12 ± 2	11 ± 4	30 ± 7
Hollow	V	1080	10	13 ± 2	12 ± 4	12 ± 3	32 ± 6
Solid	Ar	1093	10	10 ± 8	9 ± 5	9 ± 7	25 ± 16
Solid	V	1075	10	7 ± 5	8 ± 5	6 ± 2	19 ± 8
Solid	V	1080	10	15 ± 6	15 ± 3	11 ± 5	35 ± 11

Table 24: Directional shrinkage measured for solid and hollow cubes in different sinter atmospheres

It can be seen that the shrinkage in the X- and Y-direction is around the same value. The shrinkage in the Z-direction is higher in the hollow cubes sintered in argon. For the other sintered samples the shrinkage in the Z-direction is the same value as the X- and Y-direction or it is lower, which is the case with the solid cube shrinkage in vacuum on 1080. The highest volumetric shrinkage is with the hollow cubes in argon and vacuum 1080 and the solid cubes in vacuum 1080.

4.6 Testing of functional properties

Density

The density of two different shapes were measured in three different atmospheres. Table 25 shows the average density calculations for the hollow and solid cubes, measured with a caliper and scale. In the last column, the density percentage is given. The percentage is compared to the density of wrought copper, which is rho=8.93 g/cm^3 [13]. Each cube, hollow and solid, has a layer height of 100 micron, has a debinding time of 3.5 hours on 450 ℃ and the saturation level is 72 %. The only difference between the cubes are the total amount of binder in them (difference between solid and hollow cubes itself) and the atmosphere and temperature they are sintered in (difference between each hollow cube).

Shape	Atm	Temp [℃]	Time [h]	Volume [cm^3]	Weight [g]	Density [g/cm^3]	Density [%]
Hollow	-	-	-	1114.80 ± 25.6	5.12 ± 0.14	4.59 ± 0.09	51 ± 1
Hollow	Argon	1093	10	755.08 ± 64.89	4.87 ± 0.16	6.51 ± 0.74	73 ± 8
Hollow	Vacuum	1075	10	775.56 ± 74.07	5.02 ± 0.11	6.51 ± 0.49	73 ± 5
Hollow	Vacuum	1080	10	754.68 ± 64.56	4.93 ± 0.04	6.59 ± 0.62	74 ± 7
Solid	-	-	-	1141.70 ± 37.08	4.97 ± 0.31	4.35 ± 0.19	49 ± 2
Solid	Argon	1093	10	857.17 ± 197.93	4.96 ± 0.43	5.97 ± 0.87	67 ± 10
Solid	Vacuum	1075	10	918.51 ± 79.35	4.67 ± 0.19	5.13 ± 0.60	57 ± 7
Solid	Vacuum	1080	10	742.02 ± 113.28	4.61 ± 0.16	6.32 ± 0.67	71 ± 7

Table 25: Solid cube density measured with a caliper and a scale

The hollow cubes have a higher density than the solid cubes for each sinter atmosphere. The vacuum 1080 has the highest achieved average density for the hollow and solid cubes.
The density is also measured with the Archimedes method to test how accurate the method is for porous samples. Table 26 shows the comparison of the density percentage measured with a caliper (D_C) and Archimedes (D_A).

Sample	Shape	Atm	Temp [°C]	Time [h]	D_C [%]	Dry weight [g]	Wet weight [g]	D_A [g/cm^3]	D_A [%]
1	Hollow	Argon	1093	10	83	5.07	4.42	7.76	87
2	Hollow	Argon	1093	10	71	4.71	4.14	8.31	93
3	Hollow	Argon	1093	10	82	5.03	4.39	7.86	88
1	Hollow	Vacuum	1075	10	75	5.01	4.40	8.20	92
2	Hollow	Vacuum	1075	10	79	5.02	4.388	7.92	89
3	Hollow	Vacuum	1075	10	77	4.84	4.21	7.73	87
1	Hollow	Vacuum	1080	10	82	4.98	4.35	7.78	87
2	Hollow	Vacuum	1080	10	71	4.99	4.28	7.00	78
3	Hollow	Vacuum	1080	10	82	4.95	4.31	7.80	87

Table 26: Hollow cube density measured with a Archimedes

It can be seen that every measurement done with Archimedes differs highly than measurements done with a caliper. The smallest difference is 4 %, the biggest difference is 22 %.

Dimensional accuracy

Table 27 shows the average measurements in the three different directions of the samples. It also shows the standard deviation. The goal was to achieve a 0.5 mm tolerance between the STL file and the printed parts. The STL files of both solid and hollow cubes were 10x10x10 mm.

Direction	Shape	Average length [mm]	Standard deviation [mm]
X	Hollow	10.4	0.1
Y	Hollow	10.5	0.2
Z	Hollow	10.3	0.1
X	Solid	10.6	0.2
Y	Solid	10.6	0.3
Z	Solid	10.2	0.2

Table 27: Dimensional accuracy measurements of green samples

Electrical conductivity

Table 28 shows the different resistance, resistivity and electrical conductivity (EC) values. For the two atmospheres that achieved the highest density, three samples were tested. The density is measured with a caliper and scale.

Sample	Shape	Atm	Temp [℃]	Time [h]	D_C [%]	Resistance [Ohm]	Resistivity [$\times 10^{-4}$ Ohm×m]	EC [S/m]
1	Cuboid	Argon	1093	10	80	0.2	1.85	5403
2	Cuboid	Argon	1093	10	69	0.2	2.36	4241
3	Cuboid	Argon	1093	10	69	0.2	2.47	4054
1	Cuboid	Vacuum	1080	10	61	0.2	2.23	4488
2	Cuboid	Vacuum	1080	10	68	0.2	2.15	4651
3	Cuboid	Vacuum	1080	10	59	0.2	2.15	4663

Table 28: Electrical conductivity measurements of cuboids in different atmospheres

Compression, tensile and PIP testing

Table 29 shows the different compressive strength measurements for the different sinter atmospheres. For each atmosphere, three discs were tested and the average was taken. The average E modulus of wrought copper is 115 GPa [13]. There is not only a big difference between the values of different atmospheres, but also a big difference between the values in the same atmosphere.

Sample	Shape	Atm	Temp [℃]	Time [h]	D_C [%]	F_{max} [kN]	E_{mod} [MPa]
1	Disc	Argon	1093	10	51	0.1	11.8
2	Disc	Argon	1093	10	50	5.1	32.2
3	Disc	Argon	1093	10	49	0.1	9.7
1	Disc	Vacuum	1075	10	57	1.8	37.7
2	Disc	Vacuum	1075	10	59	23.0	28.9
3	Disc	Vacuum	1075	10	62	33.9	48.2
1	Disc	Vacuum	1080	10	66	30.4	19.4
2	Disc	Vacuum	1080	10	56	3.7	40.1
3	Disc	Vacuum	1080	10	61	1.1	68.6

Table 29: Compressive strength measurements of different atmospheres

Table 30 shows the tensile test values of the one sample tested. Only one dog-bone survived the printing process thus there was only one sample tested. The dog-bone was sintered for 10 hours in vacuum at 1080 ℃.

Atmosphere	Temperature [℃]	Time [h]	E_{mod} [GPa]	F_{max} [N]	UTS [MPa]	Elongation [%]
Vacuum	1080	10	0.32	96.1	2.63	0.2

Table 30: Tensile strength of sample sintered in vacuum at 1080 ℃

The dog-bone before tensile testing can be seen in figure 36a. The break in the dog-bone after tensile testing can be seen in figure 36b.

(a) Dog-bone before tensile testing

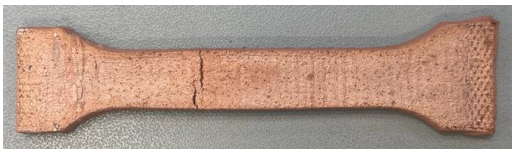

(b) Dog-bone after tensile testing

Figure 36: Dog-bone before and after tensile testing, sintered at 1080 ℃ in vacuum

The PIP testing was done on the two samples that achieved the highest density. Which were the hollow cube sintered in argon at 1093 ℃ for 10 hours. The hollow cube had an achieved density of 83 %. The other hollow cube was sintered in vacuum at 1080 ℃ for 10 hours. Both samples were tested, but unfortunately both samples gave errors during the measurement. Thus there were no PIP testing results of both cubes.
The error can be due to the input values before the measurement. Before testing, the type of material must be entered. In this case it was copper/copper-alloys. This ensures the machine knows what to expect of the material and what other data it should use for the measurement. However, the samples used for the PIP testing are porous. Therefore they can have significant lower values than the machine expects.
Furthermore the machine gave a warning the indentation tip was damaged. Which if the measurements did work, raises the question how accurate the measurements would be.

4.7 Microstructural characterisation

Figure 37 shows the edge of the hollow cube sintered in argon at 1093 ℃ for 10 hours. The hollow cube had an achieved density of 83 %. Figure 37a shows the cube with a zoom of 100x with 20.0 kV and a working distance of 14 mm. Figure 37b shows the cube with a zoom of 2000x with 20.0 kV and a working distance of 15 mm.

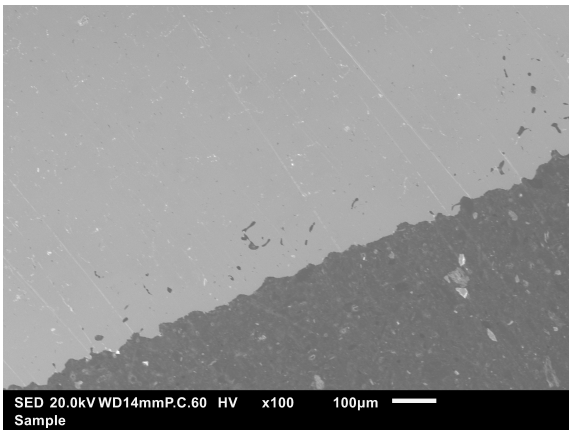

(a) Argon sample 100x

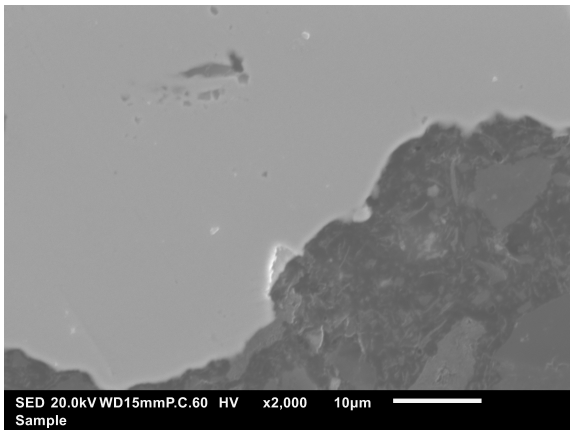

(b) Argon sample 2000x

Figure 37: SEM images of sample sintered in argon at 1093 ℃

Figure 38 shows the edge of the hollow cube sintered in vacuum at 1080 ℃ for 10 hours. The hollow cube had an achieved density of 82 %. Figure 38a shows the cube with a zoom of 100x with 20.0 kV and a working distance of 10 mm. Figure 38b shows the cube with a zoom of 2000x with 20.0 kV and a working distance of 9 mm. In both samples the pores are mostly located on the edge of the samples and less towards the center.

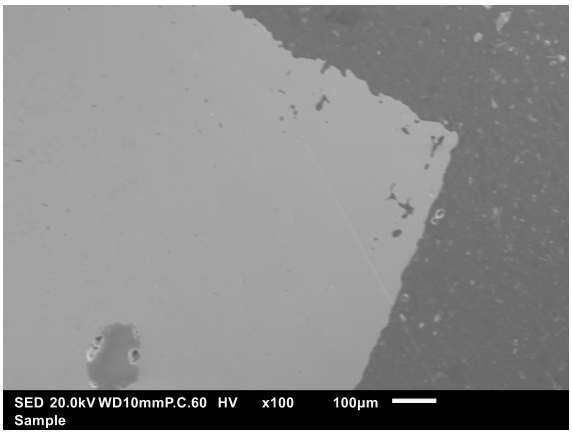

(a) Vacuum sample 100x

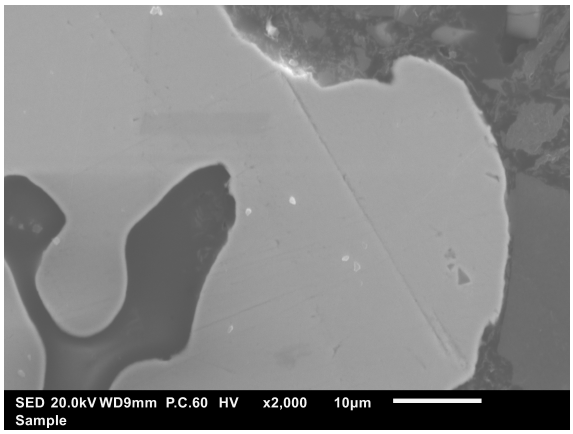

(b) Vacuum sample 2000x

Figure 38: SEM images of sample sintered in vacuum at 1080 ℃

Figure 39 shows the EDS map of the hollow cube sintered in argon with the three most present atoms.

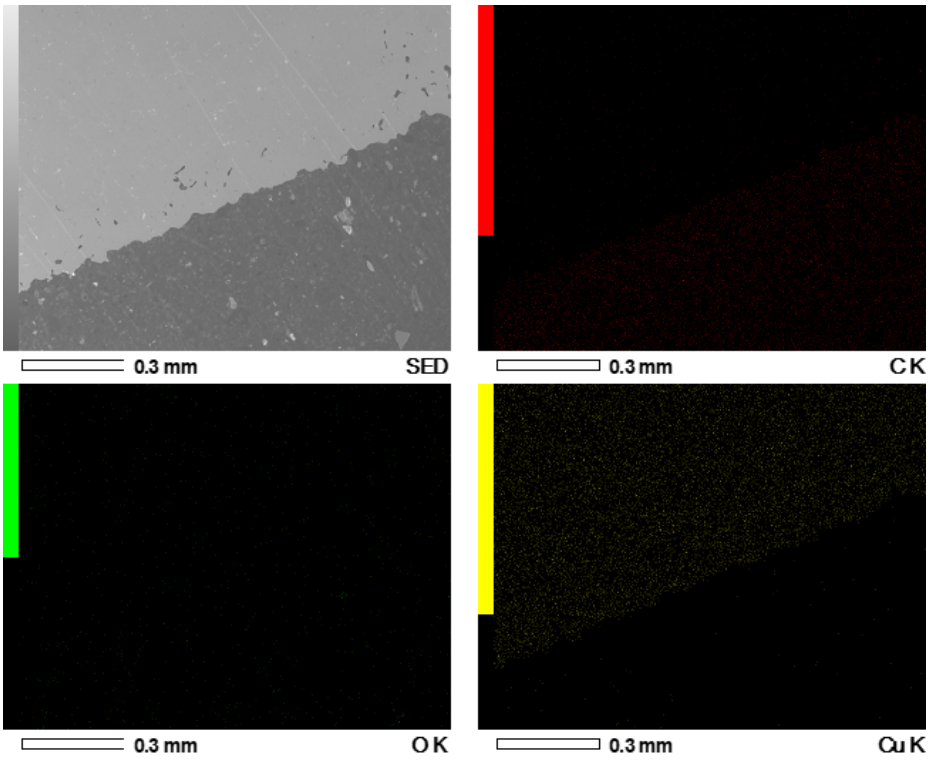

Figure 39: EDS map of argon sample

Figure 40 shows the XRD map of the hollow cube sintered in argon.

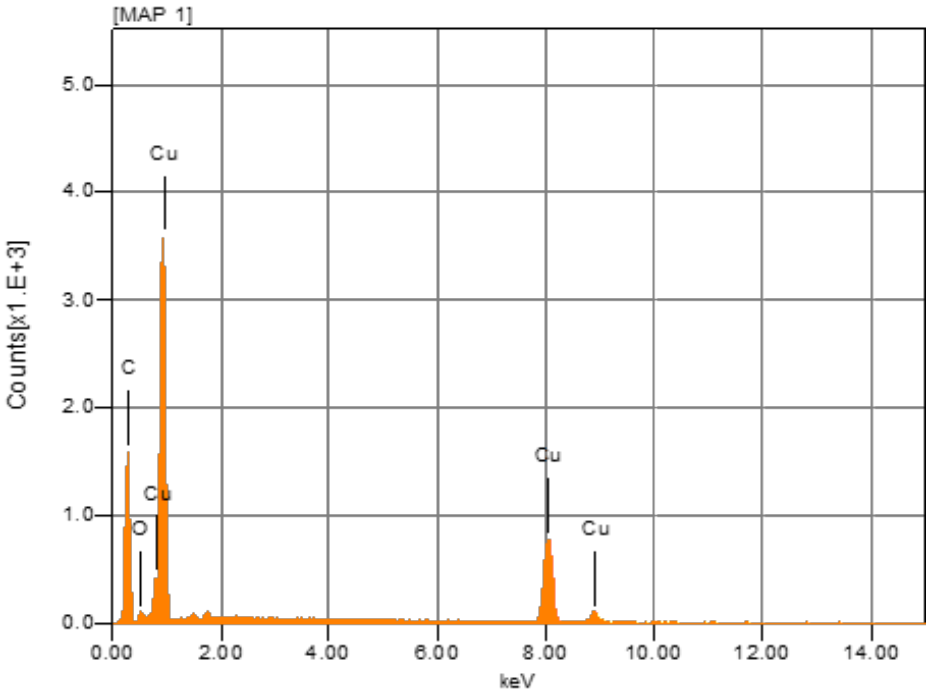

Figure 40: XRD map made by EDS of argon sample

Table 31 shows the percentages in mass and atoms of the hollow cube sintered in argon. It is important to note that the carbon percentage is very high, but the amount of carbon residue left in the sample itself is rather low. As most of the carbon is present in the material the sample holder is made of. Oxygen seems to be equally spread everywhere and not just concentrated in the sample or the sample holder.

Formula	Mass [%]	Atom [%]	Sigma	K ratio	Line
C	52.87	83.05	0.06	0.0019873	K
O	3.35	3.95	0.08	0.0004509	K
Cu	43.78	13.00	0.22	0.0234799	K

Table 31: EDS percentage of argon sample

Figure 41 shows the EDS map of the hollow cube sintered in vacuum with the three most present atoms.

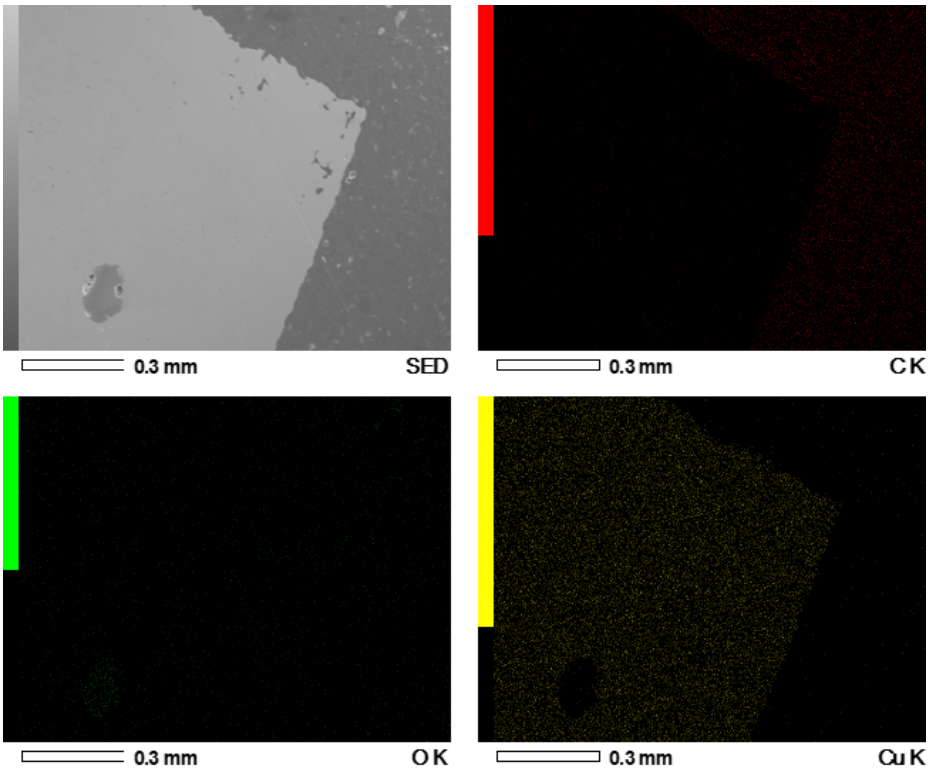

Figure 41: EDS map of vacuum sample

Figure 42 shows the XRD map of the hollow cube sintered in vacuum.

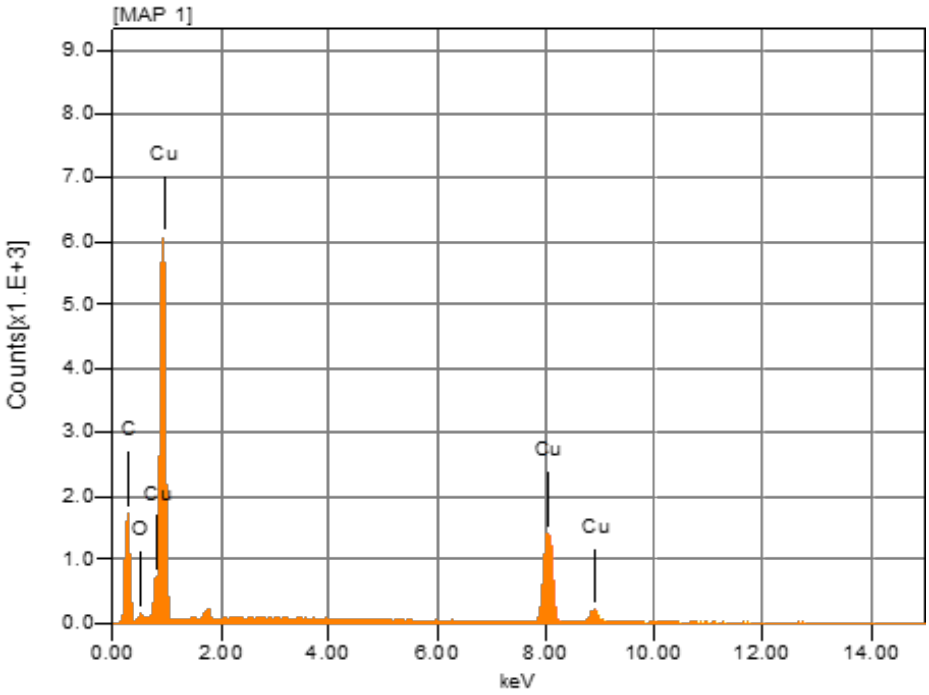

Figure 42: XRD map made by EDS of vacuum sample

Table 32 shows the percentages in mass and atoms of the hollow cube sintered in vacuum. The vacuum sample has the same high percentage of carbon which is mostly located outside the sample. The oxygen is equally present too, with a higher concentration in the dark grey eye on the left bottom corner. The copper concentration is low in this eye.

Formula	Mass [%]	Atom [%]	Sigma	K ratio	Line
C	43.06	77.93	0.07	0.002204	K
O	2.55	3.47	0.09	0.000671	K
Cu	54.38	18.47	0.31	0.047048	K

Table 32: EDS percentage of vacuum sample

5 Discussion

The different results are discussed per section of the process. The reasoning behind the choices made, is also explained. Then the results are compared to other achievements of researchers that printed copper with binder jetting and conventional manufactured copper.

5.1 Printing and Post-processing of samples

Printing experimentation

There were multiple unknowns during the printing and the debinding and sintering. A big question during the printing process is: why do the prints not survive the printing process? Table 33 shows the prints that did not survive the printing process or were not dimensionally accurate. The samples were dimensionally accurate when they were not less than 0.5 mm out of bounds after printing compared to the STL file input. Bleeding and distortion are possible reasons why the samples are not dimensionally accurate if they fall outside the 0.5 mm of the original STL size. Furthermore it shows what the reasoning is behind the failure and the calculated saturation level. The first reason behind the necessary dimensionally accurate samples, is it is wanted by the company. The second reason behind the necessary dimensionally accurate samples, is it makes the measurements for the shrinkage and density easier. When bleeding is present it is difficult to measure the volume precisely with a caliper.
Print session 1 and print session 2 were done with the Armadillo 2000 printer. Print session 3 was done with the Armadillo Chiron printer, a printer specifically for metal binder jetting. It was not possible to print the third session on the same printer, thus it is possible the prints from print session 3 have small differences. Mainly due to the Chiron printer being quite new to the team and only a few prints were done before the copper printing started. The Chiron still had some small issues that needed to be tweaked.

Green sample	Saturation Level [%]	Printed [-]	Survived [-]	Accurate [-]	Due to
ps1p1 Cu	104	11	11	0	Bleeding
ps1p2 Cu	< 70	10	2	0	Too weak
ps1p4 Cu	104	4	4	0	Oxidation
ps2p1 HC	209	9	9	0	Bleeding
ps2p2 HC	104	9	6	3	Leaking
ps2p3 HC	80	9	2	0	Removal
ps2p3 Cu	80	67	53	0	Bleeding
ps2p4 HC	80	9	7	7	
ps2p4 Cu	80	8	2	1	Short curing
ps2p4 Sp	80	3	0	0	Too thin
ps2p5 Co	80	9	5	5	
ps2p5 Do	80	3	0	3	Cracking
ps2p6 Cu	80	15	14	0	Bleeding
ps2p7 Cu	80	15	13	8	Distortion
ps2p8 Gy	80	6	4	4	Long curing
ps3p1 Do	72	10	0	0	Misalignment
ps3p4 Do	72	10	0	0	Removal print box

Table 33: Reasoning survival and accuracy of printed samples

For ps2p1 and ps2p2 only a small amount of samples could be printed as there was a significant amount of powder leakage. The leakage can be seen in figure 43. It shows how little of the area in the print box was left that was undisturbed by the created chasms due to the leaking. The small area was already taken into account and still the bottom row of samples got distorted due to the powder shortage caused by the leaking. Furthermore the feed box too had leaking issues. If there is leakage in the feed box, there will not be enough powder rolled into the print box during the printing. Thus not only will the powder in the print box leak through, resulting in powder loss, the layer height will be inconsistent too, as there will not be added enough powder. This can create chasms as well in the print box, resulting in inaccurate prints as the layer height will not be same for the different layers.

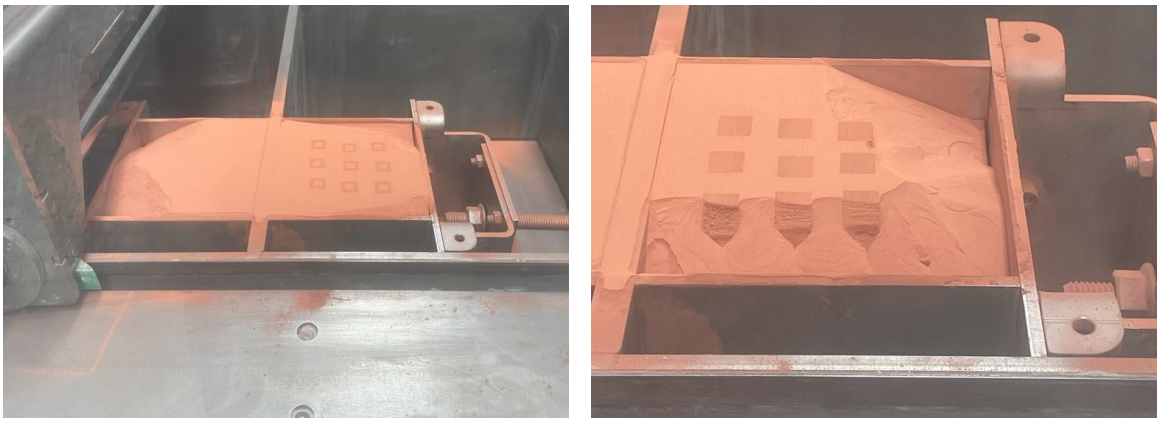

(a) Leaking of the feed box and print box (b) Close up of leaking in the print box

Figure 43: Leaking powder during printing

The leaking was the consequence of the reduction bed itself. The reduction bed is used to print on a small area, 100x100x100 mm, instead of the whole printer, which is 370 x 260 x 250 mm, to reduce time, material costs and waste. The used reduction bed was an older model used for R & D practices with bigger powder particles. To resolve the leakage issue, metal epoxy was used to seal the insides of the reduction bed, as there were visible gaps on the inside. The metal epoxy led to significantly less leaking of the powder during the printing. Furthermore a slightly larger silicone sheet was added underneath the print plate to help seal the corners during the printing. The results of the metal epoxy and silicone can be seen in figure 44.

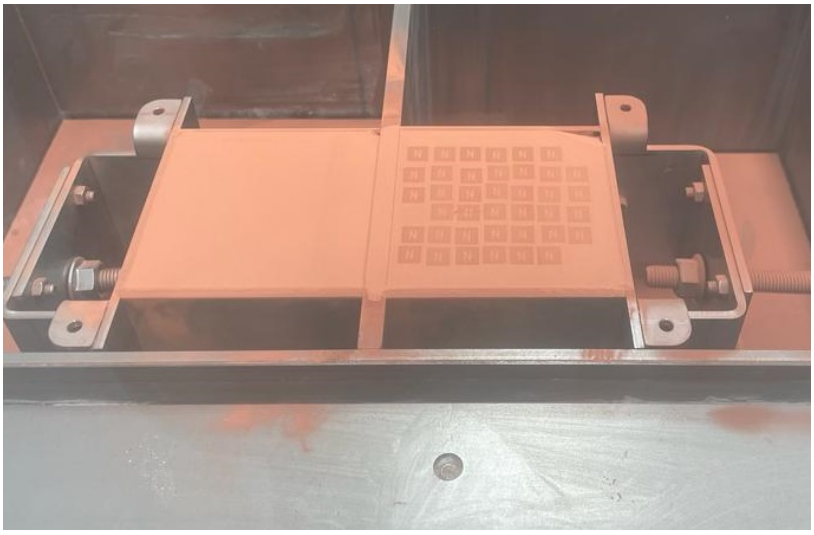

Figure 44: Less leaking with upgraded reduction bed

There is still some leakage in figure 44, but this small amount does not cause any big problems during the printing. The small leakage is due to incorrect placement of the print plate. The placement of the print plate needs to be checked to see if the silicone sheet seals the whole area around the print plate. With small adjustments the leakage should be resolved.

The second reason behind distortion of the samples can be the z-axis offset. The z-axis offset can adjust the pressure of the roller on the print box, by moving down one layer height for new powder in the print box and moving up the value of the offset. The offset value was taken from the print before the copper printing was run. The moving up and down of the print plate can be the cause of the distortion during the printing, due to the silicone sheet which is fastened on top of the printing plate. The silicone sheet is a little bit bigger than the print box and can move during the printing. When the print box goes up, the corners of the silicone sheet will go down and the center will take a convex shape. When the print box goes down the corners will go up and the center will stay down, creating a small crater shape. This normally would not create problems for small prints, but larger prints can get affected by the movement of the silicone sheet.

The third reason behind distortion of the samples can be the misalignment of the printhead in the x-direction. As the samples from ps3p1 had a line through it where the samples did not correctly align. The misalignment can be solved by adjusting the x-offset value, but it takes multiple testing prints to fully solve the issue. The distorted samples due to misalignment can be prevented by using a different orientation of the samples.

The reasoning why only one dog-bone survived the printing process is due to the removal of the print box. At least 50 dog-bones were printed, but they all broke either during the printing, the removal of the print box or during the depowdering. Even when the orientation was changed, the dog-bone was made smaller and thicker, they did not survive the printing process. There are two reasons behind the broken dog-bones. The first reason is the moving silicone sheet, which can distort long shapes placed on the bottom of the print box. The second reason is due to the design of the removal of the print box. To remove the print plate, a box is placed on top of the print plate and the print plate is moved all the way up. On the bottom of the box are four holes designed for a mechanism that slides under the print plate. These holes are not covered during the ascending print plate, meaning quite some powder leaks out. It is important the powder stays in the print box for the support of the printed samples. When the powder mostly flows away, the printed parts loose their support. This is especially important for long and thin shapes like dog-bones.

The biggest printing issue known at the start of the project, was the bleeding of the copper samples. The bleeding issue can be solved by adjusting the binder saturation, which is a combination of layer height, waveform and x-speed. The total binder saturation can also be reduced using shell printing, a method that only uses binder on the outside of the samples. It is not much discussed in literature, despite the many advantages [31]. After printing cubes and hollow cubes, it was clear to see how accurate all the hollow cubes were. The hollow cubes were dimensional accurate and had no bleeding issues. The solid cubes had either distortion or bleeding issues. Thus the shell printing has a positive effect on the dimensional accuracy of the copper powder. This is also said in literature as the binder saturation affects the resolution of the prints [34]. This can be seen in figure 45, with on the left a cube with too little binder, in the middle has a good amount of binder and the right has too much binder.

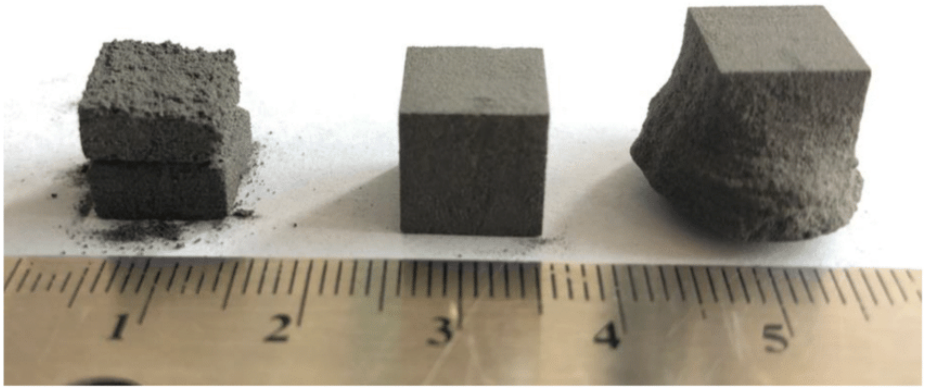

Figure 45: Difference in binder saturation on cubes [45]

The first adjustment that was done to lower the saturation level, was by changing the waveform. At first the waveform 3 pulse (3P) was changed to 1 pulse (1P). This was already an established waveform made by the company for the m-binder. But the samples made with the 1P were very weak and almost all samples broke during the depowdering. The second adjustment that was done to lower the saturation level, was by changing the x-speed. Changing the x-speed from the original 60 % to 30 % from the 3P waveform, lead to dimensional accurate samples with almost no bleeding issues. The bleeding presented itself in a small bump on the bottom of the solid cube and discs. The bleeding was less than the samples from the 60 % and the hollow cubes, cones and dog bones had no bleeding at all. Thus the thinner the sample, the less bleeding it has. The only downside of changing in x-speed, is the print time, as it took twice as long to print the same samples. To print at a higher speed again the company made a 2 pulse (2P) waveform. The 2P has the same droplet volume

at high X-speeds as the 3P has at low X-speeds. This data can be seen in table 34. The 50 and 60 % x-speed for the 3P could not be measured by the dropwatcher, the machine in which the waveform is developed. But these x-speeds are still usable. In theory it meant that a print could be run with a 2P waveform at 60 % x-speed and have the exact same results as the 3P prints at 30 %. However this has not proven the case. The prints that came out of the printer with the 2P runs, were a lot darker and had significantly more bleeding than the 3P runs. It could be possible that the 2P waveform still needs development as it is not perfected. But it is clear more binder is used as the samples appear darker and have more bleeding [45].

X-Speed	Two Pulse (2P) [pL]	Three Pulse (3P) [pL]
10%	78-85	85-105
20%	85-105	115-125
30%	115-125	130-140
40%	120-130	140
50%	125-145	-
60%	130-140	-

Table 34: Waveform M-Binder

Concluding the best working print parameters depend on the thickness of the sample. The print parameters that give dimensional accurate shapes for solid samples are the 3P waveform with a X-speed of 20 % and a layer height of 100 micron. The calculated saturation level of these samples is 72 %. This low saturation level is necessary to achieve no bleeding in the samples. When samples have walls or structures thinner than 5 mm, the saturation level needs to be 80 %, thus a 3P waveform with 30 % X-speed. This is necessary for a high enough green strength during the depowdering. The gyroids and heat exchangers both have thin structures and needed to be handled carefully. The higher saturation level gives a small boost in strength necessary for the handling of the samples, without causing bleeding issues. This could be seen in earlier prints. The gyroids printed with a 80 % saturation level had a small amount of breakage during the depowdering, compared to the 72 % saturation level gyroids. On all sides the green samples are in the tolerance of 0.5 mm of the digital shape and they are strong enough to be depowdered. The samples can take small falls of 20 cm and will not take any damages.
The print parameters that give dimensional accurate shapes for shell printed samples, with a wall of 2 mm, and prints that have a thickness of maximum 2 mm are the 3P waveform with a X-speed of 30 % and a layer height of 100 micron. This gives the samples a saturation of 80 %. The change in parameters is necessary for the extra

strength in the green sample. Especially the thin structures break somewhat easily by hand. The higher saturation level improves the green strength [46]. Due to the thinness and the shell printing the samples do not bleed, unlike solid samples that bleed a very small amount with an 80 % saturation level.
All samples need to be cured at 110 ℃ for three hours. A curing time of two hours was tested first, as this was the advised curing time. The samples need to be fully cooled down before the depowdering can begin, as some samples were still somewhat soft after they were depowdered before they fully cooled down. A curing time of two hours gave some soft samples after fully cooling down, hence the choice was made to cure the samples for three hours at 110 ℃. A much higher curing time (T $>$ 180 ℃) was tried in the beginning of the printing, but the high temperature ruined the powder and turned it into a weird mixture of caked powder that was ruined.

It could be seen in table 35, that on average a 0.5 mm tolerance of the STL files is achieved. Only the X and Y-direction have a length of 10.6 mm on average. The cause of the inaccuracy could not only be due to the switching of the printers, but also to the switching of binders just before the printing process. Like said before, the Chiron printer, on which these samples were printed, has a different fluid system. This different fluid system is less accurate due to the placement of the pump and the high fluctuating meniscus pressure. It is an older fluid system than the fluid system of the 2000 machine.

Direction	Shape	Average length [mm]	Standard deviation [mm]	Original length [mm]
X	Hollow	10.4	0.1	10
Y	Hollow	10.5	0.2	10
Z	Hollow	10.3	0.1	10
X	Solid	10.6	0.2	10
Y	Solid	10.6	0.3	10
Z	Solid	10.2	0.2	10

Table 35: Dimensional accuracy measurements of green samples

The reusage of the powder caused some issues. The biggest problem during the printing was the loss of accuracy. When powder was used that had been recycled from earlier sessions, the shapes came out rather distorted and lost all their precision. This was unexpected as the exact same parameters were used, with new powder, that gave very accurate shapes. It is possible that during the depowdering and recycling of the powder, most of the smallest particles were lost through the vacuum or left in the printer. The powder particles can be as small as 5 microns. In literature it was

tested by Pisani [30] to see how long the copper could be cured before it reached an oxygen percentage higher than 2-3 %. He concluded his pure copper powder could be cured for up to six hours in 180 ℃ until it reached an oxygen percentage of 2-3 %. With this information it was thought the powder could be reused at least three times without a risk for oxidation, furthermore the curing temperature is lower than in the literature. As 110 ℃ was used for two hours. But this was not the case as the powder had a much darker colour after using it for three printing and curing sessions. The darker colour is most likely due to copper oxidation [30]. It is possible that the oxidation may influence the particle shape of the powder, as the oxidation is formed around the copper particles. This can be seen in figure 46. But it seems that in the case of Schöß, Schulenburg and Turek [47], the spherical shape is still rather intact with a copper oxide shell around the pure copper particles. The biggest difference is mostly the size of the particles and the size of the voids. As both become bigger, some accuracy can become lost.

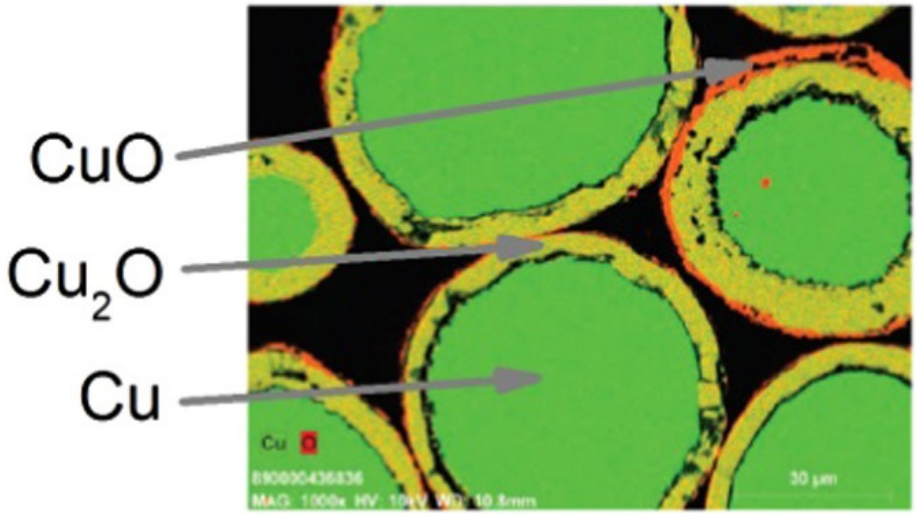

Figure 46: Particle shape of copper with a copper oxide shell [47]

It is important the particles have the correct sizes, multiple researchers [48], [49], [50] have shown that the highest density is achieved with bimodal powders. This is due to the creation of a high green packing density with the small particles filling the voids of the bigger particles. Furthermore the small particles have a high sintering driving force [49], which creates a high density sintered part printed with binder jetting.
Powders with only big particles and powders with only small particles achieve lower packing densities. In addition big particles do not have high accuracy, due to their large area and large voids. Small particles, in theory, should give the highest accuracy, smoothest surface finish and highest hardness [50], but the smaller particles will

agglomerate too much and thereby loose the accuracy it is supposed to have [37]. Figure 47 visualizes the difference in packing density with a different coarse powder fraction.

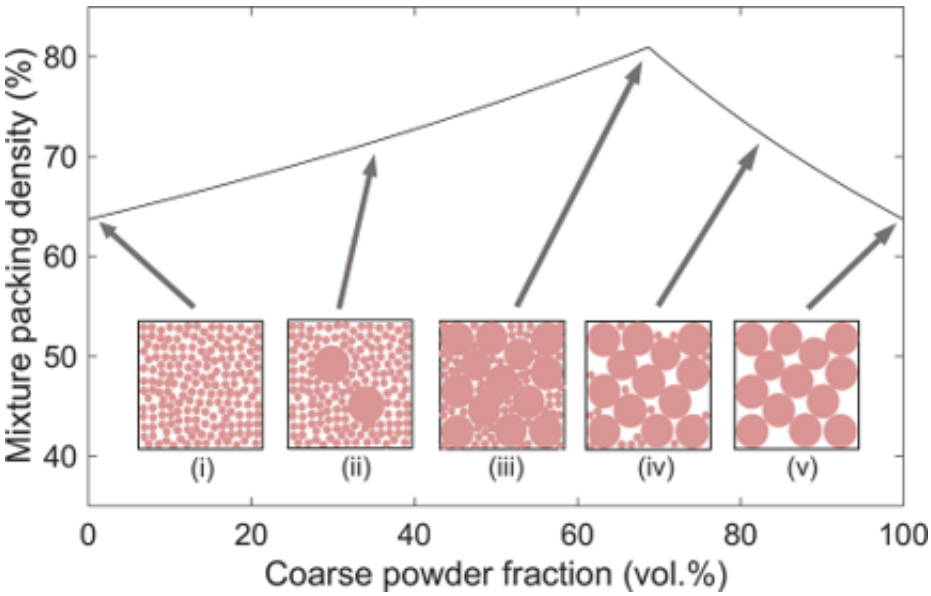

Figure 47: Packing density versus sizes particles [48]

The shape of the powder particles can influence the accuracy of the prints due to the fluid drainage of the binder in the particles. The different fluid drainage can be seen in figure 48. When the powder particles have irregular shapes, the binder will not flow where it is suppose to go, unlike with spherical shapes. The irregular shapes can also cause micro-voids in one region and macro-voids in another reason. In this case the fluid will first flow in the micro-voids before it reaches a macro-void, thus taking more time before the same amount of area is penetrated by the binder than with spherical shapes [34]. Meaning irregular shaped particles can cause inaccurate shapes due to non cohesive binder saturation.

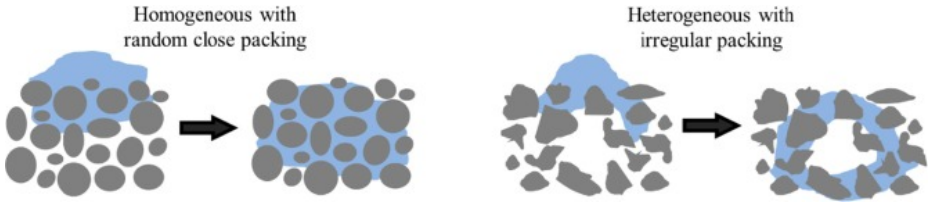

Figure 48: Fluid drainage binder in different powder particle shapes [34]

TGA

Concr3de did earlier TGA and sinter tests for copper binder jetted parts at the TU Delft. The difficulty of the sinterability is what inspired this thesis. The samples were analysed and the runs were repeated to look at the outcome of the copper. The higher temperatures of 1050 ℃ showed a shiny outside. The graphs helped determinate the debinding temperature of 450 ℃ and not 650 ℃ which was originally the debinding temperature. A lower debinding temperature was also tested, but this is right on the edge of the weight loss in the TGA graphs. To ensure that the binder fully burns out a temperature well above the this value is chosen, which is a debinding a temperature of 450 ℃.

Debinding and sintering

In the beginning it was hard to find a working temperature to sinter copper at. One of the causes for the difficulty was due to the furnace itself, as the samples are placed inside a carbon bucket and the thermocouple and pyrometer are outside of the carbon bucket. Furthermore there is quite some convective heat loss due to the argon flow and the size of the furnace. To lessen the heat loss the flow was altered from 250 l/h to 150 l/h. The heat loss can be proven by the measurements of the thermocouple and the pyrometer. As the pyrometer measures a temperature of 1093 ℃ and the thermocouple measures the true temperature, which is 1092 ℃. If there was no heat loss the samples should all be melted as the temperature is nine degrees above the melting temperature of pure copper.
Other literature uses lower temperatures in comparison, 900 ℃ [30], [26] and 1000 ℃ [26] are used and had successful results of a 91 % density. But when the lower temperatures where put into the TGA, samples were not sintered as the powder was still loose and the samples could be crushed by hand. After multiple low temperature sintering runs (1050-1085 ℃) without any results, a higher temperature of 1100 ℃ was put in and darker samples were used. It was already thought the darker samples were oxidized copper, but it was hoped the oxidized copper would not influence the results. This was due to Liu, Zhang and Cui [33] talking about the possibility to reverse copper oxidation in a high carbon environment. Unfortunately the reversing did not happen and the outcome was different than expected, which can be seen in figure 49. The dark tops of the cubes were brittle and could be lifted of the lighter coloured bottoms and there were little droplets of pure molten copper. Thus it is important that the green bodies used for sintering are not oxidized as the melting temperature of oxidized copper (T_m=1232 ℃ [51] and T_m=1326 ℃ [52]) is much higher than the melting temperature of pure copper (T_m=1083 ℃).

Figure 49: S4 samples

Finding the correct temperature and time to sinter the samples fully on the inside and outside was a very precise process. It can be seen in table 21 that the sessions eventually went up by a single degree to have no more loose powder on the outside. Furthermore 1094 ℃ was too hot and and 1093 ℃ was too cold, thus the hold time needed to be adjusted. Which in the beginning was a fixed parameter. It was interesting to see how the different shapes reacted to the sintering temperature. As the cone and dog-bone sintered easily, which was expected as they are both rather thin and have a large area. But to see the difference between the two cubes: one that was shell printed and sintered at 1093 & 1094 ℃ and one that was a solid cube that did not sinter at 1093 ℃ and melted at 1094 ℃. Meaning that the amount of binder in the same shape affects the temperature and holding time that needs to be chosen.
Increasing the run time from 5 to 7.5 hours in 1093 ℃ argon, fully sinters the outside of the samples. To try to enhance the densification even more, the run time was increased from 7.5 to 10 hours in argon. The samples were also sintered in vacuum for 10 hours in two different temperatures, 1075 ℃ and 1080 ℃. The sinter session of 1080 ℃ in vacuum for 10 hours is on the edge of the melting point of copper. As

small molten droplets were found on the plateaus, see figure 50. Thus if it is tried to further densify samples in vacuum, they cannot have a longer run time than 10 hours in 1080 ℃. The run time will need to be increased in vacuum at 1075 ℃.

Figure 50: Droplets on plateau

A heating and cooling rate is necessary to prevent distortion of long and flat samples. Without it the dog-bones will curl up which can be seen in figure 51a. After an input

of a cooling rate of 5 ℃/min, the dog-bone was not distorted anymore. This can be seen in figure 51.

(a) Distorted dog-bone (b) Non-distorted dog-bone

Figure 51: Effect of adjustment cooling rate

But when the heat exchanger was sintered, it still had some small distortion. This can be seen in figure 52. The cooling rate could be adjusted to 2 ℃/min to prevent this distortion from happening in the future.

Figure 52: Distorted heat exchanger

5.2 Testing of samples

The density measurements of all the samples show quite different values, as can be seen in table 36. It can be seen that shell printed cubes (hollow cubes) achieve higher densities than solid printed cubes, thus the total amount of binder in the samples influences the sintered density. It is possible the copper particles fuse easier due to less residual carbon left inside the samples, which leads to a higher densification [53].

Shape	Atm	Time [h]	Temp [℃]	Average density [%]	Standard deviation [%]
Hollow	Argon	1093	10	73	8
Hollow	Vacuum	1075	10	73	5
Hollow	Vacuum	1080	10	74	7
Solid	Argon	1093	10	67	10
Solid	Vacuum	1075	10	57	7
Solid	Vacuum	1080	10	71	7

Table 36: Achieved densities and standard deviations measured with caliper

First it can be seen that the hollow cubes reach a higher density in each chosen atmosphere. The best average density achieved is with vacuum at 1080 ℃, but when looked at the singular samples there is also a difference. Two of the five hollow samples in argon have achieved a density of 82 % and 83 % and three of the five solid samples in argon have achieved a density of 71 %, 75 % and 77 %. Which is both much higher than the average. This also explains the high standard deviation. The big difference in density is due to the placement of the samples inside the sinter furnace. The plateau, see figure 53a, on which the samples are placed before it goes in the furnace and the seven samples, see figure 53b, that were placed on the top level of the plateau for the argon session can be seen in figure 53.

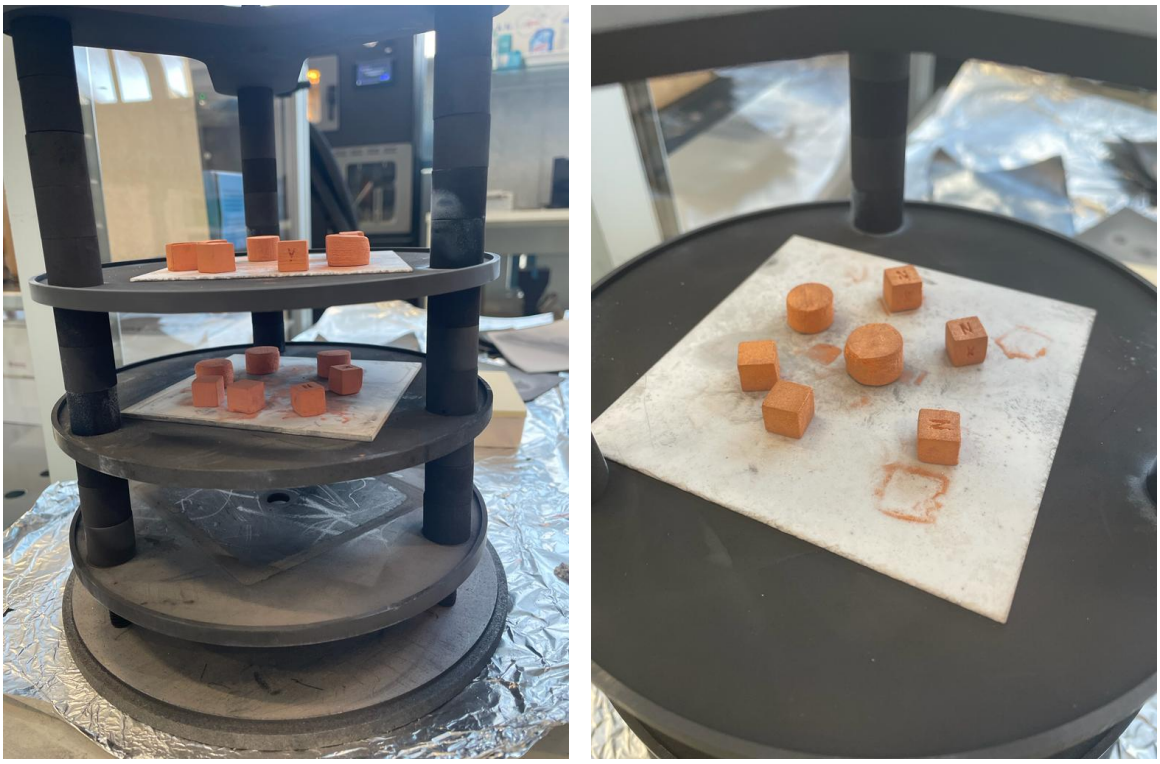

(a) Plateau on which samples are placed (b) Sintered argon samples at top level

Figure 53: Plateau sample placement

The samples that were placed on the top level had the high measured densities. Meaning that the placement of the samples on the plateau also has an effect on the achieved density of the samples. This too was the case for the sintered hollow cubes in vacuum at 1075 ℃, as the three samples placed on the top level have a density percentage between 75 % and 79 %, while the ones placed on the level lower have 65 % and 68 %. The hollow cubes in vacuum at 1080 ℃, have a density of 71 %, and twice 82 % that were placed on the top level, while the ones placed on the level lower have twice 67 %. Both sets of solid cube samples do not differ much depending on the level when sintered in vacuum. They both have one sample that has a density lower or higher of around 15 %. These two big differences can be due to the placement of the sample in the print box. As the placement of the samples influences the final density of the part due to the single roller used by the Armadillo. The parts placed closest to the feed box have a high amount of powder that is compressed by the roller on top of the samples. The parts placed furthest away from the feed box have only enough powder equal to the layer height to be placed on top of the samples. Less powder on top of the samples equals less compression by the roller, which equals to a lower green

and later sintered density. Furthermore the difference between the top level and lower levels can be explained by the gas flow, as it flows from the top to the lower levels. Most of the gas will just flow along the sides of the plateau and not between them, as the plateaus are quite close to each other in height. It can be difficult for the gas to flow through each level, which could lead to lower temperatures on lower levels and thus lower achieved densities. As it is seen that the high temperatures are necessary for the densification of the samples. In vacuum the temperature should be the same on all the levels as there is no gas flow. The difference between the different levels could be due to the debinding of the samples, as the debinding needs to happen in argon with a gas flow. It is possible that due to the lower temperatures on the lower levels, the binder is not fully burned out and leaves more carbon residue. This could lead to lower densities, just like shell printed samples have higher densities because there is less carbon residue [53].

Shrinkage measurements

The 3D laser scanner was impractical. The software gave to many polygonals that needed to be removed during the fusion of the different views to give an accurate shape. Thus the most accurate way to measure the dimensions of the samples was with a caliper. It is expected to have around the same shrinkage in the X- and Y-direction and a higher shrinkage in the Z-direction with binder jetting as it is seen in literature [26]. Table 37 shows the average shrinkage of the samples in the X/Y-direction, the Z-direction, the volumetric shrinkage and the average density. The X- and Y-direction were almost the same in every measurement in the results, thus the average is taken and used.

Shape	Atm	Temp [°C]	Time [h]	S X/Y [%]	S Z [%]	V S [%]	Density percentage [%]
Hollow	Ar	1093	10	11 ± 4	14 ± 3	32 ± 7	73 ± 8
Hollow	V	1075	10	11 ± 3	11 ± 4	30 ± 7	73 ± 5
Hollow	V	1080	10	12 ± 3	12 ± 3	32 ± 6	74 ± 7
Solid	Ar	1093	10	10 ± 6	9 ± 7	25 ± 16	67 ± 10
Solid	V	1075	10	7 ± 5	6 ± 2	19 ± 8	57 ± 7
Solid	V	1080	10	15 ± 5	11 ± 5	35 ± 11	71 ± 7

Table 37: Average measured shrinkage and density

It can be seen that the shrinkage in the Z-direction is only higher with the hollow samples sintered in argon. For the other samples it is the same value and it is even

lower for the solid cubes sintered in vacuum at 1080 ℃. But it can be seen that the highest volumetric shrinkage give the highest densities.

Electrical conductivity

Table 38 shows the comparison of the average electrical conductivity of the binder jetted cuboids with binder jetted rods by Kumar et al [10] and batch 2 of binder jetted rods by Meeder [54].

Shape	Atm	Temp [℃]	Density [%]	Conductivity [S/m]
Cuboid	Argon	1093	72 ± 5	$4.6 \pm 0.6 \times 10^3$
Cuboid	Vacuum	1080	63 ± 4	$4.6 \pm 0.08 \times 10^3$
Rod [10]	Reduced	1075	91 ± 0.3	$5.2 \pm 0.1 \times 10^7$
Rod [54]	Hydrogen	1075	82 ± 2	$3.5 \pm 0.1 \times 10^7$

Table 38: Comparison electrical conductivity

There is a big difference in the electrical conductivity of the binder jetted cuboids and the binder jetted rods.
The big difference is mostly due to the method of measuring. A two point probe multimeter was used, but the lowest value the multimeter gave, was 0.2 Ohm. Regardless how close or far away the measuring rods were placed. Silbernagel et al [55] use a four point probe to measure the electrical conductivity which is much more precise than the multimeter used. Meeder [54] uses a four point probe too and measures values of around 1.3 $10^{-}3$ Ohm. Thus different machinery needs to be used to measure the electrical conductivity of copper, but this was not available during the thesis.
Furthermore it can be seen that the density of the cuboids is rather low, the lowest was 59 % and the highest was 80 %. Which probably would have given low electrical conductivity values. It is difficult to compare how the density affects the electrical conductivity as Kumar et al [10] did not measure the density of the rods, but used different shapes for the density calculations. The real density of the rods is unknown. But Meeder [54] had three different batches and those batches have different densities. Batch 3 with the highest density 91 ± 2 % also had the highest conductivity of 4.44 ± 0.2 $\times 10^7$ S/m. Thus the higher the density the higher the electrical conductivity.
At last the electrical conductivity is best measured on samples with small areas, like the rods. The area of the rods is small enough for the probes to fully cover the area. While the dog-bones had a rather large and rectangular area. This makes it possible for the probes to be placed somewhat misaligned and thus giving small errors in the end result.

5.3 Characterization analysis

XRD

It is discussed before why oxidized copper cannot be used for the sinter sessions, as the two different copper oxides have a higher melting temperature than pure copper. Thus it is important to know when the samples are oxidized before the sintering. As concluded from session S4 oxidized copper has a darker colour, thus it should be rather easy to see when the sample is oxidized. As long as the colour of non-oxidized copper is known. Because the issue of the higher melting temperatures, it is important to know if the copper samples are oxidized before sintering. The colour is a good indication to see if it is already oxidized: if the powder is light in colour like in the top row of figure 31c then it is likely not oxidized. But when the colour is darker it is a possibility, thus XRD can be used to determine this for the darker samples. For both cube samples no oxide peaks were found. Thus the darker colour of the samples is only due to a different amount of binder in them. Both samples should sinter at the same temperatures. The gyroid that cured for 15 hours also shows no oxide peaks, just like the hollow cubes. Thus theoretically all three samples should sinter at the sinter temperature for pure copper.
This was proven faulty when the gyroid was cured next to some other samples. When sintered the gyroid was very brittle and pieces had already fallen off, which can be seen in figure 54. It looks oxidized compared to the samples around it, although according to the XRD it should not be oxidized copper. But it behaves the same as the sintered oxidized samples from the earlier run. It is not known why it behaves like oxidized copper, while the XRD shows no oxidation.

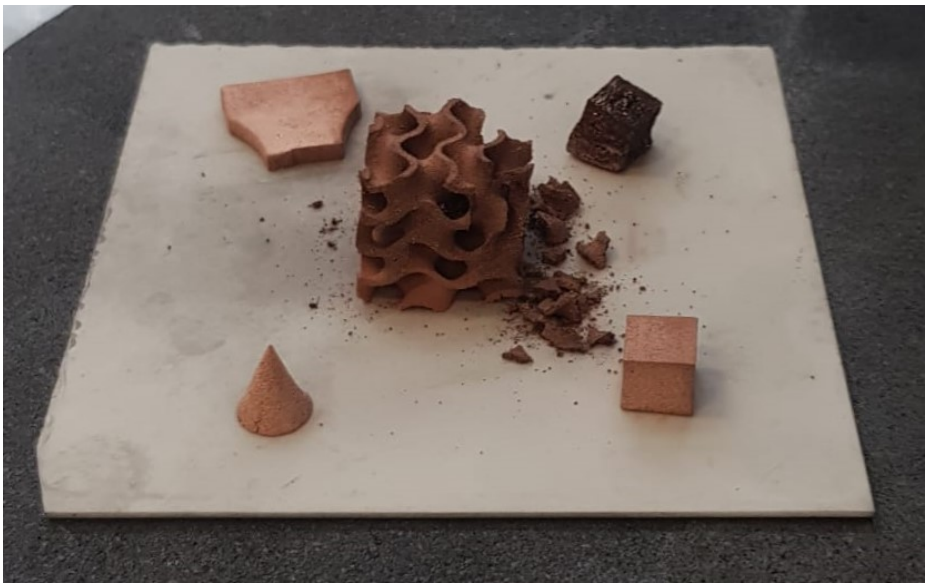

Figure 54: Sintered broken off gyroid

Table 39 shows the achieved maximum force and the E modulus tested with compression testing. The last column shows the density percentage measured with a caliper and scale.

Sample	Atm	Temp [°C]	Time [h]	Fmax [kN]	Emod [GPa]	Compressive Strength [MPa]	Density [%]
1	Argon	1093	10	0.113	0.0118	0.56	51
2	Argon	1093	10	5.088	0.0322	0.78	50
3	Argon	1093	10	0.102	0.0097	0.51	49
1	Vacuum	1075	10	1.797	0.0377	1.27	57
2	Vacuum	1075	10	23.01	0.0289	0.77	59
3	Vacuum	1075	10	33.85	0.0482	0.89	62
1	Vacuum	1080	10	30.37	0.0194	1.00	66
2	Vacuum	1080	10	3.737	0.0401	1.30	56
3	Vacuum	1080	10	1.134	0.0686	0.66	61

Table 39: Compressive strength measurements of different atmospheres

It can be seen that the two discs with the highest maximum force have the highest density. Overall the discs have a very low density compared to the sintered cubes. But this is due to the size difference of the discs. The discs have a sintered height of around 10 mm and a diameter of around 15 mm. The cubes have sintered dimensions of around 9x9x9 mm. The difference in size has an impact on the sinterability of the

material, as bigger samples need to be longer sintered than smaller samples. This lead to sintered discs where the core still had some loose powder. With the bigger discs probably having a more loose powder in the core than the smaller discs.
The low density could be seen during the compression testing, as only three of the samples did not fully break during the testing. But the compressive strength is quite low. This is also due to the F0.2, which is difficult to place when the samples are not fully solid. This low F0.2 value gives the low compressive strengths.
A dummy sample was tested before the 9 samples. This was the smallest sample taken from the batch with a height of 8.29 and a diameter of 12.8. This sample did not break as can be seen in figure 55.

Figure 55: Dummy sample for compression testing

A sample that did not fully break can be seen in figure 56. It shows the difference in height with a non-compressed sample. It also shows the small tear. The other samples broke down into loose powder that was still inside of them.

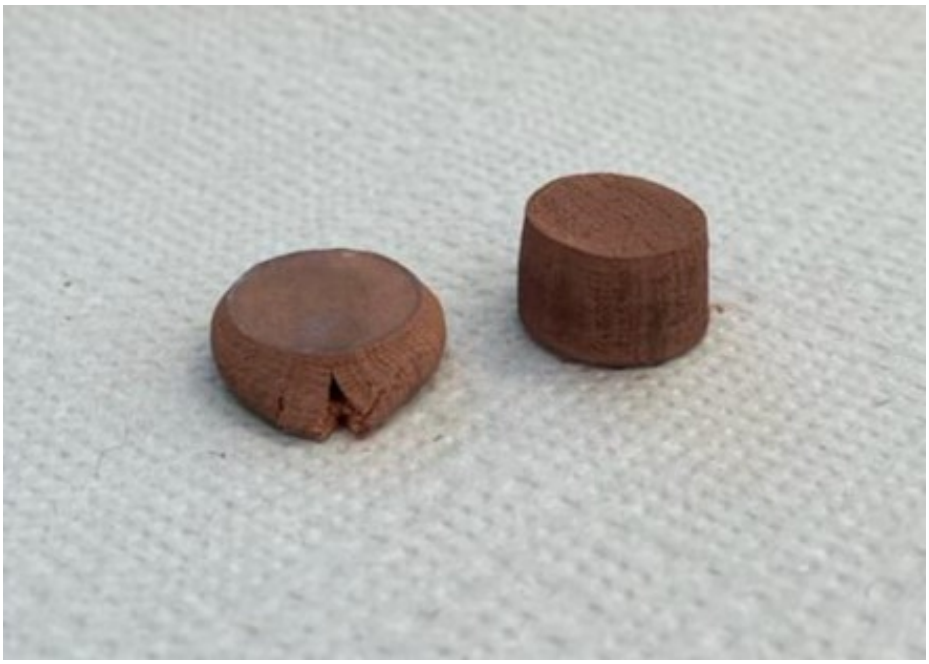

Figure 56: Compressed sample with tear

Thus it was difficult to test the compression strength of the binder jetted samples as the discs were not fully sintered. The samples that did not pulverize during the compression testing were the smallest samples of the three batches and thus had less loose powder in their core. The sample that did not tear and performed the best, was the dummy sample. This was the smallest sample (h = 8.29 mm) and was not weighed beforehand. But it was highly probable that the dummy sample had the highest density due to its small size.

Microstructural characterisation

Most of the pores were on the edge of the samples. There was not a big difference between the amount of pores that could be seen in the vacuum sample compared to the argon sample. Which can be expected as the samples were around the same density. The argon sample had a density of 83 % and the vacuum sample had a density of 82 %. The low porosity that can be seen in both figure 57a and figure 57b is due to the chosen sections being close to the surface.

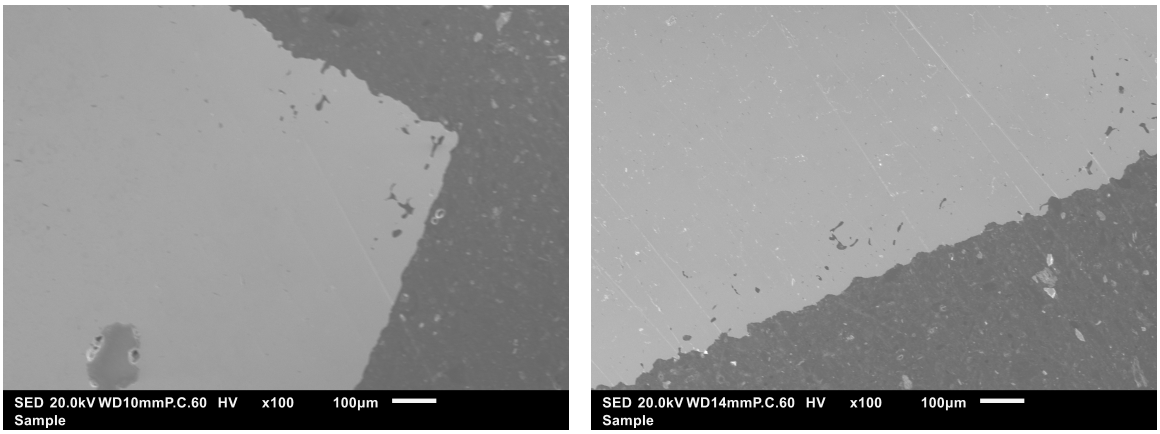

(a) Vacuum sample 100x (b) Argon sample 100x

Figure 57: SEM images of sample sintered in vacuum at 1080 ℃ and argon at 1093 ℃

There is a small amount of carbon present in both samples. It seems the carbon is located in higher concentrations in the pores on the edges of both samples. But the remaining carbon is still scattered across the surfaces. This is likely carbon residue of the binder that is left behind by the pyrolysis.

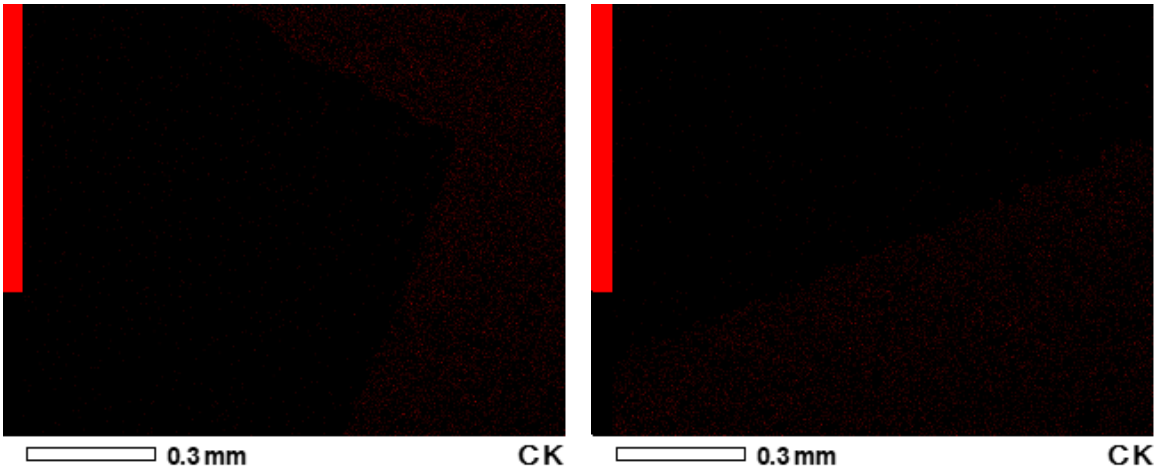

(a) Carbon in vacuum sample 100x (b) Carbon in argon sample 100x

Figure 58: EDS map of carbon in different samples

The oxygen is equally scattered across the samples and the sample holders and not concentrated in the copper. The vacuum sample oxygen map can be seen in figure

59a and the argon sample oxygen map can be seen in figure 59b. Meaning it is not necessary due to oxidation of the copper. It can be due to contamination during the preparation of the samples for the SEM. But it is interesting to see a high concentration of oxygen in the darker eye in the bottom left corner of the vacuum sample. This darker eye can be a big pore that had a small amount of oxygen inside due the printing or curing. During the debinding and sintering it is possible the oxygen became trapped and could not leave the sample.

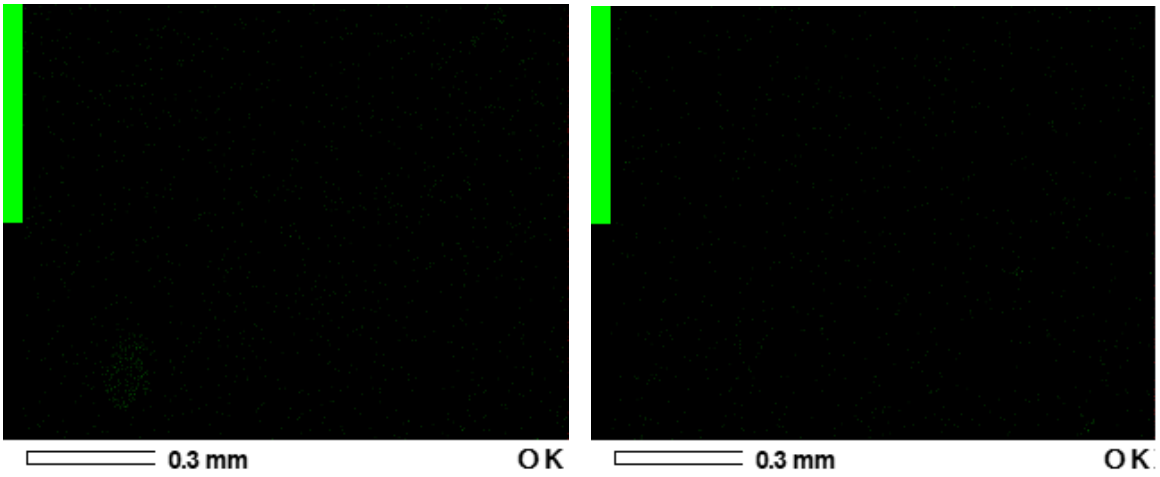

(a) Oxygen in vacuum sample 100x (b) Oxygen in argon sample 100x

Figure 59: EDS map of oxygen in different samples

5.4 Comparison to wrought copper

Table 40 shows the comparison of the achieved values with the Armadillo and how they compare to other copper binder jetted values, wrought copper and metal injected modeled copper. The average values were taken from the wrought copper values, as the values differ greatly. The Armadillo value is the highest chosen value of the three different sintering cycles per property. The same goes for the binder jetted value. It is the highest achieved value by researchers for copper binder jetting and copper binder jetting that also use HIP.

Property	Armadillo	BJT [9]	BJT & HIP [9]	Wrought [13]
Layer height [μm]	100	70	70	-
Saturation level [%]	72	100	100	-
Tensile [MPa]	2.63	144.9	176.35 ± 6.48	318
Compression [MPa]	1.3	-	-	45-330 [56]
E Modulus [GPa]	0.068	-	-	116
Density [g/cm^3]	74 ± 7 %	90.5 ± 0.3 %	97.3 ± 0.1 %	8.93
EC [$\times 10^7$ S/m]	0.00046 ± 0.000008	4.7 ± 0.1	5.2 ± 0.1	5.9

Table 40: Property comparison

The tensile, compression, elasticity modulus and the electrical conductivity values differ greatly from other binder jetted and conventionally manufactured copper. This is partly due to the samples having rather low densities. The different shapes used for the different tests were between 50 and 70 % density.
The electrical conductivity value differs greatly from the other values due to the non-precise equipment. A four-point probe could not be used in time.
The compression and elasticity modulus values are very low due to the samples not being fully sintered. Only the outsides of the discs were sintered, thus it did not behave like a copper metal.
The tensile values are low due to early breakage of the sample. The broken dog-bone did not have loose powder in the broken cross-section. It is possible the dog-bone was already put under stress during the printing and curing. This is likely as all other dog-bones did not survive this process. Therefore there can be some internal stresses inside the dog-bone, which caused the early breakage. It can also be caused by the printhead and the deposition of the binder on the sample. As vertical lines can be seen on top of the sample, which match the path of the printhead.

The highest achieved average density was 74 %, but the highest achieved density overall was 83 % with hollow cubes in argon at 1093 ℃ for 10 hours and 82 % with hollow cubes in vacuum at 1080 ℃ for 10 hours. This still leaves a big difference between the achieved density in this thesis and the achieved density in literature. This is partly due to the difference in measurements, as everybody in the literature uses the Archimedes method which can lead to false values. Table 41 compares the measured densities of the hollow cubes again. First the density was measured with a caliper and scale ($Density_C$), then it was measured with Archimedes ($Density_A$).
Another possibility is due to other researchers having optimized powder. It was said earlier the particle size distribution pays an important factor in achieving high density. Just like the type of furnace used and the gas flow.

Sample	Atm	Temp [°C]	Time [h]	$Density_C$ [%]	$Density_A$ [%]
1	Argon	1093	10	83	87
2	Argon	1093	10	71	93
3	Argon	1093	10	82	88
1	Vacuum	1075	10	75	92
2	Vacuum	1075	10	79	89
3	Vacuum	1075	10	77	87
1	Vacuum	1080	10	82	87
2	Vacuum	1080	10	71	78
3	Vacuum	1080	10	82	87

Table 41: Comparison of measured densities for hollow cubes

The low elasticity modulus and compression strength in comparison to the conventional manufactured copper are rather low. This is due to the testing of not fully sintered samples. The discs still had powder on the inside of the samples, which led to early failure during the testing and thus very low values.
Every density measured with Archimedes is higher than the densities measured with a caliper. This is due to the unknown porosity of the sample. It is expected the samples are porous, but it is unknown where the porosity is. Is it mostly on the outside or is the porosity closed off on the inside of the sample. When the sample is porous, the Archimedes method will give false results as the pores get filled with liquid. This results in a higher density. It can be prevented by blocking off the pores with oil for example. But the results will still be affected as the oil on the sample will influence the total density.

Researcher	Atmosphere	Achieved density
Pisani [30]	Vacuum	53 %
Choong [37]	Vacuum/Argon	63 %
Bai [36]	Hydrogen/Argon	85 %
Miyanaji [26]	Hydrogen	91 %
Kumar [25]	Reduced Atmosphere	91 %

Table 42: Achieved densities of different researchers

Furthermore other factors still have a big impact on the densification of the copper. Different atmospheres or a combination of them can work better. Kumar et al [9] uses a different bimodal powder which can have a big influence on the density [49] and he uses a reducing hydrogen atmosphere, where only argon and vacuum are tested in

this thesis. Table 42 shows the different densities that other researchers have achieved with the binder jetting of copper. But like said before, all these measurements are done with Archimedes, thus it is not known how accurate these results are.

6 Conclusions and Future Scope

1. What are the optimized print parameters?
   (a) What layer height achieves 0.5 mm dimensional accurate shapes?
   (b) What saturation level achieves 0.5 mm dimensional accurate shapes with no bleeding issues?
   (c) What temperature and time need to be used for curing to achieve strong enough green parts that survive the depowdering process?
   (d) How many times can the copper powder be reused for the printing process?
2. What are the optimized post-process parameters?
   (a) What is the debinding temperature that fully burns out the binder?
   (b) What are the sintering temperature and time that fully sinter the samples?
   (c) Which atmosphere or atmospheres, to debind and sinter the samples in, achieves the highest density?
3. What is the effect of the above mentioned optimized process parameters on the functional properties?
   (a) What is the highest achieved density?
   (b) What is the lowest achieved porosity?
   (c) What is the shrinkage in the X-, Y- and Z-direction?
   (d) What is the highest achieved compressive strength?
   (e) What is the highest achieved conductivity?
   (f) How do the achieved functional properties compare to conventional manufactured parts?

High density, small (max 10x10x10 mm) copper parts of 74 $\pm$ 7 % with an accuracy of less than 0.5 mm were successfully printed and post-processed with an Armadillo binder jet printer. The aim of this thesis will be answered by answering the three sub-questions made in the introduction.

What are the optimized print parameters?

The achievement of accurate prints depends on the thickness of the shape and if it is shell printed or not. For both shapes a layer height of 100 micrometer is used with a 3 pulse waveform. Structures with walls less than 5 mm are dimensional accurate with a X-speed of 30 %, which gives a saturation level of 80 %. The solid and shell printed

samples are dimensional accurate with a X-speed of 20 %, which gives a saturation level of 72 %. Both shapes need to be cured for three hours in 110 ℃, so they will be strong enough to not break during the depowdering. With the optimized print parameters the average length of the printed samples is inside the 0.5 mm tolerance. Furthermore the powder can be reused two times before it is oxidized and becomes unusable as it will not give accurate shapes and sinter at the correct temperatures.

What are the optimized post-process parameters?

The post-processing is done in the HTG 200-300/22-1G made by Carbolite Gero 30-3000 ℃. The green parts can be debinded in 100 % argon for 3 hours in 450 ℃ to fully burn out the binder. The debinding is directly followed by the sintering which can be done in different atmospheres. Small shapes, not bigger than 15x15x15 mm can be fully sintered in argon at 1093 ℃ for 10 hours, or in vacuum at 1075 ℃ for 10 hours or in vacuum at 1080 ℃ for 10 hours. The heating and cooling rate of both 5 ℃/min are necessary to prevent distortion of simple shapes like cubes and discs. With more intricate shapes, like the heat exchanger, a lower heating and cooling rate is necessary to prevent distortion. The flow of the argon is 150 l/h, which is relatively low for the furnace to minimize the convectional heat loss during the debinding and sintering.

What is the effect of the above mentioned optimized process parameters on the functional properties?

The highest average achieved density is 74 ± 7 % for 2 mm shell printed (hollow) cubes that were sintered at 1080 ℃ in vacuum for 10 hours. The achieved density is compared to the density of wrought copper, which is 8.93 g/cm^3. But the two hollow cubes that were placed at the top level of the plateau in the sinter furnace both achieved a density of 82 %. This is the same as the two hollow cubes placed on the top level in argon at 1093 ℃. They achieved a density of 83 ± 0.5 %. The density is measured with a caliper and not the Archimedes method. As the Archimedes method gives a false density varying of 4 up to 22 % density due to the porosity of the samples. The average shrinkage of the hollow cubes in vacuum at 1080 ℃ is 13 ± 2 % n the X-direction, 12 ± 4 % in the X-direction and 12 ± 3 % in the Z-direction. The average volumetric shrinkage was 32 ± 6 %. The top level hollow cubes had a shrinkage in the X-direction of 15 ± 0.5 %, in the Y-direction is 16 ± 2 % and the Z-direction is 16 ± 2 %. They both had a volumetric shrinkage of 40 %. Both hollow cubes in argon at 1093 ℃ had a volumetric shrinkage of 40 % too. Thus a higher shrinkage equals a higher density, but the vacuum does not achieve a higher density in this case. The highest achieved compressive strength is 1.3 MPa which is

1 % of conventional manufactured copper. This value is very low due to the discs not being fully sintered. They had a sintered shell and loose powder in the core. One dog-bone was tested and the achieved UTS is 2.63 MPa which is 1 % of conventional manufactured copper. This low value is probably due to internal stresses inside the dog-bone, which was caused by the printing and curing process. Or it can be due to inefficiency of the printhead on the location of the break. The PIP testing could not be performed due to errors given by the machine. The electrical conductivity could not be measured correctly as there was no access to precise enough equipment.

6.1 Recommendations for future research

There are multiple recommendations for future research. These recommendations are either coming from limitations from this research, were outside of the scope, or there were technical limitations.

Influence of placement in print bed

How will the placement of the samples in the print bed influence the properties of the sintered samples? Which orientation will be the strongest? Studies have shown that the compression done by the roller differs on the location in the print bed. At the start of the print bed the compression will be higher than at the end of the print bed, which will affect the green strength and sintered strength of the samples. The orientation affects the strength too as it is dependent on the binding strength between the particles [34]. It is interesting to see what the differences will be for copper printed with an Armadillo binder jet printer.

Influence of compression before and during printing on print bed

How can compression on the print and feed bed influence the density of the green and sintered parts. The print and feed bed can be compressed by hand before printing, but this is not accurate as the amount of force added is different each time. During the printing the print bed can be compressed by having an z-axis offset. It is interesting how different offsets and compression before printing can influence the density, but also the accuracy of the prints.

Influence of flow rate during post processing

How does the flow rate influence the sintering of the samples? It is possible for the flow rate to influence the debinding and the sintering process. In this thesis a very low flow is taken, to minimize the convectional heat loss. However it might be interesting to see if the flow has other influences on the sinterability of the copper.

Influence of different atmospheres during post processing on functional properties

How can different atmospheres influence the sintering of the samples? In this thesis only 100 % argon and vacuum are used. In the TGA a combination of hydrogen and argon is used, but the hydrogen was not used during the sintering due to the costs. It is interesting to see how the copper will react to the other atmospheres of inert gasses or a combination of them. Which atmosphere will achieve the highest density.

Influence of big and thick shapes on the post processing parameters

How much do the post process parameters need to be changed when big and thick shapes are printed with binder jetting. This thesis only focused on small and thin shapes, but it is a different optimisation process for big and thick shapes. Is it possible to create some kind of formula that helps determining the perfect sinter temperature and holding time?

Possibility of reversing copper oxidation during post processing

How can the debinding and sintering cycle be adjusted to reverse the copper oxidation into pure copper. Copper powder is expansive and can only be reused a handful of times. Thus it can be useful when slightly oxidized, accurate green parts can still be sintered and come out as pure copper. Liu, Zhang and Cui [33] talk about the possibility of the reduction of copper oxide by mechanically alloying with graphite. With a higher carbon content almost all copper oxide could be converted back into copper. The LHTG 200-300/22-1G has a carbon bucket in which the samples are placed, thus it has a high carbon environment.

Possibility of improving density with different factors

Which extra treatments can be done to further improve the density after the sintering? Kumar [25] already showed Hot Isostatic Pressing can improve the density of binder jetted copper up to 99 % if the density before HIP is already above 90 %. Are there other methods that can be used to improve the density to almost 100 %? Or can different binders improve the density of copper printed binder jetting. Bai and Williams [35] already concluded denser centers were achieved, but a more porous outer shell. It is interesting to see if this can be further optimized.

A Printlog

The print log is divided into three printing sessions. The first printing session was to get familiar with the printer and with significant help from the company. The samples printed were used for the TGA sessions. Old printing parameters were used to see how the green parts would come out. The second printing session was to optimize the printing parameters so dimensional accurate prints would come out. The dimensional accurate prints were for the optimization of the post-process parameters. The third printing session was to print the necessary dimensional accurate shapes for the statistical values of the density, shrinkage and mechanical testing measurements.

A.1 First session

The first print session done was largely a get to know the printer and see how the prints will appear. Only a small amount of samples was printed to get familiar with the machine and see how it runs. The printed samples can be seen in table 43.

Print	Shape	Waveform	X-speed [%]	Layer height [μm]	Amount printed	Survived
ps1p1	Cu	3P	60	100	11	11
ps1p1	He	3P	60	100	1	1
ps1p1	Gy	3P	60	100	1	1
ps1p2	Cu	1P	60	100	10	2
ps1p2	He	1P	60	100	1	0
ps1p2	Gy	1P	60	100	1	0
ps1p3	Cu	3P	60	100	4	4
ps1p3	HC	3P	60	100	4	3
ps1p4	Cu	3P	60	100	4	4
ps1p4	HC	3P	60	100	4	4

Table 43: Prints from printing session 1

Two prints were run and only the waveform was changed from 3P to 1P to see the difference of the saturation level. As all the cubes (Cu) printed with 3P had bleeding on the bottom. The gyroid (Gy) and heat exchanger (He) had no bleeding issues, mostly due to their thin walls. When 1P was used to see if there would be no bleeding issues, almost all samples broke during the depowdering. Making the 1P waveform to weak to work with for copper. For print 2, 3 and 4 the powder was reused for printing. Print 3 and especially print 4 turned out darker than the previous samples. This is due to the oxidation of the copper that happens during the curing. Even

though most of the prints of print 3 and 4 survived, they became less dimensional accurate every print, due to excessive bleeding. A view during the printing of print number 1 can be seen in figure 60.

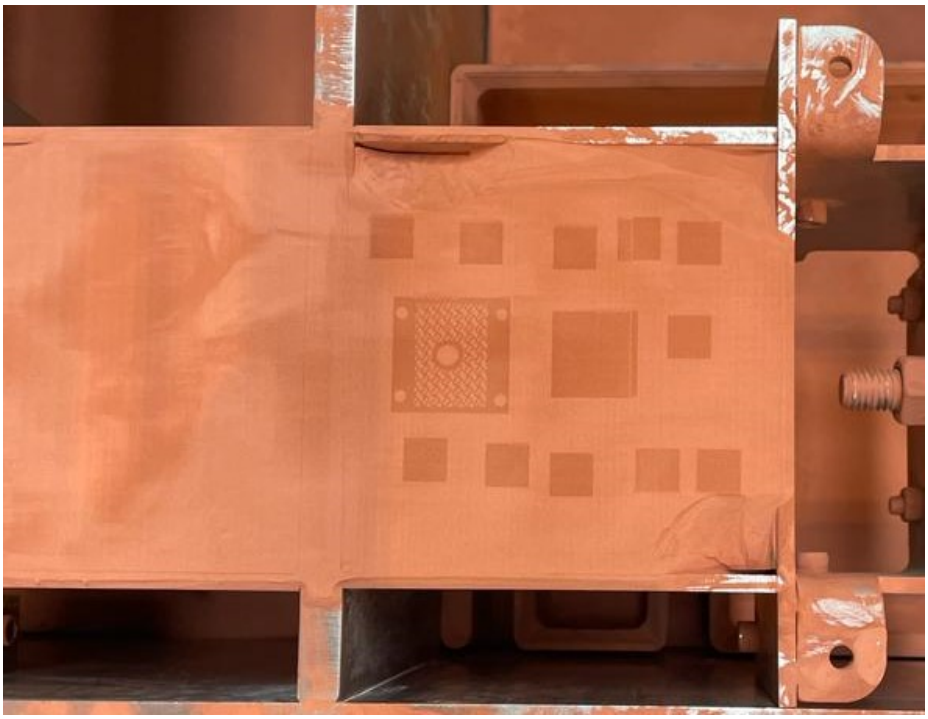

Figure 60: View during print number 1 of print session 1

Concluding that the 3P waveform at 60 % with a layer height of 100 micron has a too high saturation level. Furthermore, powder should not be reused more than once to prevent it from oxidizing during the curing, as the oxidation negatively affects the dimensional accuracy.

A.2 Second session

Print session 2 was for optimizing the printing parameters so the printer gave dimensional accurate shapes. The dimensional accurate shapes can be used for the optimisation of the post-process parameters. Thus many different printing parameters were tried and many samples were printed. Mostly due to the big amount of samples were necessary for the amount of sintering sessions needed to achieve the right temperature and time. All the different samples printed can be seen in table 44. The cubes and the hollow cubes are both 10x10x10 mm, the hollow cubes have 2 mm thick walls thus a volume of 8x8x8 mm is void on the inside. The cones are ...

mm high and they have a diameter of ... mm. The discs are ... mm high and have a diameter of ... mm. The dog-bones follow the standard of ISO 6892-1, they have a length of ... mm. The gyroid is .. mm high, . mm wide and . mm deep. The heat exchanger is .. mm high, . mm wide and . mm deep. The orientation of the samples is for some more important than others. The solid cubes have calibration markings on them, they have an X-, Y- and N-side, thus they need to be placed in the correct planes. The hollow cubes can be placed perpendicular of the X-, Y- and Z-directions. The cones, discs and the dog-bones need to be placed flat on the print plate. This is due to the irregular shrinkage, as the x- and y-direction should have the same amount of shrinkage, the Z-direction shrinkage will likely be higher. Thus to keep the radius of the cones and discs more or less the same in every direction, the cones and discs need to be placed the right side up. The dog-bone needs to be laid flat on the print plate, for the same reason as the discs and cones. The Z-direction, in this case the height, is fine if it shrinks more, but the X- and Y-direction are in proportion and need to shrink at the same percentage. The gyroid and heat exchanger just need to be placed the right side up.

Print	Shape	Waveform	X-speed [%]	Layer height [μm]	Amount printed	Survived
ps2p1	HC	3P	60	50	9	9
ps2p2	HC	3P	60	100	9	6
ps2p3	HC	2P	60	100	9	2
ps2p3	Cu	2P	60	100	67	53
ps2p3	Co	2P	60	100	9	4
ps2p4	Do	3P	30	100	7	0
ps2p4	Di	3P	30	100	4	2
ps2p4	Cu	3P	30	100	8	2
ps2p4	HC	3P	30	100	9	7
ps2p4	Co	3P	30	100	9	5
ps2p4	Sp	3P	30	100	3	0
ps2p5	Do	3P	30	100	3	0
ps2p5	HC	3P	30	100	9	7
ps2p5	Co	3P	30	100	9	5
ps2p5	Cu	3P	30	100	9	0
ps2p6	Cu	2P	60	100	15	14
ps2p6	Di	2P	60	100	4	4
ps2p6	HC	2P	60	100	9	8
ps2p6	Co	2P	60	100	9	7
ps2p7	Cu	2P	30	100	15	13
ps2p7	Di	2P	30	100	4	4
ps2p7	HC	2P	30	100	9	9
ps2p7	Co	2P	30	100	9	8
ps2p8	Gy	3P	30	100	6	4

Table 44: Prints from printing session 2

Printing number 1 had hollow cubes to see if they would bleed or not. As the hollow cubes only have binder on the outsides of the cube and loose powder on the inside, the total amount of binder in them would be much lower compared to normal cubes. The hollow cubes had a smaller layer height, meaning the binder saturation would even be higher. They had small bumps on the bottom. Thus they had small bleeding issues. The only problem was the leaking powder on the edges. To still print successfully a rather high feed height was put in.
Printing number 2 printed 9 hollow cubes again, but with a bigger layer height and thus lower saturation level. The leaking was significant during the printing and 3 out of 9 hollow cubes were distorted. These hollow cubes with a lower binder saturation

still had a small bump on each bottom. Both views during the printing of print 1 and print 2 can be seen in figure 61.

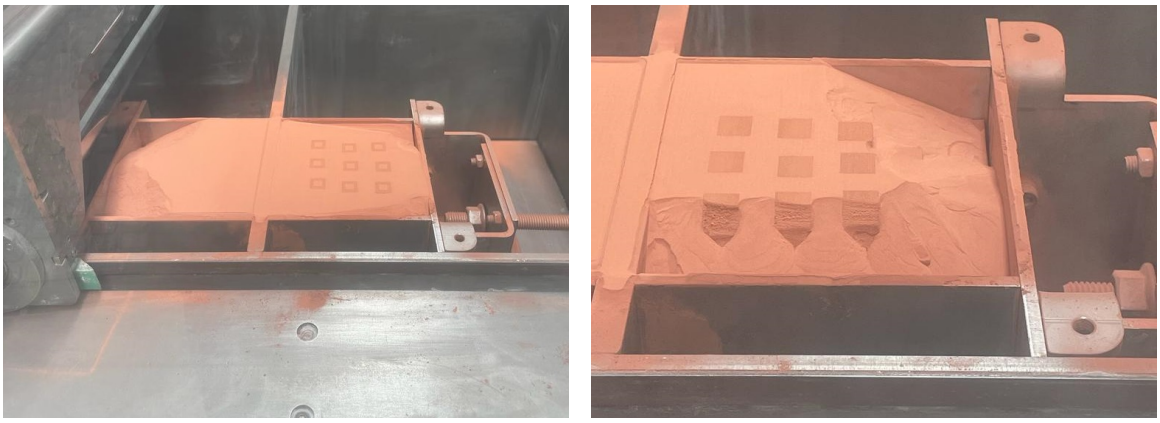

(a) View of print number 1 (b) View of print number 2

Figure 61: Leaking powder during printing

Thus the binder saturation was still too high, even when an infill pattern was used. To change the saturation level, the layer height could be adjusted higher, the waveform could be changed or the X-speed could be adjusted lower. As the layer height of 100 micron is already rather high, it was chosen to keep the layer height on 100 micron and to adjust first the waveform and later the X-speed of the print head. The other problem of leaking powder was mostly fixed by filling the edges of the reduction bed with metal epoxy. Furthermore a different waveform was made by the company. This 2P waveform should have less pL of binder than the 3P waveform. Thus the saturation level should technically be lower.

Printing number 3 was a big print, as it was expected the samples would come out well with a lower saturation level and have less leaking. The leaking problem had been mostly solved, as there were only small corners that leaked powder. But these leaking corners stayed small during the printing, meaning the 95 % of print plate could be used for placing samples. Multiple samples did not survive the printing and depowdering process. This was possibly due to the failed removal of the print bed where the samples on the bottom were accidentally destroyed by the removing contraption, a small pitchfork. Over half of the hollow cubes and cones (Co) did not survive, these were also the thinnest samples of the print number, making them more fragile than the solid cubes. After curing the samples looked darker and were anything but dimensional accurate. They had bleeding issues on the bottom and the layers itself seemed to bleed to the outsides. Furthermore the outsides of the cubes

looked porous as holes could clearly be seen all around the surface.

Although the 2P waveform should have a lower saturation level according to the dropwatcher, the outcome proved otherwise. The saturation level seemed higher than with the 3P, as the samples displayed a darker colour and not only bleeding issues on the bottom, but also on the sides. It seems that the 2P waveform is not yet stable enough to use.

Print number 4 printed many different shapes with a 3P waveform at a lower X-speed of 30 %. Thus a lower saturation level. The reasoning behind the non-survived samples probably is the rather quick removal of the samples out of the curing oven. The dog-bones were not all fully cooled before the depowdering started, which made the samples still a bit soft. The discs (Di) were temporarily stuck to each other, as they probably were too close on top of each other. They could be separated by hand and had small bleeding issues on the bottom. The spirals (Sp) were just to small and thin for these print parameters. The cones were still a bit soft and could be slightly pushed in, but it seemed there were almost no bleeding issues, only the cubes had the slightest bumps on the bottom.
Print number 5 printed more shapes with 3P at 30 % X-speed. The dog-bones (Do) already broke during the printing, which is probably due to the z-axis offset. The silicone sheet changes shape during the moving up and down of the print plate when the z-axis offset has a value. The shape changing of a convex to a crater shape and back again may be the reason behind the cracks in the dog-bones. When the z-axis offset is zero, the print plate will only move down and the silicone sheet should stay in the same shape. Multiple cubes had soft bottoms that could be pushed together and the cones were rather weak too. Before printing there were some air bubbles in the re-circulation system of the printhead. This caused a need for different settings of the pressure of the fluids until there were no bubbles left. This was probably due to small temperature and humidity changes of the air around the printer. The change of these settings may lead to a slight difference in the saturation level. Although some prints were still somewhat soft, the hollow cubes came out very dimensional accurate with no bleeding issues.

Thus the 3P waveform at 30 % causes almost no bleeding issues for the hollow cubes and the thin shapes, the dog-bones and cones. The solid cubes and discs had small bumps each, but these were significantly smaller than the bumps at 60 % or with the 2P waveform. It may be better to cure the samples a little bit longer in the oven to prevent the possibility of distorting the samples during the depowdering. The 2 hours of curing in the oven is changed to 3 hours. Furthermore the samples need to be fully cooled down before the depowdering can start.

Print 6 and 7 was used to double check how the 2P prints came out. Print 6 repeated the already used before printing parameters of 2P and 60 % X-speed and print 7 had 2P and 40 % X-speed to see how the lower saturation level would look. Both prints had a high amount of samples that survived the printing process. It seemed the cones especially were a little bit stronger due to the longer curing time. Printing 6 had some leaking issues in the beginning, but these were solved by moving the print plate and adjusting the feed height to a higher value. Just like before with the 2P prints, the prints still came out rather dark with lots of bleeding issues. The 40 % still had more bleeding issues than the 3P prints. The top of the 40 % hollow cubes samples was light, but the bottom had a darker colour. Meaning there is possibly a big change in the saturation level of the top of the hollow cubes compared to the bottom of the hollow cubes. There was no difference in powder as the powder in the feed box was from the sample container.

Thus it is clear the 2P should be further developed by the company. The 3P with 30 % maximum should be used for now as it has the least amount of bleeding issues. The curing time change seemed to work well and is kept at 3 hours from now.

Print 8 were six gyroids with 3P at 30 % X-speed. Two of the six gyroids broke, most likely during the printing. They were the two closest to the feed bed. There was a mishap by the removal of the print box out of the curing oven. Instead of the predetermined 3 hours, the prints cured overnight, which was about 15 hours. The prints had a dark colour, likely due to oxidation and during the depowdering some corners broke, but this is due to the fragile design of the gyroid itself.

Concluding print session 2, the best print parameters are a layer height of 100 microns and a waveform of 3P with a maximum of 30 % X-speed. It is good to test the 20 % X-speed to see if this solves the bleeding issues on the solid cubes. A curing time of 3 hours works well. It should not be less as the prints can be soft and it should not be longer as the prints will come out oxidized.

A.3 Third session

The third print session done was to print dimensional accurate objects for the final measurements and testing. The samples are printed with the optimized print parameters. At least five shapes for each post-processing session are printed, with five shapes extra to accommodate for breakage or distortion during printing, depowdering or transport. The shapes printed are cubes, hollow cubes, discs, dog-bones and two difficult, but thin shapes, like a gyroid. The printed samples can be seen in table 45.

Print	Shape	Waveform	X-speed [%]	Layer height [μm]	Amount printed	Survived
ps3p1	Cu	3P	20	100	10	8
ps3p1	HC	3P	20	100	10	8
ps3p1	Do	3P	20	100	10	0
ps3p1	Di	3P	20	100	10	10
ps3p2	Cu	3P	20	100	10	8
ps3p2	HC	3P	20	100	10	7
ps3p2	Do	3P	20	100	10	0
ps3p2	Di	3P	20	100	10	8
ps3p3	Cu	3P	20	100	10	9
ps3p3	HC	3P	20	100	10	8
ps3p3	Do	3P	20	100	10	1
ps3p3	Di	3P	20	100	10	7
ps3p4	Do	3P	20	100	10	0
ps3p5	He	3P	20	100	4	2
ps3p5	Gy	3P	20	100	2	2

Table 45: Prints from printing session 3

The first two prints were done on the Armadillo 2000 printer. That printer was the only R& D printer of the company at the moment and everything was printed on it, from ceramics to wood to stone to metal. Furthermore this meant that multiple different binders were used and tested to print dimensional accurate samples. These binders vary from organic to inorganic formulas and are not always compatible. To change the binder in the machine is dependent on the compatibility of the binder a time consuming process. When the binders are compatible, the new binder can be switched out for the old binder and the system can be flushed. When the binders are not compatible, there needs to be a liquid, also called flush, that is compatible with both binders. The flush is used to flush out the old binder, when that is done the flush can be flushed out with the new binder. Not only the flushing takes a long time, the new liquid in the system needs to settle for preferably 24 hours. Not only had the R & D department access to three printers instead of one, to prevent the time consuming process of switching between incompatible inks, each printer got its own binder type that should be printed with. This meant there was a new printer, the Armadillo Chiron, specifically used for metal binder jetting.
There can be some inconsistencies with the new printer, the fluid system is a bit different and can cause issues as it is less stable than the fluid system of the Armadillo 2000. On top of a different fluid system, there was a binder change. The new binder needs to settle preferably for a full day. Furthermore, as the printer was an old model

and it just got placed, some parameters were still unknown, like the x offset that needs to be adjusted to prevent a misalignment in the print. Figure 62a shows how the misalignment looks in the print bed during the first print on the Chiron. Figure 62b shows a layer of print five with four heat exchangers on the left and two gyroids on the right. After ps1p1 x offset was adjusted, so no more misalignment was visible.

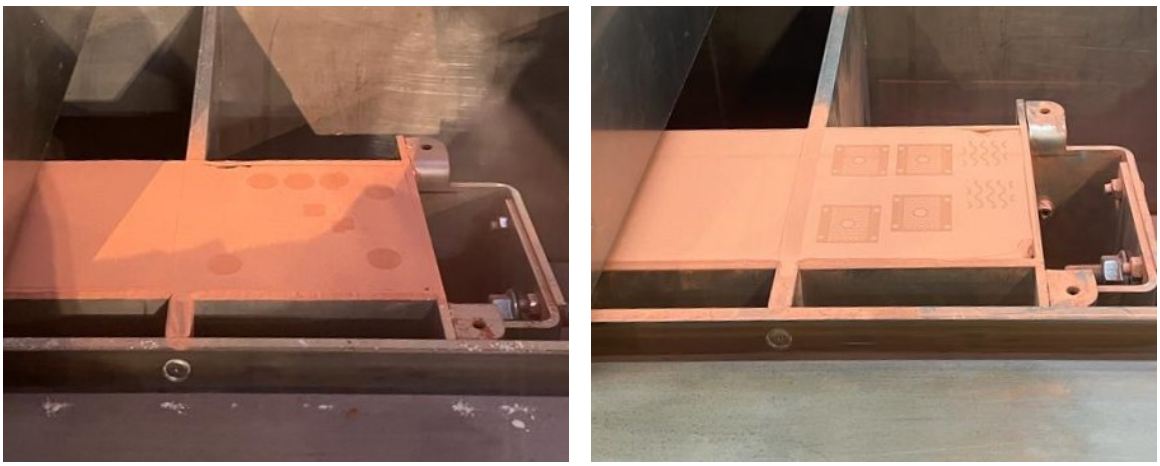

(a) Misalignment in print bed during ps3p1 (b) View of heat exchangers during ps3p5

Figure 62: Prints during print session 3

B TGA graphs

In figure 23 to 64 the different TGA graphs can be seen. There were four runs, the data can be seen in table 46. As said before the third test went wrong, the copper was molten when it was removed from the crucible. This was probably due to the high usage of the thermocouple, it was already scheduled for a renewal. Due to the high usage, the temperature went higher than it was supposed to and it melt the copper instead of only sintering it.

	Debinding		Sintering		Atmosphere
Sample #	Temp [℃]	Time [h]	Temp [℃]	Time [h]	
T1	600	3	1050	5	80% Ar 20% H
T2	450	3	1050	5	80% Ar 20% H
T3	400	3	1050	5	80% Ar 20% H
T4	400	3	1025	5	80% Ar 20% H

Table 46: TGA input data

B.1 Debinding temperature

The second sample is tested at a lower debinding temperature to see if the the sample will correctly debind. Figure 63a shows the TGA of sample T2 and figure 63b shows the derivative of the TGA of sample T2, this time it is not zoomed in on the debinding temperature. Figure 63 show the same peak around the same temperature. The mass is flat just a bit after the temperature reaches 450 ℃, meaning all the possible mass is burned out during the debinding process.
The third sample melted and will not be further discussed.
The fourth sample has a debinding temperature of 400 ℃. Figure 64 shows the TGA and the derivative in one figure of sample T4. It can be seen that during the debinding, the mass still very slightly decreases. Meaning it needs a little bit of a higher temperature to fully burn out the binder, as the mass is flat for sample T2. Furthermore the sample came out black, a lot of carbon was still on the outside of the sample which was left over from the binder. The carbon is easily wiped away, but there was a lot less carbon on sample T2 when it came out of the TGA when compared to T4. Thus the best debinding temperature is $T_d = 450$ ℃.

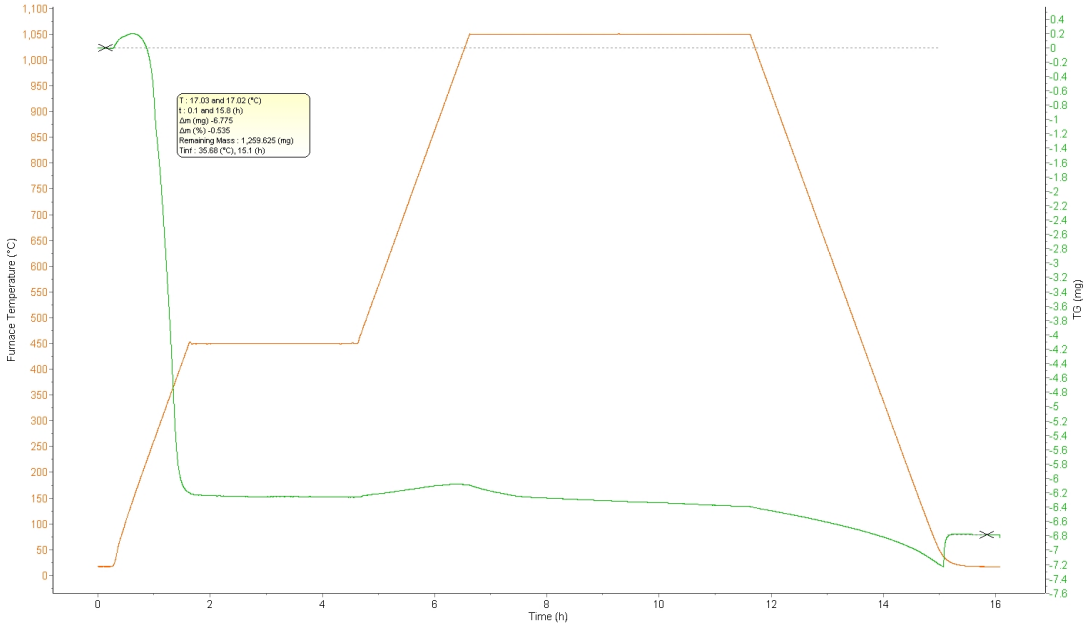

(a) TGA T2

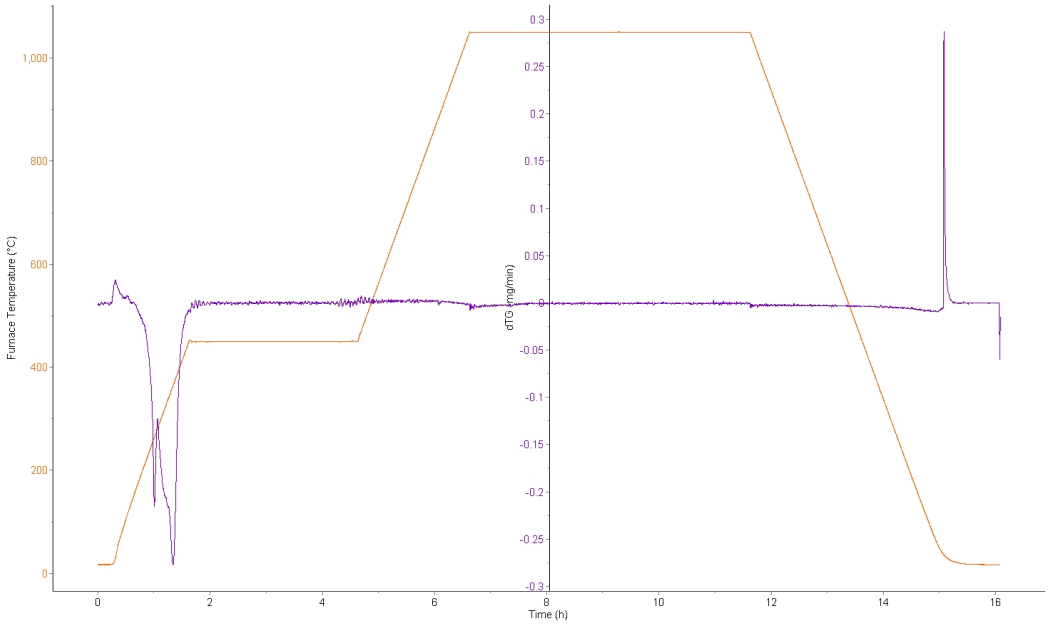

(b) TGA derivative T2

Figure 63: TGA and TGA derivative of sample T2

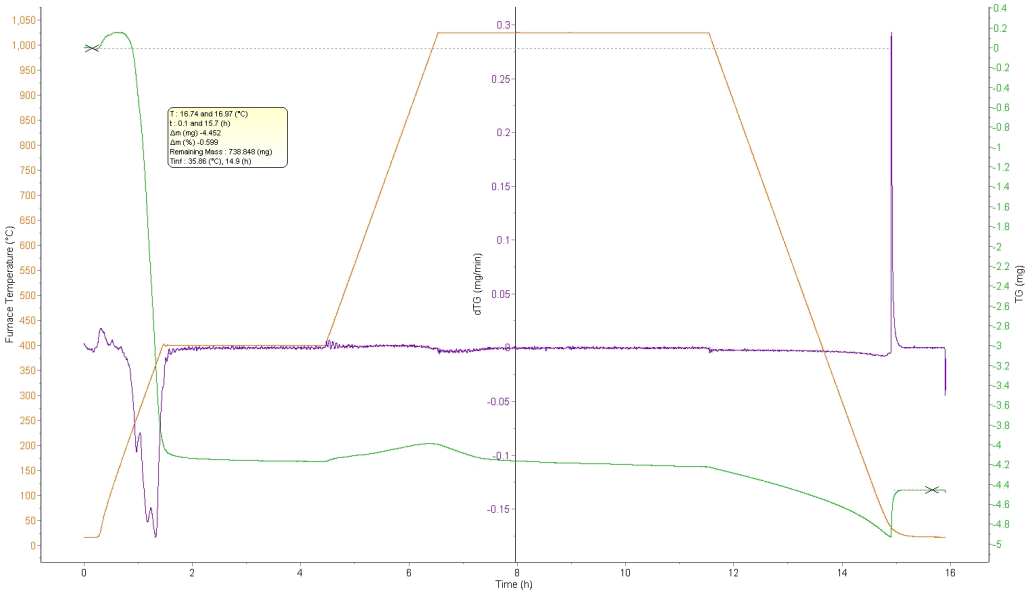

Figure 64: TGA and derivative T4

C Debinding and Sintering log

The debinding and sintering happened in multiple sessions after each printing session. The sinter and debinding sessions, from now on, called sinter sessions (S#) as the debinding and sintering happens as one process. The sinter sessions will be divided in which printing it was printed.

First session

The input data for the first debinding and sinter sessions, can be seen in table 47.
For the first sinter run, the same parameters were used from the TGA data. As the T2 run gave good results, they were repeated for the S1 run. The S1 samples however did not sinter, they still had loose powder on them. To try to get sintered samples, the temperature was increased to 1075 for S2 and 1085 for S3. But just like the samples from S1, the samples from S2 and S3 were not sintered fully. One of the samples fell on the ground during the removal and it broke in two. Meaning the whole sample did not come close to sintering even.
As seen in earlier research and being this close to the melting temperature of copper (T_m = 1083 ℃), the samples should at least show some form of sintering. There are two known reasons behind the uncompleted sintering.
The first one is due to the usage and placement of the pyrometer. The sintering furnace uses two ways to measure the temperature: a pyrometer and a thermocouple. The thermocouple measures the true temperature, which is a few degrees off of the input temperature. Furthermore the pyrometer and the thermocouple are placed outside of the bucket, while the samples are placed inside of the bucket.
The second reason behind the unsintered parts is due to the convectional heat loss of the gas flow. The first run has a flow of 250 l/h argon, but this was lowered to 150 l/h to minimize the convectional heat loss. The argon gas comes in on the outside of the bucket next to the heating elements and it is suctioned out, on the bottom on the inside of the bucket. The argon has a flow of 150 l/h, making it possible the temperature is influenced by the new gas that comes in and thus cooling the inside down.
A possible solution to this problem, is to equip the furnace with a new thermocouple that will go straight into the bucket from the top. The furnace has the ability to add this feature. In this case the temperature will be measured right next to the samples, which will give the most accurate results. This change was however not made during this thesis.

	Debinding		Sintering		Atmosphere	
Batch	Temp [℃]	Time [h]	Temp [℃]	Time [h]	Type	Flow [l/h]
S1	450	3	1050	5	Argon	250
S2	450	3	1075	5	Argon	150
S3	450	3	1085	5	Argon	150
S4	450	3	1100	5	Argon	150
S5	450	3	1092	5	Argon	150
S6	450	3	1095	5	Argon	150

Table 47: Input data sinter session 1

The second three sinter runs (S4, S5 & S6), gave other problems. A higher temperature was put into the machine for S4, but this temperature was too high. Furthermore a different sample was used, one that appeared darker than the other used samples, possibly it being oxidized copper. It was hoped the oxidized copper would not give issues, as some research explained it could be possible to reverse the oxidization. Due to the presence of carbon it is possible for the copper oxides to transform back into pure copper with carbon dioxide [33]. This reaction however did not happen. The results of S4 can be seen in figure 65.

Figure 65: S4 samples

Figure 49 shows small droplets of molten copper, a darker area on top of the cube and a lighter area on the bottom. The darker top was hard and could be lifted off the cube, the lighter area was still powder. The reasoning behind the three different results on the same cube is the powder being copper oxides in combination with pure copper. The copper oxides, tenorite (T_m=1326℃) and cuprite (T_m=1232℃), have higher melting points than pure copper. Any pure copper that was still in the cube has melted, due to the temperature being above the melting temperature of copper right next to the samples, while the rest of the cube is still powder as they are copper oxides. Figure ... shows S5 and S6 cubes that still have loose powder coming from them. Meaning they are not fully sintered. Furthermore they could be compressed by a finger and leave an impression.

Second session

During other experiments of the sintering furnace, there were some issues and the thermocouple broke down. This meant that a new thermocouple needed to be installed, thus giving different values and having a different temperature offset.
Table 48 shows the sinter sessions with a new thermocouple and thus a different true temperature. The old thermocouple needed a higher temperature for the input, while the new thermocouple needs a lower temperature for the input.
The sessions S7 to S11 were done in Argon, as the correct sintering temperature was found in argon. Session S12 was done in vacuum to see how the samples will compare in different atmospheres. It is important to note that the session cannot start in vacuum. Thus the debinding is done under argon with a gas glow of 150 l/h, until the samples have debinded for three hours. Then the cycle is done in vacuum until the sintering is done and the furnace has reached a temperature again of 300, then the furnace is flushed with argon and it cools down to room temperature.

	Debinding		Sintering		Heating & cooling rate		Atmosphere	
Batch	Temp [℃]	Time [h]	Temp [℃]	Time [h]	Heating [℃/min]	Cooling [℃/min]	Type	Flow [l/h]
S7	450	3	1075	5	5	-	Argon	150
S8	450	3	1090	5	5	-	Argon	150
S9	450	3	1095	5	5	-	Argon	150
S10	450	3	1093	5	5	-	Argon	150
S11	450	3	1094	5	5	5	Argon	150
S12	450	3	1093	7	5	5	Argon	150
S13	450	3	1075	7.5	5	5	Vacuum	150
S14	450	3	1080	7.5	5	5	Vacuum	150

Table 48: Input data sinter session 2

Sessions S7 and S8 were still not sintered fully. The sintering temperature of S7 was still much too low, thus the temperature was increased with twenty ℃. The S8 samples did show some kind of sintering, as it was smaller than the samples of S7. It also had a pincushion distortion and still had some loose powder on it. The samples can be seen next to each other in figure 66. A little bit of copper powder, left behind by sample S8, can still be seen in the right bottom corner.

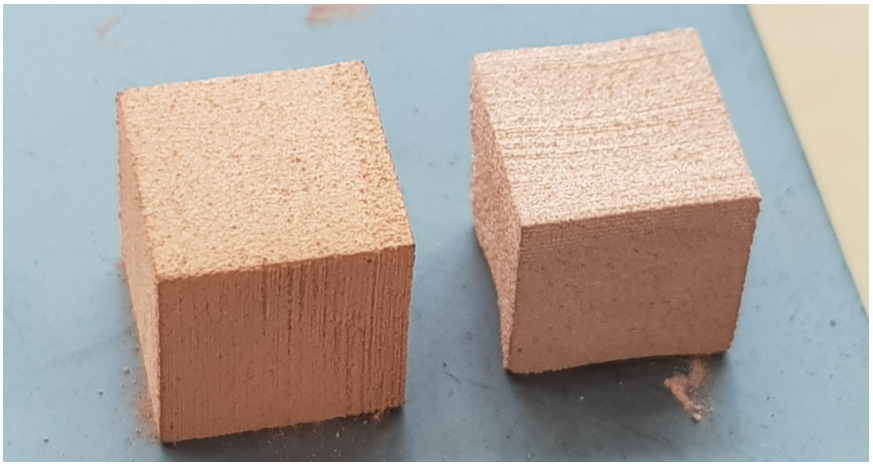

Figure 66: Difference between sintered samples S7 (left T_s=1075℃) and S8 (right T_s=1090℃)

For S9 a different sample was added to see how it would come out next to the normally used sample. The green samples can be seen in figure 67a. The shell printed cube is on the top and the cube with x, y and n engraved on it is on the bottom. This cube

is printed with binder on the whole area of the cube for each layer. The cube has little distortion, but as it is only used for finding the correct sintering temperature and not other measurements, it should not be an issue. The outcome for the S9 run is interesting, see figure 67b. The fully filled binder sample has melted partially and has carbon residue all over it from the burned out binder, while the shell printed sample was sintered fully. Thus the amount of binder can influence the sintering of the copper samples.

(a) Green samples S9

(b) Sintered samples S9

Figure 67: Samples S9 T_s=1095℃

To prevent the samples from melting and to see how different shapes would react to the sintering process, four different samples were placed inside the furnace. The green samples can be seen in figure 68a. A cone and dog bone were added and the input temperature was two degrees lower. This resulted in the cubes being almost fully sintered, but they still left a small amount of powder behind. The cone was perfectly sintered and the broken dog bone was fully sintered as well, see figure 68b. But the dog bone was distorted, the top had more shrinkage than the bottom.

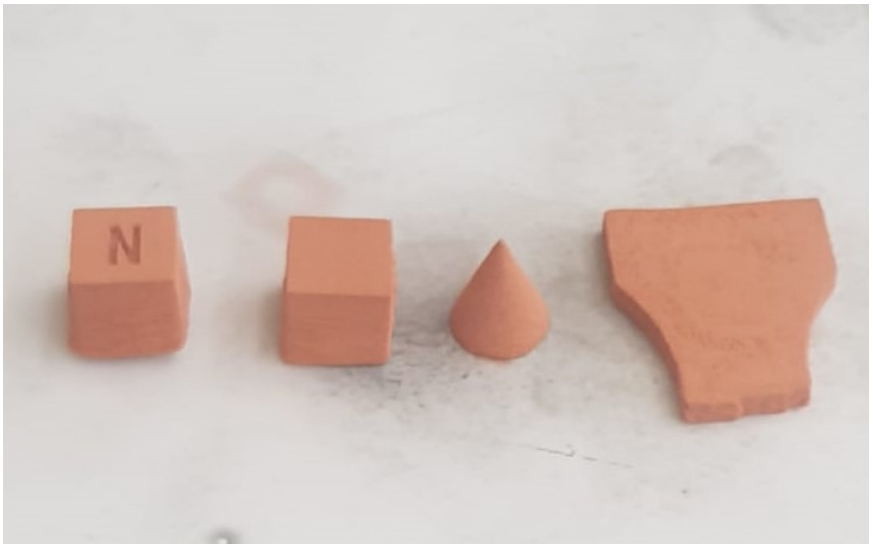

(a) Green samples S10

(b) Sintered samples S10

Figure 68: Samples S10 T_s=1093℃

It was tested to see if 1094 ℃ would be the solution and sinter all the samples fully and not melt them. Furthermore the cooling rate was changed. As earlier the system was cooled down naturally. This probably caused the distortion we saw in the dog bone in figure 25a. For session S11 the cooling down was set to a 5 ℃/min rate, until the temperature inside the furnace reached a temperature of 600 ℃. Below the 600 ℃ the system cools down naturally again. Next to the dog bone, cubes and cone a gyroid sample was added to see how it would react to the sintering, see figure 69a. It turns out that 1094 ℃ is too hot, as the cube with more binder again partially melted. The gyroid was not fully sintered and had broken pieces surrounding it. But the cone, shell printed cube and dog bone were all fully sintered. There was also no distortion in the dog bone, meaning the cooling rate should probably be used for further sinter sessions. A small crack can be seen in the cone after the sintering, this crack was already present in the green part and has not been caused by the sintering.

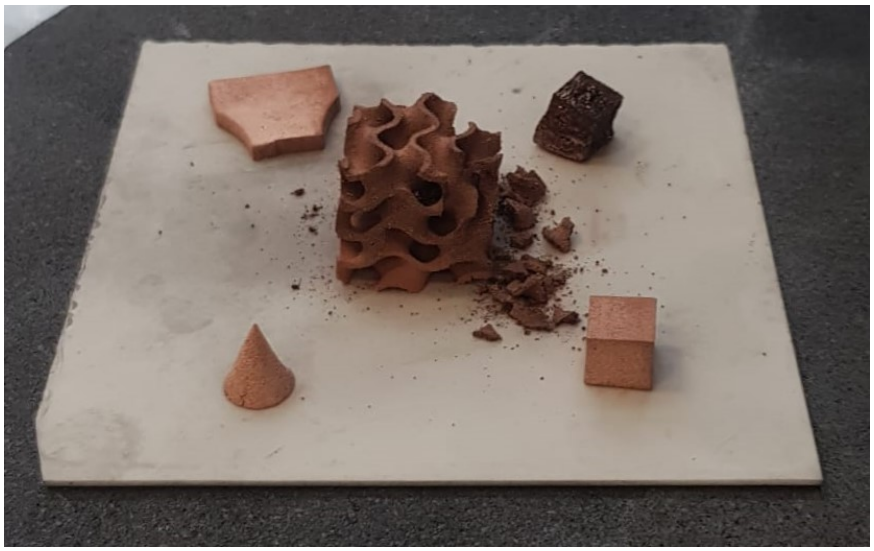

(a) Green samples S11

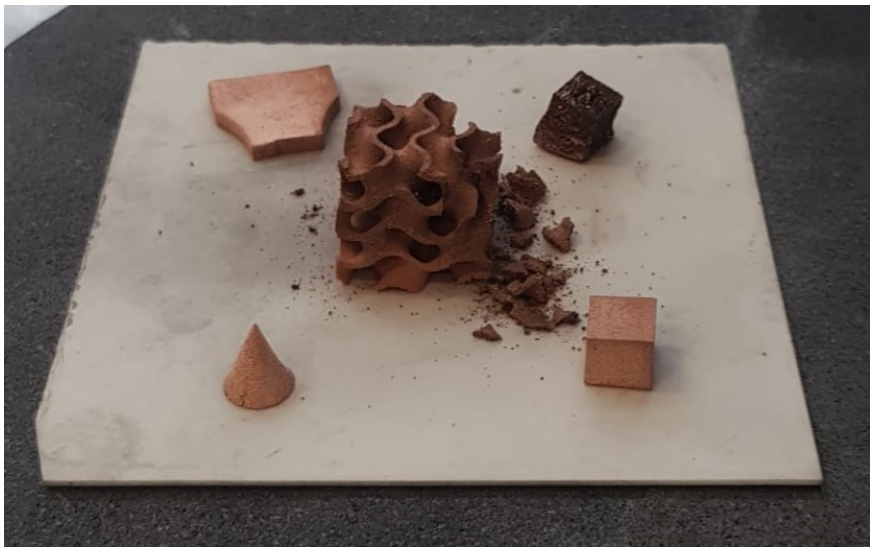

(b) Sintered samples S11

Figure 69: Samples S11 T_s=1094℃

As 1094 ℃ is too high and 1093 is too low, another run is done where the temperature is 1093 ℃, but instead of sintering for five hours it is held at this temperature for 7.5 hours. The longer run time sintered the outside of the samples fully.
As the temperature and run time in argon was found, two temperatures were tried in vacuum. It was expected that finding the temperature in vacuum would be easier due to the absent gas flow. The debinding still happens in an argon atmosphere, as

it is not possible to start a run in vacuum with the furnace used. A run in vacuum at 1075 ℃ for 7.5 hours and a run in vacuum at 1080 ℃ were done. Both sets of samples came out fully sintered on the outside.

Third session

Now the sinter atmospheres, temperatures and run times are known. The final sinter runs were done. The three successful sinter runs were repeated where each five solid cubes, five hollow cubes and five discs were sintered. After the sinter runs, the samples could be measured and compared to see which atmosphere and temperature performs the best. The run time was increased to ten hours to ensure a fully sintered outside of the samples. Table 49 shows the sinter runs that were done with the samples from the third print session.

	Debinding		Sintering		Heating & cooling rate		Atmosphere	
Batch	Temp [℃]	Time [h]	Temp [℃]	Time [h]	Heating [℃/min]	Cooling [℃/min]	Type	Flow [l/h]
S15	450	3	1093	10	5	5	Argon	150
S16	450	3	1075	10	5	5	Vacuum	150
S17	450	3	1080	10	5	5	Vacuum	150
S18	450	3	1093	7.5	5	5	Argon	150
S19	450	3	1080	7.5	5	5	Vacuum	150

Table 49: Input data sinter session 3

The sample set of the three different sinter runs can be seen in figures. Figure 70 shows the argon run at 1093 ℃, figure 71 shows the vacuum run at 1075 ℃ and 72 shows the vacuum run at 1080 ℃.

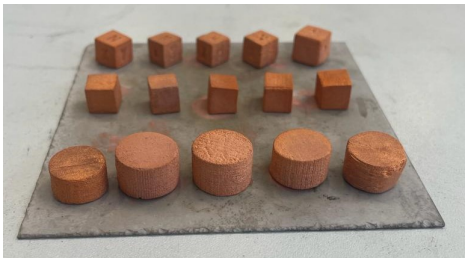

Figure 70: S15 sample set at 1093 ℃ in argon for 10 hours

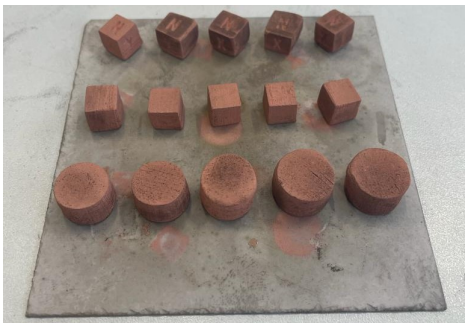

Figure 71: S16 sample set at 1075 ℃ in vacuum for 10 hours

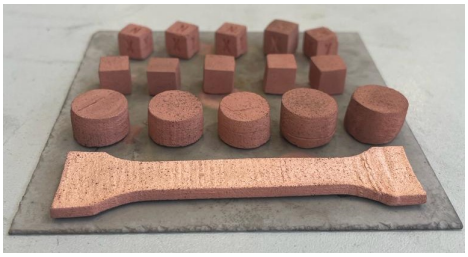

Figure 72: S17 sample set at 1080 ℃ in vacuum for 10 hours

The last sinter runs were for sintering broken dog-bones and heat exchangers. The broken dog-bones were sintered in the atmospheres that achieved the highest density. These were argon at 1093 ℃ and vacuum at 1080 ℃. The broken dog-bones were for the electrical conductivity testing. The run time was decreased to 7.5 hours as the heat exchanger has such thin walls it was believed that ten hours would possibly melt or distort the shape. The sintered heat exchanger and gyroid can be seen next to a green heat exchanger and gyroid in figure 73. The heat exchanger had a small distortion on the bottom. Thus the heating and cooling rate needs to be adjusted to a lower value than 5 ℃/minute.

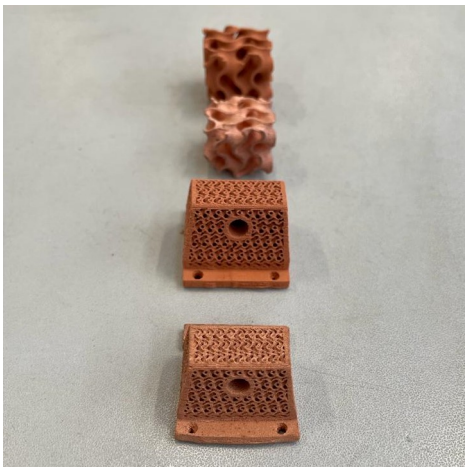

Figure 73: Sintered heat exchanger and gyroid next to green heat exchanger and gyroid

References

[1] I. Gibson, D. W. Rosen, B. Stucker and M. Khorasani, 'Additive manufacturing technologies,' in 3rd ed. Springer, 2021, ch. 8, ISBN: 9780198520115. DOI: 10.1007/978-3-030-56127-7. [Online]. Available: https://doi.org/10.1007/978-3-030-56127-7.

[2] W. E. Frazier, 'Metal additive manufacturing: A review,' *Journal of Materials Engineering and Performance*, vol. 23, pp. 1914–1928, 2014. DOI: 10.1007/s11665-014-0958-z. [Online]. Available: https://doi.org/10.1007/s11665-014-0958-z.

[3] Q. Jiang, P. Zhang, Z. Yu *et al.*, 'A review on additive manufacturing of pure copper,' *Coatings*, vol. 11, no. 6, 2021, ISSN: 2079-6412. DOI: 10.3390/coatings11060740. [Online]. Available: https://www.mdpi.com/2079-6412/11/6/740.

[4] S. Alghamdi, S. John, N. Roy Choudhury and N. Dutta, 'Additive manufacturing of polymer materials: Progress, promise and challenges,' *Polymers*, vol. 13, p. 5, Feb. 2021. DOI: 10.3390/polym13050753.

[5] W. Gao, Y. Zhang, D. Ramanujan *et al.*, 'The status, challenges, and future of additive manufacturing in engineering,' *Computer-Aided Design*, vol. 69, pp. 65–89, 2015, ISSN: 0010-4485. DOI: https://doi.org/10.1016/j.cad.2015.04.001. [Online]. Available: https://www.sciencedirect.com/science/article/pii/S0010448515000469.

[6] J. Slotwinski, 'Additive manufacturing: Overview and nde challenges,' *AIP Conference Proceedings*, vol. 1581, Jan. 2014. DOI: 10.1063/1.4864953.

[7] 'Additive manufacturing,' in A. Bandyopadhyay and S. Bose, Eds., 2nd ed. 2020, pp. 458–459, ISBN: 978-1-138-60925-9.

[8] A. P. 'The complete guide to binder jetting in 3d printing.' (2019), [Online]. Available: https://www.3dnatives.com/en/powder-binding100420174/#! (visited on 09/06/2023).

[9] A. Yegyan Kumar, Y. Bai, A. Eklund and C. B. Williams, 'The effects of hot isostatic pressing on parts fabricated by binder jetting additive manufacturing,' *Additive Manufacturing*, vol. 24, pp. 115–124, 2018, ISSN: 2214-8604. DOI: https://doi.org/10.1016/j.addma.2018.09.021. [Online]. Available: https://www.sciencedirect.com/science/article/pii/S2214860418304007.

[10] A. Yegyan Kumar, J. Wang, Y. Bai, S. T. Huxtable and C. B. Williams, 'Impacts of process-induced porosity on material properties of copper made by binder jetting additive manufacturing,' *Materials & Design*, vol. 182, p. 108 001, 2019, ISSN: 0264-1275. DOI: https://doi.org/10.1016/j.matdes.2019.108001. [Online]. Available: https://www.sciencedirect.com/science/article/pii/S0264127519304393.

[11] T.-T. Ikeshoji, K. Nakamura, M. Yonehara, K. Imai and H. Kyogoku, 'Selective laser melting of pure copper,' *JOM*, vol. 70, no. 3, pp. 396–400, Mar. 2018, ISSN: 1543-1851. DOI: 10.1007/s11837-017-2695-x. [Online]. Available: https://doi.org/10.1007/s11837-017-2695-x.

[12] R. Guschlbauer, A. K. Burkhardt, Z. Fu and C. Körner, 'Effect of the oxygen content of pure copper powder on selective electron beam melting,' *Materials Science and Engineering: A*, vol. 779, p. 139 106, 2020, ISSN: 0921-5093. DOI: https://doi.org/10.1016/j.msea.2020.139106. [Online]. Available: https://www.sciencedirect.com/science/article/pii/S0921509320301945.

[13] M. material property data. 'Overview of materials for wrought copper.' (), [Online]. Available: https://www.matweb.com/search/datasheet.aspx?matguid=cf4172b712124a66a3c1644fa79846a2&ckck=1 (visited on 24/06/2023).

[14] L. A. Chavez, P. Ibave, B. Wilburn *et al.*, 'The influence of printing parameters, post-processing, and testing conditions on the properties of binder jetting additive manufactured functional ceramics,' *Ceramics*, vol. 3, no. 1, pp. 65–77, 2020, ISSN: 2571-6131. DOI: 10.3390/ceramics3010008. [Online]. Available: https://www.mdpi.com/2571-6131/3/1/8.

[15] S. Shrestha and G. Manogharan, 'Optimization of binder jetting using taguchi method,' *JOM*, vol. 69, no. 3, pp. 491–497, Mar. 2017, ISSN: 1543-1851. DOI: 10.1007/s11837-016-2231-4. [Online]. Available: https://doi.org/10.1007/s11837-016-2231-4.

[16] R. Koseski, P. Suri, N. Earhardt and Y.-S. Kwon, 'Microstructural evolution of injection molded gas- and water-atomized 316l stainless steel powder during sintering,' *Materials Science and Engineering A*, vol. 390, pp. 171–177, Jan. 2005. DOI: 10.1016/j.msea.2004.08.002.

[17] A. Balakrishnan, P. Pizette, C. Martin, S. Joshi and B. Saha, 'Effect of particle size in aggregated and agglomerated ceramic powders,' *Acta Materialia*, vol. 58, no. 3, pp. 802–812, 2010, ISSN: 1359-6454. DOI: https://doi.org/10.1016/j.actamat.2009.09.058. [Online]. Available: https://www.sciencedirect.com/science/article/pii/S1359645409006648.

[18] F. Dini, S. A. Ghaffari, J. Jafar, R. Hamidreza and S. Marjan, 'A review of binder jet process parameters; powder, binder, printing and sintering condition,' *Metal Powder Report*, vol. 75, no. 2, pp. 95–100, 2020, ISSN: 0026-0657. DOI: https://doi.org/10.1016/j.mprp.2019.05.001. [Online]. Available: https://www.sciencedirect.com/science/article/pii/S0026065719301705.

[19] S. I. Yanez-Sanchez, M. D. Lennox, D. Therriault, B. D. Favis and J. R. Tavares, 'Model approach for binder selection in binder jetting,' *Industrial & Engineering Chemistry Research*, vol. 60, no. 42, pp. 15 162–15 173, 2021. DOI: 10.1021/acs.iecr.1c02856. [Online]. Available: https://doi.org/10.1021/acs.iecr.1c02856.

[20] A. Lores, N. Azurmendi, I. Agote, E. Espinosa and M. B. García-Blanco, 'A study of parameter and post-processing effects on surface quality improvement of binder jet 3d-printed invar36 alloy parts,' *Progress in Additive Manufacturing*, vol. 7, no. 5, pp. 917–930, Oct. 2022, ISSN: 2363-9520. DOI: 10.1007/s40964-022-00267-w. [Online]. Available: https://doi.org/10.1007/s40964-022-00267-w.

[21] T. Romano and M. Vedani, 'Additive manufacturing of pure copper: Technologies and applications,' in Sep. 2022, ISBN: 978-1-80356-510-1. DOI: 10.5772/intechopen.107233.

[22] R. German, '1 - thermodynamics of sintering,' in *Sintering of Advanced Materials*, ser. Woodhead Publishing Series in Metals and Surface Engineering, Z. Z. Fang, Ed., Woodhead Publishing, 2010, pp. 3–32, ISBN: 978-1-84569-562-0. DOI: https://doi.org/10.1533/9781845699949.1.3. [Online]. Available: https://www.sciencedirect.com/science/article/pii/B9781845695620500017.

[23] M. Ziaee and N. B. Crane, 'Binder jetting: A review of process, materials, and methods,' *Additive Manufacturing*, vol. 28, pp. 781–801, 2019, ISSN: 2214-8604. DOI: https://doi.org/10.1016/j.addma.2019.05.031. [Online]. Available: https://www.sciencedirect.com/science/article/pii/S2214860418310078.

[24] A. Lores, N. Azurmendi, I. Agote and E. Zuza, 'A review on recent developments in binder jetting metal additive manufacturing: Materials and process characteristics,' *Powder Metallurgy*, vol. 62, no. 5, pp. 267–296, 2019. DOI: 10.1080/00325899.2019.1669299. [Online]. Available: https://doi.org/10.1080/00325899.2019.1669299.

[25] A. Kumar, Y. Bai, A. Eklund and C. B. Williams, 'Effects of hot isostatic pressing on copper parts fabricated via binder jetting,' *Procedia Manufacturing*, vol. 10, pp. 935–944, 2017, 45th SME North American Manufacturing

Research Conference, NAMRC 45, LA, USA, ISSN: 2351-9789. DOI: https://doi.org/10.1016/j.promfg.2017.07.084. [Online]. Available: https://www.sciencedirect.com/science/article/pii/S2351978917302664.

[26] H. Miyanaji, K. M. Rahman, M. Da and C. B. Williams, 'Effect of fine powder particles on quality of binder jetting parts,' *Additive Manufacturing*, vol. 36, p. 101 587, 2020, ISSN: 2214-8604. DOI: https://doi.org/10.1016/j.addma.2020.101587. [Online]. Available: https://www.sciencedirect.com/science/article/pii/S2214860420309593.

[27] Y. Wang and Y. F. Zhao, 'Investigation of sintering shrinkage in binder jetting additive manufacturing process,' *Procedia Manufacturing*, vol. 10, pp. 779–790, 2017, 45th SME North American Manufacturing Research Conference, NAMRC 45, LA, USA, ISSN: 2351-9789. DOI: https://doi.org/10.1016/j.promfg.2017.07.077. [Online]. Available: https://www.sciencedirect.com/science/article/pii/S2351978917302597.

[28] A. Mostafaei, S. H. V. R. Neelapu, C. Kisailus, L. M. Nath, T. D. Jacobs and M. Chmielus, 'Characterizing surface finish and fatigue behavior in binder-jet 3d-printed nickel-based superalloy 625,' *Additive Manufacturing*, vol. 24, pp. 200–209, 2018, ISSN: 2214-8604. DOI: https://doi.org/10.1016/j.addma.2018.09.012. [Online]. Available: https://www.sciencedirect.com/science/article/pii/S2214860418304810.

[29] A. Mostafaei, E. L. Stevens, J. J. Ference, D. E. Schmidt and M. Chmielus, 'Binder jetting of a complex-shaped metal partial denture framework,' *Additive Manufacturing*, vol. 21, pp. 63–68, 2018, ISSN: 2214-8604. DOI: https://doi.org/10.1016/j.addma.2018.02.014. [Online]. Available: https://www.sciencedirect.com/science/article/pii/S2214860418300526.

[30] S. Pisani, 'Binder jetting 3d printing of copper,' M.S. thesis, Politecnico di Milano, 2020.

[31] G. Miao, M. Moghadasi, M. Li, Z. Pei and C. Ma, 'Binder jetting additive manufacturing: Powder packing in shell printing,' *Journal of Manufacturing and Materials Processing*, vol. 7, p. 4, Dec. 2022. DOI: 10.3390/jmmp7010004.

[32] S. Choudhary, J. V. N. Sarma, S. Pande *et al.*, 'Oxidation mechanism of thin cu films: A gateway towards the formation of single oxide phase,' *AIP Advances*, vol. 8, no. 5, p. 055 114, 2018. DOI: 10.1063/1.5028407. [Online]. Available: https://doi.org/10.1063/1.5028407.

[33] L. Liu, T. J. Zhang, K. Cui and Y. D. Dong, 'Reduction of copper oxide with graphite by mechanical alloying,' *Journal of Materials Research*, vol. 14, no. 10, pp. 4062–4069, Aug. 1999, ISSN: 2044-5326. DOI: 10.1557/JMR.1999.0548. [Online]. Available: https://doi.org/10.1557/JMR.1999.0548.

[34] A. Mostafaei, A. M. Elliott, J. E. Barnes *et al.*, 'Binder jet 3d printing—process parameters, materials, properties, modeling, and challenges,' *Progress in Materials Science*, vol. 119, p. 100 707, 2021, ISSN: 0079-6425. DOI: https://doi.org/10.1016/j.pmatsci.2020.100707. [Online]. Available: https://www.sciencedirect.com/science/article/pii/S0079642520300712.

[35] Y. Bai and C. B. Williams, 'Binder jetting additive manufacturing with a particle-free metal ink as a binder precursor,' *Materials & Design*, vol. 147, pp. 146–156, 2018, ISSN: 0264-1275. DOI: https://doi.org/10.1016/j.matdes.2018.03.027. [Online]. Available: https://www.sciencedirect.com/science/article/pii/S0264127518302065.

[36] Y. Bai and C. Williams, 'An exploration of binder jetting of copper,' *Rapid Prototyping Journal*, vol. 21, pp. 177–185, Mar. 2015. DOI: 10.1108/RPJ-12-2014-0180.

[37] Y. H. Choong, M. Krishnan and M. Gupta, 'A printability evaluation of fine and coarse powder in binder jetting of dense and porous copper parts,' *Progress in Additive Manufacturing*, Dec. 2022, ISSN: 2363-9520. DOI: 10.1007/s40964-022-00380-w. [Online]. Available: https://doi.org/10.1007/s40964-022-00380-w.

[38] Terra. 'Tag.' (), [Online]. Available: https://www.terraanaliz.com/tag-1 (visited on 24/11/2023).

[39] C. Gero. 'Laboratory furnace, graphite insulation (lht gr).' (2023), [Online]. Available: https://www.carbolite-gero.com/products/vacuum-furnace/laboratory-furnaces/lhtg/ (visited on 26/07/2023).

[40] C. Gero, *Vacuum, inert and reactive gas furnaces up to 3000 ℃*, Accessed: 2023-07-26. [Online]. Available: https://www.carbolite-gero.com/files/15236/vacuum-inert-and-reactive-gas-furnaces-up-to-3000-c.pdf.

[41] N. Aramesh, A. R. Bagheri, T. A. Nguyen and M. Bilal, '3 - characterization techniques for nanomaterials used in nanobioremediation,' in *Nano-Bioremediation : Fundamentals and Applications*, ser. Micro and Nano Technologies, H. M. Iqbal, M. Bilal and T. A. Nguyen, Eds., Elsevier, 2022, pp. 29–43, ISBN: 978-0-12-823962-9. DOI: https://doi.org/10.1016/B978-0-12-823962-9.00018-0. [Online]. Available: https://www.sciencedirect.com/science/article/pii/B9780128239629000180.

[42] A. 3D. 'Artic space spider: Technical specifications.' (), [Online]. Available: https://www.artec3d.com/portable-3d-scanners/artec-spider#specifications (visited on 28/09/2023).

[43] PX. 'Supercharged mechanical testing.' (), [Online]. Available: https://plastometrex.com/pip-vs-tensile/ (visited on 10/12/2023).

[44] T. Theivasanthi and M. Alagar, *X-ray diffraction studies of copper nanopowder*, Accessed: 2023-09-21. [Online]. Available: https://arxiv.org/ftp/arxiv/papers/1003/1003.6068.pdf.

[45] R. Jiang, L. Monteil, K. Kimes, A. Mostafaei and M. Chmielus, 'Influence of powder type and binder saturation on binder jet 3d–printed and sintered inconel 625 samples,' *The International Journal of Advanced Manufacturing Technology*, vol. 116, pp. 1–12, Oct. 2021. DOI: 10.1007/s00170-021-07496-3.

[46] R. K. Enneti and K. C. Prough, 'Effect of binder saturation and powder layer thickness on the green strength of the binder jet 3d printing (bj3dp) wc-12%co powders,' *International Journal of Refractory Metals and Hard Materials*, vol. 84, p. 104 991, 2019, ISSN: 0263-4368. DOI: https://doi.org/10.1016/j.ijrmhm.2019.104991. [Online]. Available: https://www.sciencedirect.com/science/article/pii/S0263436819302446.

[47] M. A. Schöß, F. Schulenburg and T. Turek, 'Oxidation of copper at high temperature as an example for gas-solid reactions in a downer reactor – experiments and model-based analysis,' *Chemical Engineering Science*, vol. 151, pp. 116–129, 2016, ISSN: 0009-2509. DOI: https://doi.org/10.1016/j.ces.2016.05.004. [Online]. Available: https://www.sciencedirect.com/science/article/pii/S0009250916302342.

[48] W. Du, J. Roa, J. Hong, Y. Liu, Z. Pei and C. Ma, 'Binder Jetting Additive Manufacturing: Effect of Particle Size Distribution on Density,' *Journal of Manufacturing Science and Engineering*, vol. 143, no. 9, p. 091 002, Mar. 2021, ISSN: 1087-1357. DOI: 10.1115/1.4050306. [Online]. Available: https://doi.org/10.1115/1.4050306.

[49] Y. Bai, G. Wagner and C. B. Williams, 'Effect of Particle Size Distribution on Powder Packing and Sintering in Binder Jetting Additive Manufacturing of Metals,' *Journal of Manufacturing Science and Engineering*, vol. 139, no. 8, p. 081 019, Jun. 2017, ISSN: 1087-1357. DOI: 10.1115/1.4036640. [Online]. Available: https://doi.org/10.1115/1.4036640.

[50] A. Averardi, C. Cola, S. E. Zeltmann and N. Gupta, 'Effect of particle size distribution on the packing of powder beds: A critical discussion relevant to additive manufacturing,' *Materials Today Communications*, vol. 24, p. 100 964, 2020, ISSN: 2352-4928. DOI: https://doi.org/10.1016/j.mtcomm.2020.100964. [Online]. Available: https://www.sciencedirect.com/science/article/pii/S235249281931596X.

[51] Wikipedia. 'Copper(i) oxide.' (), [Online]. Available: https://en.wikipedia.org/wiki/Copper(I)_oxide (visited on 16/11/2023).

[52] Wikipedia. 'Copper(ii) oxide.' (), [Online]. Available: https://en.wikipedia.org/wiki/Copper(II)_oxide (visited on 16/11/2023).

[53] K. M. Rahman, A. Wei, H. Miyanaji and C. B. Williams, 'Impact of binder on part densification: Enhancing binder jetting part properties through the fabrication of shelled geometries,' *Additive Manufacturing*, vol. 62, p. 103 377, 2023, ISSN: 2214-8604. DOI: https://doi.org/10.1016/j.addma.2022.103377. [Online]. Available: https://www.sciencedirect.com/science/article/pii/S2214860422007667.

[54] M. P. Meeder, 'Modeling the thermal and electrical properties of different density sintered binder jetted copper for verification and revision of the wiedemann-franz law,' M.S. thesis, Virginia Polytechnic Institute and State University, 2016.

[55] C. Silbernagel, L. Gargalis, I. Ashcroft, R. Hague, M. Galea and P. Dickens, 'Electrical resistivity of pure copper processed by medium-powered laser powder bed fusion additive manufacturing for use in electromagnetic applications,' *Additive Manufacturing*, vol. 29, p. 100 831, 2019, ISSN: 2214-8604. DOI: https://doi.org/10.1016/j.addma.2019.100831. [Online]. Available: https://www.sciencedirect.com/science/article/pii/S2214860418309916.

[56] Azom. 'An introduction to copper.' (), [Online]. Available: https://www.azom.com/properties.aspx?ArticleID=597 (visited on 26/11/2023).